National Library of Canada
Bibliothèque nationale du Canada

Canadian Theses Service
Service des thèses canadiennes

Ottawa, Canada
K1A 0N4

NOTICE

The quality of this microform is heavily dependent upon the quality of the original thesis submitted for microfilming. Every effort has been made to ensure the highest quality of reproduction possible.

If pages are missing, contact the university which granted the degree.

Some pages may have indistinct print especially if the original pages were typed with a poor typewriter ribbon or if the university sent us an inferior photocopy.

Reproduction in full or in part of this microform is governed by the Canadian Copyright Act, R.S.C. 1970, c. C-30, and subsequent amendments.

AVIS

La qualité de cette microforme dépend grandement de la qualité de la thèse soumise au microfilmage. Nous avons tout fait pour assurer une qualité supérieure de reproduction.

S'il manque des pages, veuillez communiquer avec l'université qui a conféré le grade.

La qualité d'impression de certaines pages peut laisser à désirer, surtout si les pages originales ont été dactylographiées à l'aide d'un ruban usé ou si l'université nous a fait parvenir une photocopie de qualité inférieure.

La reproduction, même partielle, de cette microforme est soumise à la Loi canadienne sur le droit d'auteur, SRC 1970, c. C-30, et ses amendements subséquents.

NL-339 (r. 88/04) c

Canada

UNIVERSITY OF ALBERTA

A STUDY OF FLAME STRUCTURE WITH ELECTRICALLY INDUCED TURBULENCE

by

MICHAEL J. SZELEWICKI

A THESIS

SUBMITTED TO THE FACULTY OF GRADUATE STUDIES AND RESEARCH

IN PARTIAL FULFILLMENT OF THE REQUIREMENTS FOR THE DEGREE

OF MASTER OF SCIENCE

DEPARTMENT OF ELECTRICAL ENGINEERING

EDMONTON, ALBERTA

SPRING 1990

National Library of Canada
Bibliothèque nationale du Canada

Canadian Theses Service
Service des thèses canadiennes

Ottawa, Canada
K1A 0N4

NOTICE

The quality of this microform is heavily dependent upon the quality of the original thesis submitted for microfilming. Every effort has been made to ensure the highest quality of reproduction possible.

If pages are missing, contact the university which granted the degree.

Some pages may have indistinct print especially if the original pages were typed with a poor typewriter ribbon or if the university sent us an inferior photocopy.

Reproduction in full or in part of this microform is governed by the Canadian Copyright Act, R.S.C. 1970, c. C-30, and subsequent amendments.

AVIS

La qualité de cette microforme dépend grandement de la qualité de la thèse soumise au microfilmage. Nous avons tout fait pour assurer une qualité supérieure de reproduction.

S'il manque des pages, veuillez communiquer avec l'université qui a conféré le grade.

La qualité d'impression de certaines pages peut laisser à désirer, surtout si les pages originales ont été dactylographiées à l'aide d'un ruban usé ou si l'université nous a fait parvenir une photocopie de qualité inférieure.

La reproduction, même partielle, de cette microforme est soumise à la Loi canadienne sur le droit d'auteur, SRC 1970, c. C-30, et ses amendements subséquents.

ISBN 0-315-60180-9

NL-339 (r. 88/04) c

Canada

UNIVERSITY OF ALBERTA

RELEASE FORM

NAME OF AUTHOR: MICHAEL J. SZELEWICKI

TITLE OF THESIS: A STUDY OF FLAME STRUCTURE WITH ELECTRICALLY INDUCED TURBULENCE

DEGREE: MASTER OF SCIENCE

YEAR THIS DEGREE GRANTED: SPRING 1990

PERMISSION IS HEREBY GRANTED TO THE UNIVERSITY OF ALBERTA LIBRARY TO REPRODUCE SINGLE COPIES OF THIS THESIS AND TO LEND OR SELL SUCH COPIES FOR PRIVATE, SCHOLARLY OR SCIENTIFIC RESEARCH PURPOSES ONLY.

THE AUTHOR RESERVES OTHER PUBLICATION RIGHTS, AND NEITHER THE THESIS NOR EXTENSIVE EXTRACTS FROM IT MAY BE PRINTED OR OTHERWISE REPRODUCED WITHOUT THE AUTHOR'S WRITTEN PERMISSION.

(SIGNED) M. Szelewicki

PERMANENT ADDRESS:

10249 - 158 Street

Edmonton, Alberta

T5P 2Y1

DATE: April 5, 1990

THE UNIVERSITY OF ALBERTA

FACULTY OF GRADUATE STUDIES AND RESEARCH

The undersigned certify that they have read, and recommend to the Faculty of Graduate Studies and Research, for acceptance, a thesis entitled A STUDY OF FLAME STRUCTURE WITH ELECTRICALLY INDUCED TURBULENCE submitted by Michael J. Szelewicki in partial fulfillment of the requirements for the degree of MASTER OF SCIENCE in ELECTRICAL ENGINEERING.

Peter R Smy

DR. P.R. SMY
Supervisor

J.D. Dale

DR. J.D. DALE

DR. J. TULIP

Date April 4/90

Abstract

A better understanding of the roles of turbulence and plasma mixing from electric sparks is gained from an experimental investigation of pulsed plasma jets and conventional igniters. Studies of luminosity, ionization, burning velocity, and flame structure were performed with these igniters. It is shown that electrically induced turbulence is responsible for large increases in the effective values of gaseous thermal conductivity and diffusion. This enhancement is sufficient to explain the substantial increases in flame speed which are observed. Data was collected using conventional photography, Langmuir probes, image intensified streak photography, single and dual photomultiplier measurements of laser schlieren, and optical measurements of high speed schlieren video images.

Acknowledgments

I would like express my gratitude to Dr. Peter Smy for the opportunity to write this thesis. It is his patience, understanding, and passion for the quest of new knowledge that has provided inspiration and motivation, making this learning experience a tremendously enjoyable and memorable one. The aformentioned attributes are perhaps the essence of this Master's thesis.

I am indebted to Mr. James Dawe, with gratification, for his extraordinary editing abilities and enlightening comments. A man whose patience and organization has helped make the transcription of information and ideas, clear and meaningful.

I would also like to thank Mr. Richard Haley for answering a multitude of questions, making many eye-opening explanations, and for his participation in the burning velocity study; moreover, for making three years of existence in the lab, interesting and fun.

Finally, I would like to thank Bording Ostergaard for his help with AutoCAD, and a special thanks to Jackie George for her participation in the luminosity study.

This thesis is dedicated to my equine and feline friends:

Leane and Sheba.

Table of Contents

Chapter		Page
1.	Introduction	1
	1.1 Pulsed Plasma Jet Igniter	2
	1.2 Purpose	8
	1.3 Content	11
2.	Apparatus	13
	2.1 Combustion Chamber	13
	2.2 Optical Bench	15
	2.3 Power Supply	17
	2.4 Surface Gap Igniter	20
	2.5 Plasma Jet Igniter	22
3.	Diagnostics	25
	3.1 Image Intensified Streak Camera	26
	3.2 Schlieren Optical Measurements	28
	3.3 Langmuir Probe	33
	3.4 Discussion on Probes	38
	3.5 Photomultiplier	44
4.	Experimental Studies	47
	4.1 Luminosity Measurements	48
	4.1.1 Experimental Design	48
	4.1.2 Results	51
	4.1.3 Conclusion	57

Chapter Page

4.2 Image Intensified Streak Photography 60

4.2.1 Experimental Design 60

4.2.2 Results 62

4.2.3 Conclusion 68

4.3 Ionization Measurements 70

4.3.1 Experimental Design 70

4.3.2 Results 74

4.3.3 Conclusion 79

4.4 Relative Burning Velocity 80

4.4.1 Experimental Design 80

4.4.2 Results 82

4.4.3 Conclusion 86

4.5 Flame Structure Mechanisms 87

4.5.1 Theory 88

4.5.2 Experimental Design 93

4.5.3 Results 96

4.5.4 Conclusion 123

5. Summary of Results from all Experimental Studies 127

References 131

Appendix I 134

1. Introduction 134

2. Experimental Design 134

3. Experiment Considerations 137

Chapter Page

4. Time Domain Model 139

4.1 Normal Input Intensity 139

4.2 High Input Intensity 143

4.3 Excessively High Input Intensity 146

5. Phosphor Decay Case 149

6. Time Exposure Model 150

7. Conclusion 154

List of Tables

Table — Page

4.1 Flame Front 10% to 90% Rise Time (μs),
- a. Surface Gap Igniter 99
- b. Plasma Jet Igniter 99

4.2 Instantaneous Velocity (m/s)
- a. Surface Gap Igniter 102
- b. Plasma Jet Igniter 102

4.3 Flame Front Thickness (mm)
- a. Surface Gap Igniter 105
- b. Plasma Jet Igniter 105

4.4 Flame Front Thickness (mm), by Optical Probe 110

4.5 Thermal Conductivity (mJ / m s K)
- a. Surface Gap Igniter 113
- b. Plasma Jet Igniter 113

4.6 Turbulent Diffusion (m^2/s)
- a. Surface Gap Igniter 123
- b. Plasma Jet Igniter 123

List of Figures

Figure		Page
1	Plasma Plug Igniter	3
2.1	Luminosity Measurement Experiment	14
2.2	Langmuir Probe Flame Structure Experiment	16
2.3	Igniter Power Supply Schematic	18
2.4	Plasma Jet Igniter	21
3.1	Image Intensified Streak Camera Experiment	27
3.2	Schlieren Laser Experiment	29
3.3	Schlieren Cinematography Experiment	32
3.4	Langmuir Probe Setup	35
3.5	Apparent Flame Front Thickness Graph	40
3.6	Laser Schlieren Dual Photomultiplier Experiment	42
3.7	Typical Photomultiplier Oscillogram of Light Intensity from a Flame	46
4.1	Luminosity Measurement Experiment	49
4.2	Luminosity Travel Time Graph	54
4.3	Luminosity Relative Amplitude Graph	54
4.4	Image Intensified Streak Camera Experiment	61
4.5	Langmuir Probe Ionization Experiment	71
4.6	Langmuir Probe - Luminosity Comparison	78
4.7	Schlieren Cinematography Experiment	81
4.8	Flame Front Distance Graph	84
4.9	Temperature Profile of Wavefront	91

Figure — Page

4.10 Langmuir Probe and Laser Schlieren Experiment 94

4.11 Typical Photomultiplier Output Graph of Langmuir Probe 97

4.12 Wavefront Distance Graph
a. Surface Gap Igniter 100
b. Plasma Jet Igniter 100

4.13 Flame Front Thickness Graph
a. Surface Gap Igniter 103
b. Plasma Jet Igniter 103

4.14 Ambient Temperature Flame Front Thickness Graph . 106

4.15 Ambient Temperature Instantaneous Velocity Graph 106

4.16 Typical Oscillogram of Optical Probe: Voltage vs Time Graph 109

4.17 Thermal Conductivity with respect to Air Graph
a. Surface Gap Igniter 111
b. Plasma Jet Igniter 111

4.18 Thermal Conductivity with respect to Stoichiometric Ratio Graph
a. Surface Gap Igniter 114
b. Plasma Jet Igniter 114

4.19 Igniter Comparison of Thermal Conductivity 116

4.20 Diffusion with respect to Air Graph
a. Surface Gap Igniter 118
b. Plasma Jet Igniter 118

4.21 Diffusion with respect to Stoichiometric Ratio Graph
a. Surface Gap Igniter 119
b. Plasma Jet Igniter 119

4.22 Igniter Comparison of Thermal Diffusion 121

Figure		Page
I.1	Image Intensifier Experiment	135
I.2	Normal Input Intensity	142
I.3	High Input Intensity	145
I.4	Excessively High Input Intensity	148
I.5	Output-to-Input Luminosity Area vs Input Voltage	156

List of Plates

Plate		Page
4.1	3000 ASA Polaroid Photograph of Plasma Plume	52
4.2	20,000 ASA Polaroid Photograph of Plasma Plume ...	52
4.3	Typical Photomultiplier Luminosity Oscillogram ...	53
4.4	Oscillogram of Simultaneous Schlieren and Photomultiplier Outputs	53
4.5	Polaroid of Plasma Jet Igniter in Nitrogen	63
4.6	Polaroid of Plasma Jet Igniter in Air	63
4.7	Polaroid Photographs of Plasma Jet Igniter in Propane-Air Mixtures	
	a. 0.5% Propane	65
	b. 1.0% Propane	65
	c. 2.0% Propane	66
	d. 2.5% Propane	66
	e. 4.02% Propane	67
4.8	Polaroid of Surface Gap Igniter in Stoichiometric Mixture of Propane-Air	67
4.9	Oscillogram of Ion Density	76
4.10	Schlieren Photograph of Relative Burning Velocity	83
I.1	Oscillogram of Image Intensifier's Output, excited by Normal Input Intensity	142
I.2	Oscillogram of Image Intensifier's Output, excited by High Input Intensity	145
I.3	Oscillogram of Image Intensifier's Output, excited by Excessively High Input Intensity ...	148

1. INTRODUCTION

Spark ignition engines consume more than a billion gallons of gasoline daily, or roughly one-third of the total annual world petroleum production (Keck, 1982). Internal combustion engines are also a major source of air pollution. Thus, increasing fuel efficiency and reducing emissions from these engines is a matter of considerable practical importance, and one that has become a major goal of current combustion research. Of particular interest is the development of theories, which explain the influence of turbulence on the flame speed of combustion (Weinberg, 1986). Such turbulence could be effective in both enhancing the performance of existing engines utilizing lean fuel mixtures, and in improving the design of future engines, because turbulence can enhance the burning rate of combustion.

As a result of studies carried out over more than half a century, it has been established (Andrews et al, 1975) that turbulence does play some role in combustion. Although a great deal of experimental data has been accumulated, and numerous theories have been proposed, a completely satisfactory theory for predicting the influence of turbulence on burning rates has not yet been developed. A review of current theories of turbulence, and their compatibility with different models of turbulent flame propagation, was made by Andrews and others in 1975. It is

clear from this review that the development of models for turbulent combustion based on fundamental principles is a formidable task, and one unlikely to be completed in the near future. However, a model which considers the turbulent enhancement of heat conduction (turbulence) and particle diffusion (chemical), both of which affect flame speed, would seem to have some application at the present time (Weinberg, 1986). These two turbulent enhancement mechanisms are thought to arise in pulsed plasma jet igniters.

1.1 PULSED PLASMA JET IGNITER

In recent years, growing concern about pollution and escalating fuel prices led to the a study of plasma jets as ignition sources, primarily as a possible means of enhancing the performance of internal combustion engines. In order to improve engine emission characteristics and efficiencies, development has concentrated on the use of leaner mixtures. However, the optimum conditions, both for minimum fuel consumption and for minimizing the various pollutants, occur somewhere near the lean mis-fire limit -- the point at which combustion becomes erratic because of the dilute fuel mixture. Successful combustion at these lower fuel-air ratios requires increased rates of flame propagation, and more effective and reliable ignition sources. The pulsed plasma jet igniter is an ignition

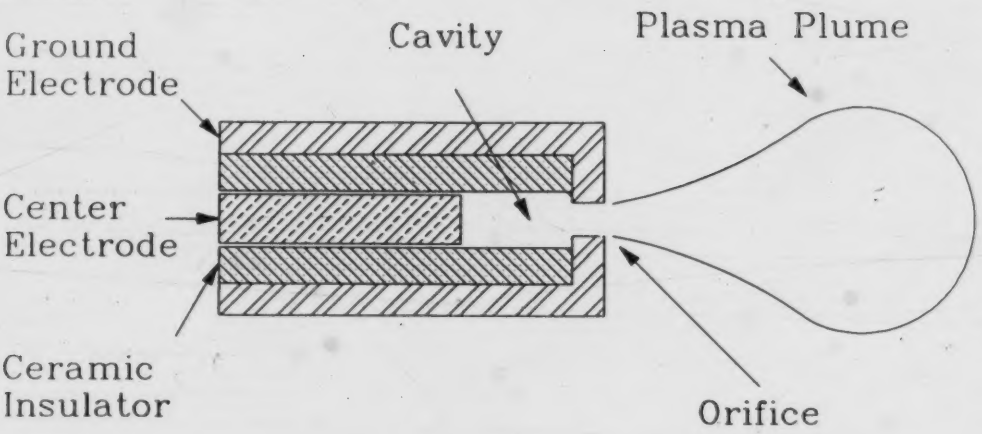

Figure 1 Plasma Jet Igniter

source which achieves these ends because of the turbulence it creates. The plasma igniter is the subject of a recent study on electrically induced turbulence by Haley et al (1989).

The plasma jet igniter (Figure 1) is essentially a modified spark plug in which the discharge, instead of occurring between two exterior electrodes, is constrained within a small cavity (less than 10 microliters) which can be filled with a suitable fuel-air medium such as gasoline-air, propane-air, or methane-air. Rapid heating by an electric discharge causes the medium to dissociate; the plasma thus created is then expelled at high velocity through the orifice, preceded by a shock wave. By varying the size and shape of the aperture in relation to the volume of the cavity, and to the energy input, one can control plasma temperature, radical production, and the fluid dynamics of the jet. Fluid dynamics include both depth of penetration and the amount of turbulence generated.

When a plasma plug is discharged, the plume penetrates much further into the combustible mixture than a conventional spark plug, and in so doing increases the rate of combustion. In comparison with a conventional spark plug, the increase in speed is dramatic (Weinberg, 1986). A conventional igniter ignites a mixture as a point source, which then develops into a flame kernel and propagates

radially outwards as a spherical flame front. In contrast, the plasma plug expels a high velocity plume of high pressure and high temperature plasma. The turbulent boundary layer of this plume causes many flame kernels to develop in and along the plume's wake, which subsequently combine to form a radially propagating flame front around an already large volume of burnt gas. This large radial flame front ignites a greater quantity of mixture per unit time than can be lit by a point source.

Mixture ratio is defined as the stoichiometric mixture volume ratio over the actual mixture volume ratio, and is denoted by λ:

$$\lambda = \frac{\text{stoichiometric mixture volume ratio}}{\text{actual mixture volume ratio}}$$

The stoichiometric ratio (λ=1.0) for methane in air is 9.5% by volume, and 4.02% by volume for propane in air (Lewis and von Elbe, 1961). Mixture ratios greater than unity indicate lean mixtures, while ratios less than one indicate rich mixtures.

Lean fuel mixtures ignited by a conventional spark plug ordinarily burn more slowly than stoichiometric mixtures. However, using the plasma jet igniter, the burning rate for lean mixtures can be increased until it equals the combustion rate for stoichiometric mixtures (Dale, 1981; Weinberg, 1984). The result could be more efficient use of fuel in a system using a lean mixture and

a plasma jet igniter.

Fluid mechanical effects determine the structure and turbulence of the jet, and hence the initial location and surface area of the flame kernel (Weinberg, 1986). The rate of volume consumption of the reactants at any instant is proportional to the flame area, as well as to the burning velocity. Experimental work has shown that when plasma jets are allowed to interact with already propagating flames, the flame speed can be considerably increased -- even under conditions where the radicals have been "quenched out" (Zhang et al, 1982).

As has been stated, pulsed plasma ignition shows great promise, especially for igniting lean fuel mixtures. Comparisons have been carried out between conventional ignition systems and plasma jet igniters on various internal combustion engines burning gasoline, propane, and methane (Dale et al, 1978; Edwards et al, 1983; Tozzi et al, 1982). Various attempts have been made to relate the depth of penetration of the expanding jet to the energy dissipated, and to the geometry of the cavity/orifice combination (Grant et al, 1983; Cetegen et al, 1980; Smy et al, 1982). The jet has been shown to be substantially supersonic (Smy et al, 1982) and the blast wave has been estimated to carry about one-tenth of the electrical energy dissipated in the igniter during the first half cycle of the discharge (Topham et al, 1975).

Studies of the contributions of aerodynamic and chemical effects suggests it is important that they be considered together (Orrin et al, 1981; Clements et al, 1984; Weinberg, 1983). The rate of flame propagation is increased by both types of effects if the volumetric rate of reactant consumption is equal to the product of laminar burning velocity and flame area. Chemistry controls the burning velocity, and turbulence strongly influences the flame area. The usefulness of the two effects depends on the stoichiometry of the mixture to be burned. Turbulence appears most useful for near stoichiometric mixtures where radical shortage is not critical, and where increasing the fundamental burning velocity can cause the flame to laminarize. These studies have also found that for very lean mixtures the chemical mechanism offers unique radical transport advantages, whereas for near stoichiometric conditions it is better to design plugs that generate maximum turbulence.

Pulsed plasma jets are potentially useful in many combustion applications including cold-starting of diesel engines, more reliable ignition in furnaces (where failure to ignite rapidly might constitute a major explosion hazard), and re-ignition (following flame-out) in jet engines. The disadvantage of using pulsed plasma jets is that, burning transiently, they are incapable of flame holding. Thus, in the case of jet engines operating at

high altitudes, they could not prevent flame-out, but only provide reliable relighting following re-establishment of flammable conditions. Current power supply designs fire repetitively up to 300 Hertz and the energy dissipated in a discharge can be up to 2000 Joules.

1.2 PURPOSE

The study of combustion enhancement mechanisms, especially the role of radicals in the form of activated molecular species in gaseous mediums (like nitrogen, air, methane-air, and propane-air) is the main focus of the experimental studies of Chapter 4, conducted for this thesis. Moreover, the mechanism by which radicals are transported and thus promote combustion is studied in terms of the ability of radicals to mix (i.e. diffuse) with cold gas. As heated gas (radicals) move from the plasma plume to the wavefront in the non-combustible case, or from the reaction zone to the pre-heat zone in the flame front of the combustible case, cold gas is heated. This characteristic is considered from the point of view of the igniter. In comparison with the normal activation of radicals from a conventional igniter, such as the surface gap igniter, electrically induced turbulence produced by the plasma jet igniter (Haley, 1989) is the important mechanism by which these radicals are created and formed into "hot pockets" (Weinberg, 1986).

Chemical effects of the plasma jet igniter were studied in terms of luminosity and ionization. Luminosity photographs of excited nitrogen states were taken in nitrogen mixed with varied amounts of oxygen. Nitrogen was used because it was a suitable neutral medium to visibly observe the activated species. More informative observations were made with the aid of an Image Intensified Streak Camera. Streak photographs from this camera provided information about flame front velocity and enhanced the observations of both activated species ahead of the plume and the presence of these radicals with respect to time. Ionization measurements were also carried out in nitrogen, air, and in a combustible mixture of propane. Propane was used because it was a suitable fuel to study ionization, and because it has current applications in the world as automotive fuel. Measurements of ionization gave information about the thickness, density, and resistivity of the chemical activity region produced by the flame.

Additionally, it was established that the luminous ionization cloud (no combustion) from the plasma plug is the same cloud that was found to be heated and sharply defined in the work of Weinberg (1983). Evidence for this was in the form of an oscillogram of simultaneous signals from an ionization probe and from a laser schlieren photomultiplier output. This finding was also supported by ionization results of the wavefront.

The secondary purpose of this study was to determine whether the increased rate of combustion of a plasma jet igniter is caused by chemical effects or turbulence. This distinction was made by first determining the (relative) burning velocity of a flame front with respect to the mixture preceding it. Next, the instantaneous velocities and flame front thicknesses from both the plasma jet and the surface gap igniters were determined. These and other appropriate quantities were then substituted into the derived equations of heat conduction and turbulent diffusion.

The measured thermal (heat) conductivity of a lean mixture compared with thermal conductivity of a stoichiometric mixture shows whether turbulence is dependent upon the mixture strength. A comparison of thermal conductivity from the plasma jet to that from the surface gap igniter, for all mixture ratios, shows how flame enhancement is promoted by turbulent activity.

Turbulent radical diffusion within a lean mixture compared with turbulent radical diffusion within a stoichiometric mixture shows whether or not the transport and mixing of radical hot-pockets is dependent upon the mixture strength. A comparison of radical diffusion from the plasma jet to the surface gap igniter, for all mixture ratios, shows how flame enhancement is promoted by the mixing activity of radicals with cold gas.

Experimental observations of flame structure and burning velocity are used to support both heat conduction and turbulent diffusion transport process theories, which results in a model of the role these mechanisms play in increasing flame speed that is in good agreement with nature.

To obtain evidence of increased flame speed of combustion processes, the following variants were studied: igniter type, fuel-air mixture ratio, and ambient temperature. The studies incorporated both probe and optical measurements, including those from Langmuir probes, image intensified streak photography, schlieren photography, photomultipliers, and a schlieren laser technique.

1.3 CONTENT

This thesis consists of five chapters and one appendix. Chapter Two, entitled Apparatus, discusses the various components used in experiments conducted as part of this study: Combustion Chamber, Optical Bench, Power Supply, Surface Gap Igniter, and Plasma Jet Igniter.

Chapter Three, Diagnostics, gives explanations on each sensing method and device used to obtain experimental data: Image Intensified Streak Camera, Schlieren Laser Technique, Schlieren Cinematography, Langmuir Probe, and Photomultiplier.

Chapter Four outlines five separate studies conducted on igniters: Luminosity Measurements, Image Intensified Streak Photography, Ionization Measurements, Relative Burning Velocity, and Flame Structure Mechanisms. Each individual study introduces the experiment, presents results, and draws conclusions.

Chapter Five summarizes the results of the five studies, and draws a final conclusion based on these findings.

Finally, Appendix I is a chapter on the use of the image intensified streak camera as a linear light amplifier to produce enhanced luminosity photographs.

2. APPARATUS

This chapter discusses the major components used in the experiments described in chapter 4: Combustion Chamber, Optical Bench, Power Supply, Plasma Jet Igniter, and Surface Gap igniter. All of the combustion and non-combustion experiments were performed within the confines of the combustion chamber. The optical bench held all components in place and provided a means to adjust their alignment. The power supply was used as the energy source for both the plasma plug and the surface gap igniter. Either igniter could be mounted in the wall of the combustion chamber. The plasma jet igniter was fired into non-combustible mixtures of air, nitrogen, and nitrogen-oxygen, and combustible mixtures of propane-air, and methane-air. Similarly, the surface gap igniter was discharged in identical mixtures and the laminar flame it created compared with the pulsed plasma jet's characteristically turbulent flame.

2.1 COMBUSTION CHAMBER

The combustion chamber, or bomb, consists of a stainless steel cylinder with 1 centimeter thick walls, capped at each end with 2.54 cm (1 inch) thick schlieren quality (perfectly flat and parallel) Pyrex glass windows. Entering the cylinder at various locations are fittings for the gas inlet and exhaust, the igniter, and the Langmuir probe. With internal dimensions of eight centimeters in

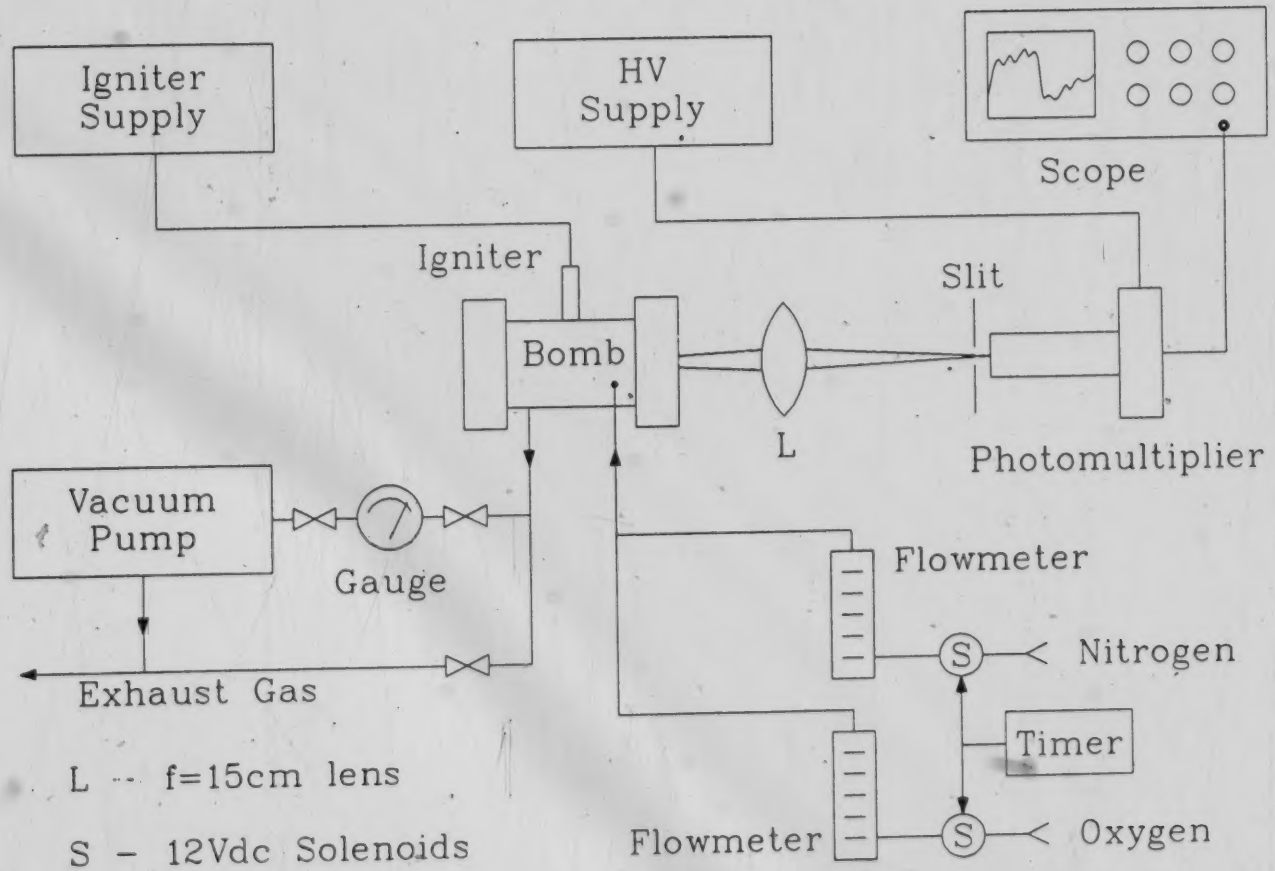

Figure 2.1 Luminosity Measurement Experiment

diameter and ten centimeters in length, the bomb encloses a five hundred milliliter volume.

2.2 OPTICAL BENCH

A 1.8 meter optical rail held all the necessary components in proper alignment for the luminosity experiments (Figure 2.1). The bomb was mounted in a double "V" holder with leveling adjustments, and this in turn sat on an optical rail car, located midway on the optical rail. Located at one end of the rail was either a Polaroid camera or the Image Intensified Streak Camera. For the experiments involving luminosity photographs, a sheet of Mylar located at seventy centimeter from the camera, acted as a light diffuser, and illumination was provided by a light source mounted at one hundred centimeters distance from the camera. In the case of the intensified image, a fifty millimeter lens located one centimeter down the rail from the camera, focused the image from the point of interest (just below the igniter within the bomb) onto the camera's slit and shutter arrangement.

For the Flame Structure observations, the bomb was also located midway on the optical rail (Figure 2.2). Located at one end of the rail was the laser beam point source: a Helium-Neon (HeNe) laser of 632.8 nanometer (nm) wavelength, 1 millimeter beam diameter and 1 milliwatt power. Thirty centimeters down the rail, an adjustable iris

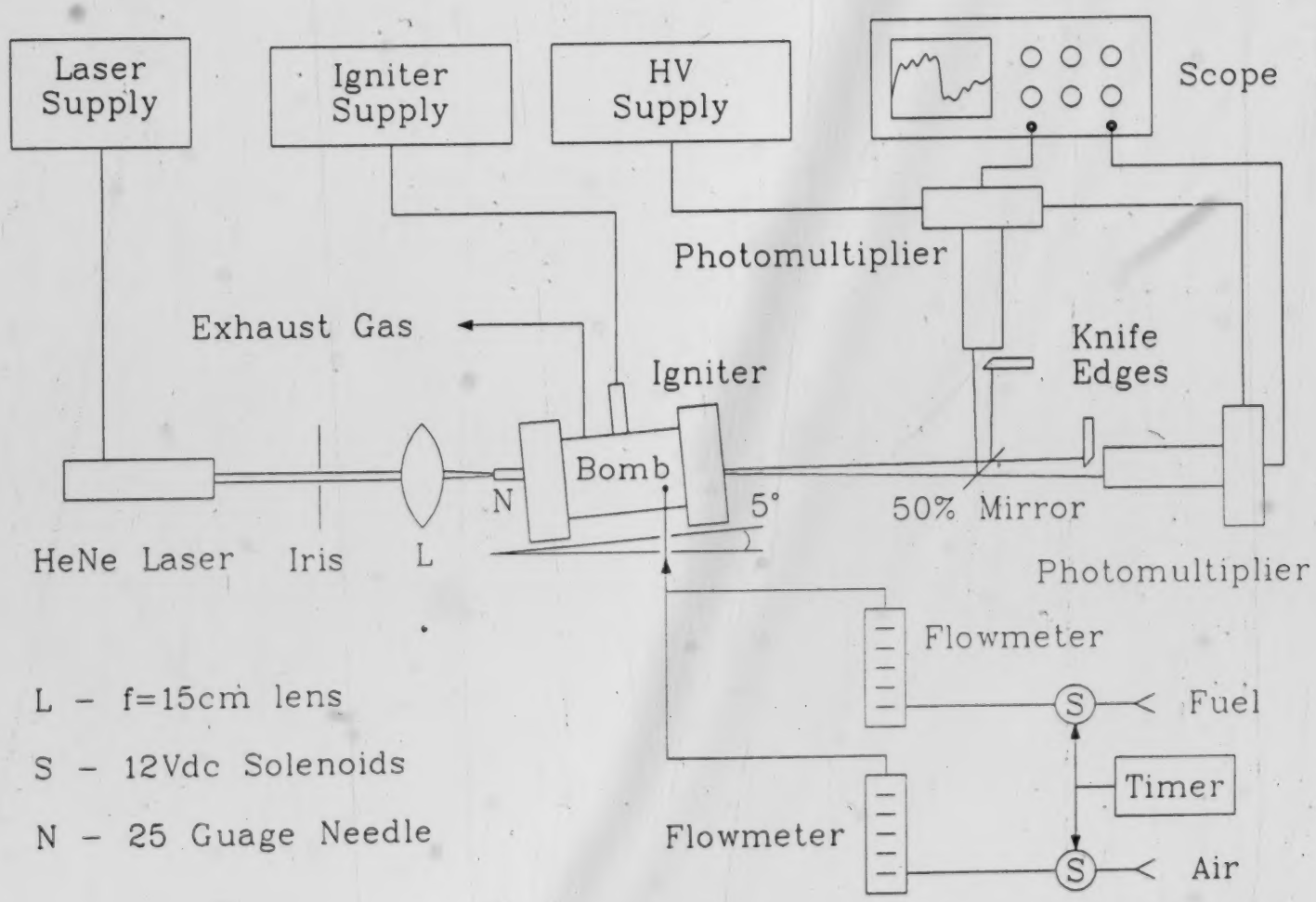

Figure 2.2 Laser Schlieren Dual Photomultiplier Experiment

removed any beam divergence and scatter, limiting the laser to a clean parallel beam. At forty-five centimeters, a convex lens with a focal length of fifteen millimeters focused the beam to a 0.1 millimeter convergence at the tip of a hollow needle (N in Figure 2.2). The needle was mounted in the end of a 3.175 mm (1/8 inch) brass tube itself set in a 1 inch thick Plexiglas window, which was substituted for one of the Pyrex bomb windows. The beam then diverged as it left the pointed needle tip inside the bomb. A fifty-percent reflective mirror was located at the seventy centimeter position, splitting the beam equally onto two photomultiplier knife-edge arrangements mounted at one hundred centimeters distance from the point source.

2.3 POWER SUPPLY

The power supply (Figure 2.3), which served as the ignition source for both the plasma jet and the surface gap igniters, was built in two sections. The first section was a low power automotive spark coil with triggering circuitry. When used alone it supplied the low energy spark required by the surface gap igniter. Used with the second, high energy, section, it provided an initial breakdown path for a high energy release through the triple electrode spark gap. The energy from the high energy section was set at 660 millijoules, with a duration of 80 microseconds. This was found to be sufficient to drive the plasma jet for experimental purposes.

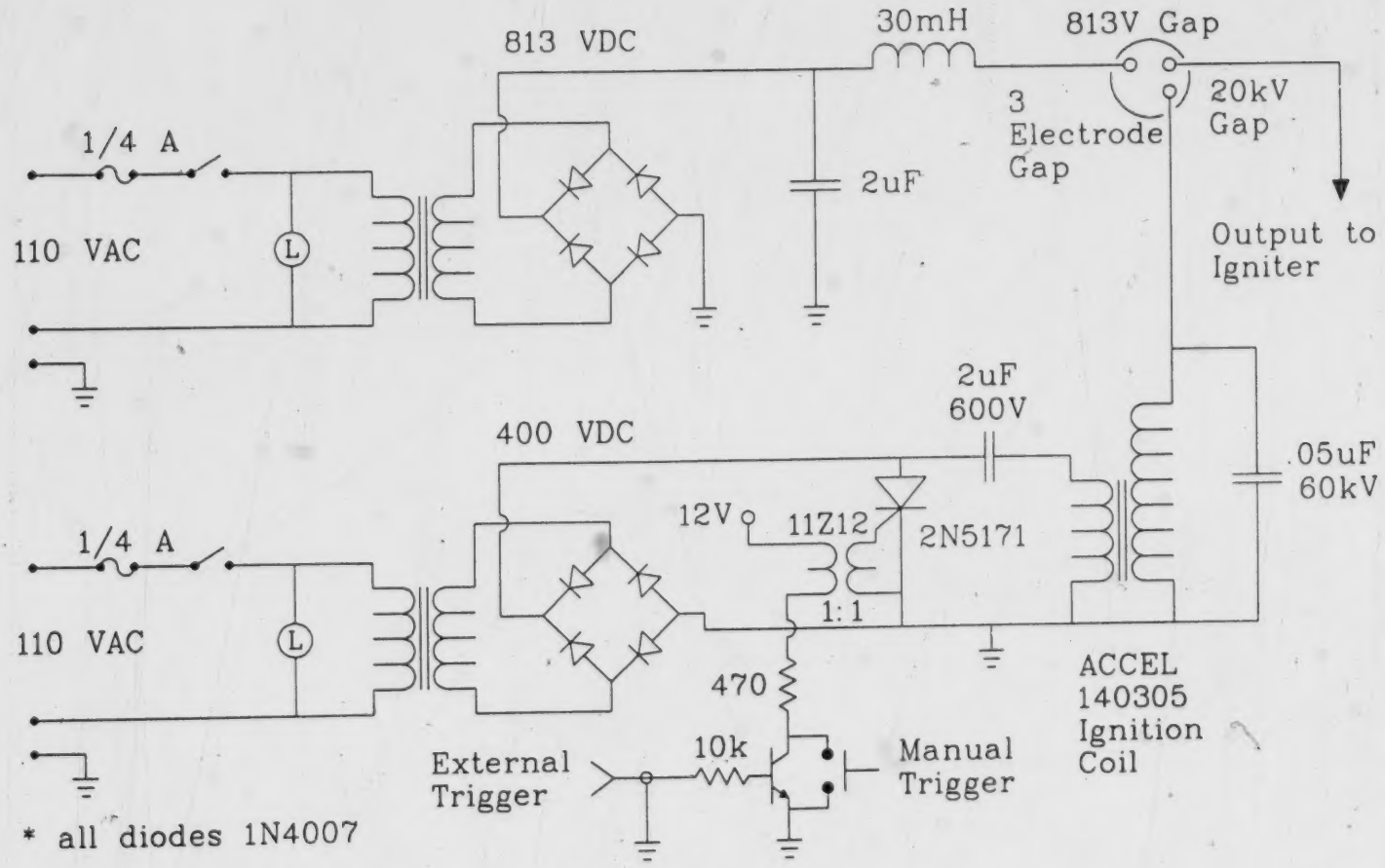

Figure 2.3 Igniter Power Supply Schematic

The first section of the power supply stepped up and rectified the 110V AC line voltage to 400V DC. This supply charged a 2 microfarad capacitor with 160 millijoules of energy through the primary windings of a conventional automobile ignition coil. The stored energy discharge could either be triggered manually or by an external signal from an oscilloscope. Momentarily depressing the push button applied a positive pulse to the primary winding of a one-to-one pulse transformer. This transformer then applied the pulse across the gate of the thyristor (SCR). Upon gating, the SCR connected the positive terminal of the charged 2 microfarad capacitor to ground. Thus, the capacitor dumped its stored energy through the primary winding of the ignition coil, and the secondary winding of the ignition coil stepped up the voltage to the thirty thousand volts necessary for gap breakdown to occur. The current was then fed to a 0.05 microfarad capacitor until enough charge had been collected for breakdown to occur between two of the electrodes in the three electrode spark gap.

As with the first section, the second section stepped up and rectified the 110 V AC line voltage to 813V DC. A 2 microfarad, 2 kilovolt storage capacitor charged to 660 millijoules with this potential applied across it. When the first section's high voltage automotive spark jumped between the first and second electrodes of the 3-electrode gap, the second electrode was raised sufficiently to allow

breakdown to occur between the second and third electrodes. In this way the energy stored in the power supply was dumped through the triple gap and onwards to the plasma jet igniter.

2.4 SURFACE GAP IGNITER

The surface gap igniter (Champion L-77V) is a plug design used today in many marine and aircraft applications. The electrode arrangement consists of a short central stub anode separated by a 3 millimeter semiconductive ceramic surface from a surrounding, flush mounted, circular ring cathode. When energy is released from the power supply, one or more sparks occur between the center and ground electrodes anywhere around the 360 degree perimeter. This arrangement ensures a spark will always occur because of the constant gap separation between the electrodes. If obstructions, such as corrosion or oil deposits, are formed on the electrodes, a spark will occur between the next cleanest electrode surfaces. Thus, breakdown can occur at relatively low potentials, and the igniter can also operate at high temperatures.

For the purpose of these experiments, an igniter such as the surface gap plug which created a spark perpendicular to the probe was required. In this way, a laminar burning flame front was achieved within the fuel mixture. The behavior of this flame could be compared with the turbulent combustion created by the pulsed plasma plug.

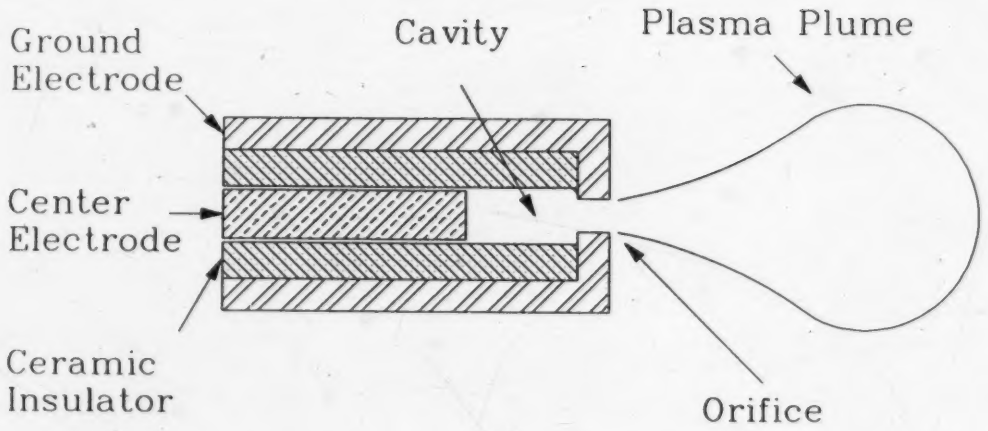

Figure 2.4 Plasma Jet Igniter

2.5 PLASMA JET IGNITER

The plasma jet igniter (Figure 2.4) used in these experiments consists of a 1.588 mm (1/16 inch outer diameter) tungsten electrode mounted in a 6.35 mm (1/4 inch outer diameter) ceramic tube. The ceramic tube is mounted with Swage-Lock fittings in a conventional spark plug style threaded casing. Instead of protruding, the electrode is recessed into the ceramic by 4 millimeters, and the casing is capped with an orifice plate having a 1.588 mm (1/16 inch) hole. With these dimensions, the cavity contains a volume of eight microliters.

The construction of the cavity within the plug is crucial to the performance characteristics desired. By changing the tungsten electrode diameter, and thus the ceramic tube diameter, the cavity volume can be changed. Increasing the electrode diameter will naturally increase the cavity volume, allowing a greater volume of plasma to be produced. If the cavity volume is made too large for the size of the orifice, however, expulsion of the plasma plume will be restricted. Varying the orifice diameter effectively changes the nozzle velocity at which the plasma is expelled. Decreasing the diameter results in a plume with greater velocity and penetration into the combustible mixture. However, if the orifice is too small, it may be impossible for the cavity pressure to drive a large enough

plume to ignite the mixture. Finally, if the electrode separation is increased too much, electrical breakdown cannot occur, since the minimum breakdown potential is not achieved. The optimum electrode separation is just within the limit of electrical breakdown. Obviously, a balance of these variables is required for optimization, such as in an engine application. For the purpose of experiments conducted as part of this thesis, a non-optimal plasma jet igniter was sufficient because only the turbulent structure of the extruding plume was of interest.

Refueled and at rest, the fuel-air mixture within the bomb also fills the plasma plug cavity. When a high energy spark occurs between the electrode and orifice, the contents of the cavity heats to a high temperature and pressure, causing dissociation of the reactant molecules into ions and electrons. This ion/electron dense cloud is neutrally charged as a whole and is called a plasma. As the temperature-driven pressure builds within the cavity, the plasma is expelled as a plume into the combustion mixture through the orifice plate. Upon expulsion, the friction at the boundary layer between the the plasma plume and the combustion mixture causes turbulent eddies to occur along the sides of the plasma plume. Turbulence produced in this manner is known as electrically induced turbulence (Haley et al, 1989).

As mentioned in Chapter 1 on page 4, the characteristic turbulence of the plasma jet gives it many advantages over conventional igniters. The plasma jet can ignite a greater quantity of fuel in a shorter period of time than can a conventional igniter. It can ignite very lean fuel-air mixtures reliably. The resulting combustion is significantly lower in toxic emissions and harmful by-products because of improved mixing within the mixture. Improved mixing allows more oxygen (i.e. air) to be mixed with the fuel, causing a homogeneous mixture. When combustion occurs in these circumstances, less toxic emissions and less harmful by-products are produced. An increased rate of reaction is an additional benefit of the igniter's characteristics.

The turbulent nature of the plasma jet contrasts with the laminar flow of the surface gap igniter in terms of two enhancement mechanisms: heat conduction and radical diffusion. These mechanisms are discussed in Section 5 of Chapter 4.

3. DIAGNOSTICS

This chapter discusses the diagnostic techniques of Langmuir probes, Image intensified streak photography, schlieren optical measurements, and photomultiplier luminosity measurements used in the experimental studies of Chapter 4. The Langmuir probe was responsible for measurements of ionization and flame structure. Probe ionization measurements give flame front velocity and flame thickness. Image intensified streak photography provides light amplified luminosity photographs of flames and plasma plumes. These streak photographs show the distance that the luminosity travels along the vertical axis, versus persistence along the horizontal time axis. The instantaneous slope of this luminosity curve is a velocity profile of the wavefront, and specific values of velocity can be obtained by taking tangents to this curve. Two schlieren optical techniques were used: laser schlieren measurement and schlieren cinematography. The laser schlieren technique gives a temperature profile of the plume/flame based on changes in its refractive index resulting from temperature changes. Schlieren cinematography is similarly based on temperature dependent changes in refractive index; it produces two dimensional images of flames or plasma plumes. Observations of displacement can be made as images are stepped through individual sequential frames. This allows information on

relative displacement and velocity to be taken. Finally, photomultiplier observations provide a method for detecting the presence and magnitude of luminosity at one specific point of interest.

3.1 IMAGE INTENSIFIED STREAK CAMERA

The image intensified streak camera photographs time versus distance images of combustion reactions. These high speed streak photographs of the expanding flame plume reveal radicals ahead of the flame plume. Examination of these plume formations is instrumental in determining if radicals contribute to increasing flame speed.

As in a conventional camera, where the time exposure of film is most important, the correct time exposure of photographs is also of concern in the streak camera. However, the sweep-time and slit-width characteristics of the streak camera reduce the apparent intensity of the illuminating light source; moreover, the self-illumination of the combustible reaction is sometimes not even bright enough to correctly expose the Polaroid film used in the camera. Therefore, using an image intensifier's linear light gain to enhance the self-illumination of the reaction, as discussed in Appendix I, served to provide improved experimental photographs.

This apparatus (Figure 3.1) consists of a millisecond rotating-mirror camera fitted with a shutter and various lenses. The camera is focused within the combustion

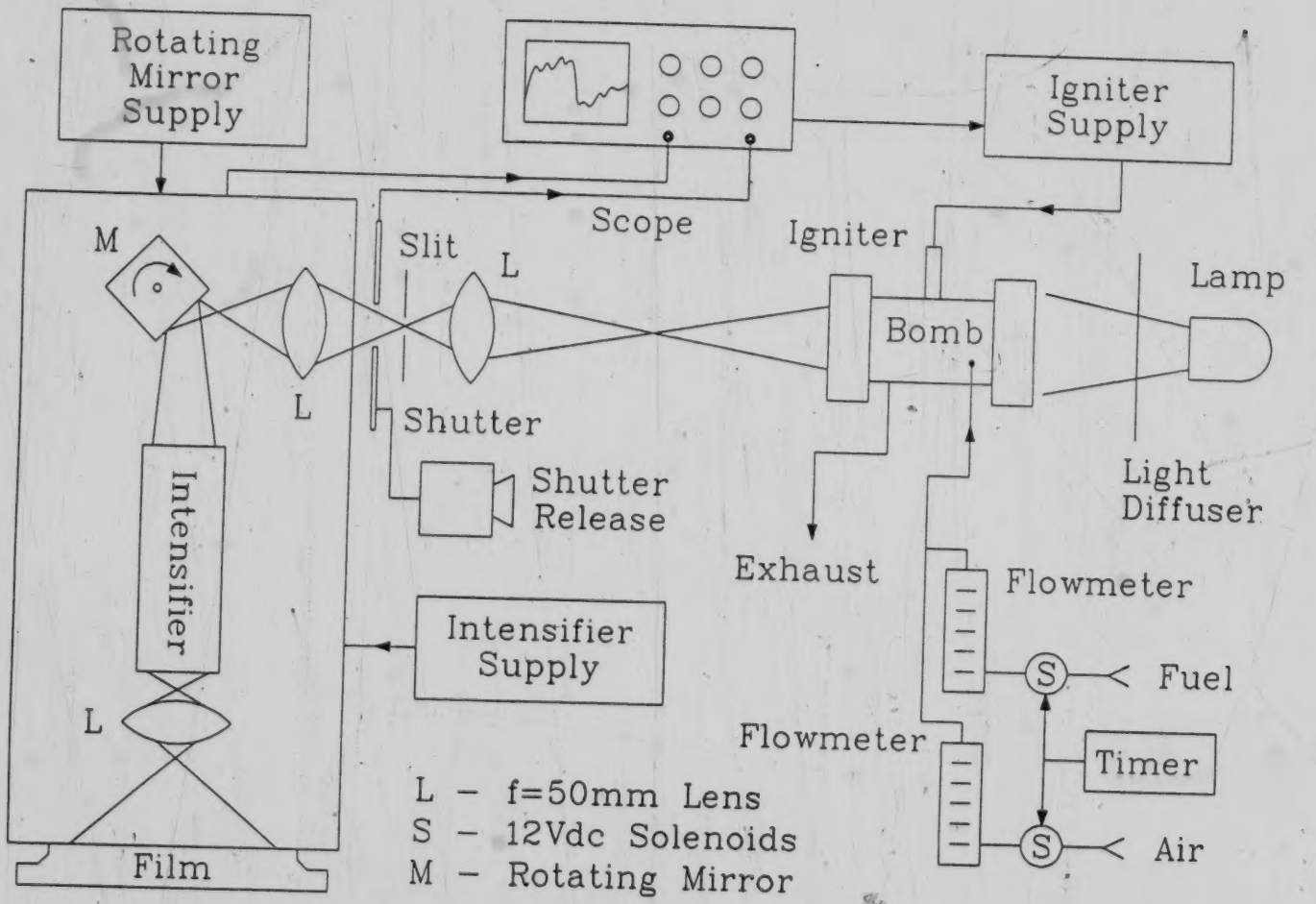

Figure 3.1 Image Intensified Streak Camera Experiment

chamber, and streak images are recorded on high speed 3000 ASA, and very high speed 20,000 ASA Polaroid film.

An oscilloscope acted as a delay timer and coordinated the sequence of events required to operate the camera. With the shutter cocked and the bomb recharged, a manual cable-release mechanism simultaneously triggered the shutter to open and reset the oscilloscope for triggering from the rotating mirror within the camera. The trigger signal came from a magnetic sensor which was able to detect the presence of a magnet mounted on one corner of the mirror. When the mirror rotated to precisely the right position, a trigger signal was sent from the magnetic sensor to the oscilloscope. The scope initiated a timing delay and upon completion, triggered the power supply to dump its stored energy into the igniter. Consequently, the igniter was fired at precisely the right moment for its slit image to be swept across the Polaroid film within the camera. (All runs were performed in a darkened room so ambient room light would not affect the results.)

3.2 SCHLIEREN OPTICAL MEASUREMENTS

Although image intensified streak photography of visible light emitted from a flame provided a satisfactory method for locating the front, it gave very little information about the zone structure and thickness of the flame front. To obtain such information, schlieren optical

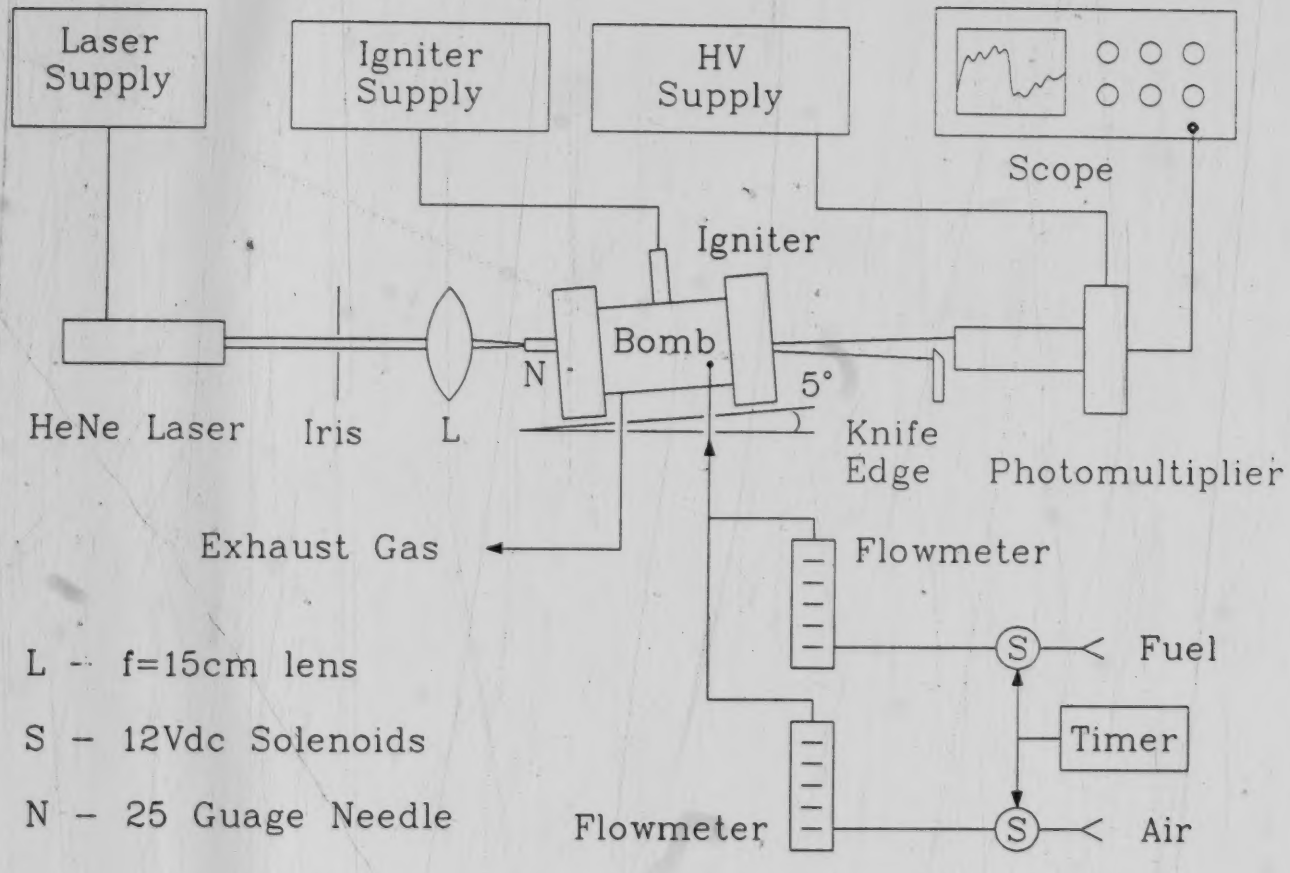

Figure 3.2 Schlieren Laser Experiment

measurements were used. The term "schlieren" is a German word which describes "regions of varying refraction in a transparent medium, often caused by pressure or temperature differences, and detectable especially by optically monitoring the passage of a beam of light" (Webster's, 1973).

The schlieren laser system (Figure 3.2) used consisted of a Helium-Neon laser focused through an array of lenses to a 0.1 millimeter beam at the point of observational interest. The light beam was then projected onto a knife edge with a light sensitive photomultiplier immediately behind it. When a parallel beam of light was focused to a point, and a knife edge intercepted the beam, 50% of the light was transmitted to the photomultiplier. However, if the parallel light was disturbed by regions of different refractive index, which varies with temperature, less of the light rays would be blocked by the knife edge from the photomultiplier.

A beam of light was sent through the test section containing, in this case, the flame front structure of a methane-air flame. A flame, which is hot compared to the surrounding gas, has a lower refractive index than its surroundings. Thus, light which passes through the edge of the flame will be deflected toward the cold gas with its higher index of refraction. Light which enters and exits the flame front will be relatively undisturbed. Therefore,

the light which passes through the leading edge of the flame front will be deflected past the knife edge and recorded on the oscilloscope. This deflection is explained by the equation:

$$\alpha = \frac{dn}{dy} \Delta x \qquad (3.1)$$

where

α is the laser beam deflection angle;
n is the index of refraction;
Δx is the change in the x-coordinate, of the refractive region;
y is the y-coordinate of the refractive region.

The schlieren cinematography experiment, as seen in Figure 3.3, consisted of a Gallium-Arsenide (GaAs) diode laser (904 nm wavelength) focused through an iris and an array of beam expanding lenses (L1 and L2) to a 25 mm spherical mirror, M1. A parallel light beam was reflected from this mirror to a second 25 mm spherical mirror, M2. The bomb was placed in the observational range between the two mirrors at a distance of twice the mirror focal length from the mirror M2. The second spherical mirror, M2, reflected the beam in a convergent manner onto a third flat mirror, M3. This mirror could only reflect wavelengths of light greater than 850 nm, and therefore removed light from the visible spectrum. Continuing from mirror M3, the beam was focused through an iris and a lens, L3, onto the charge-coupled-device (CCD) sensor of the Kodak Spin Physics SP2000 camera.

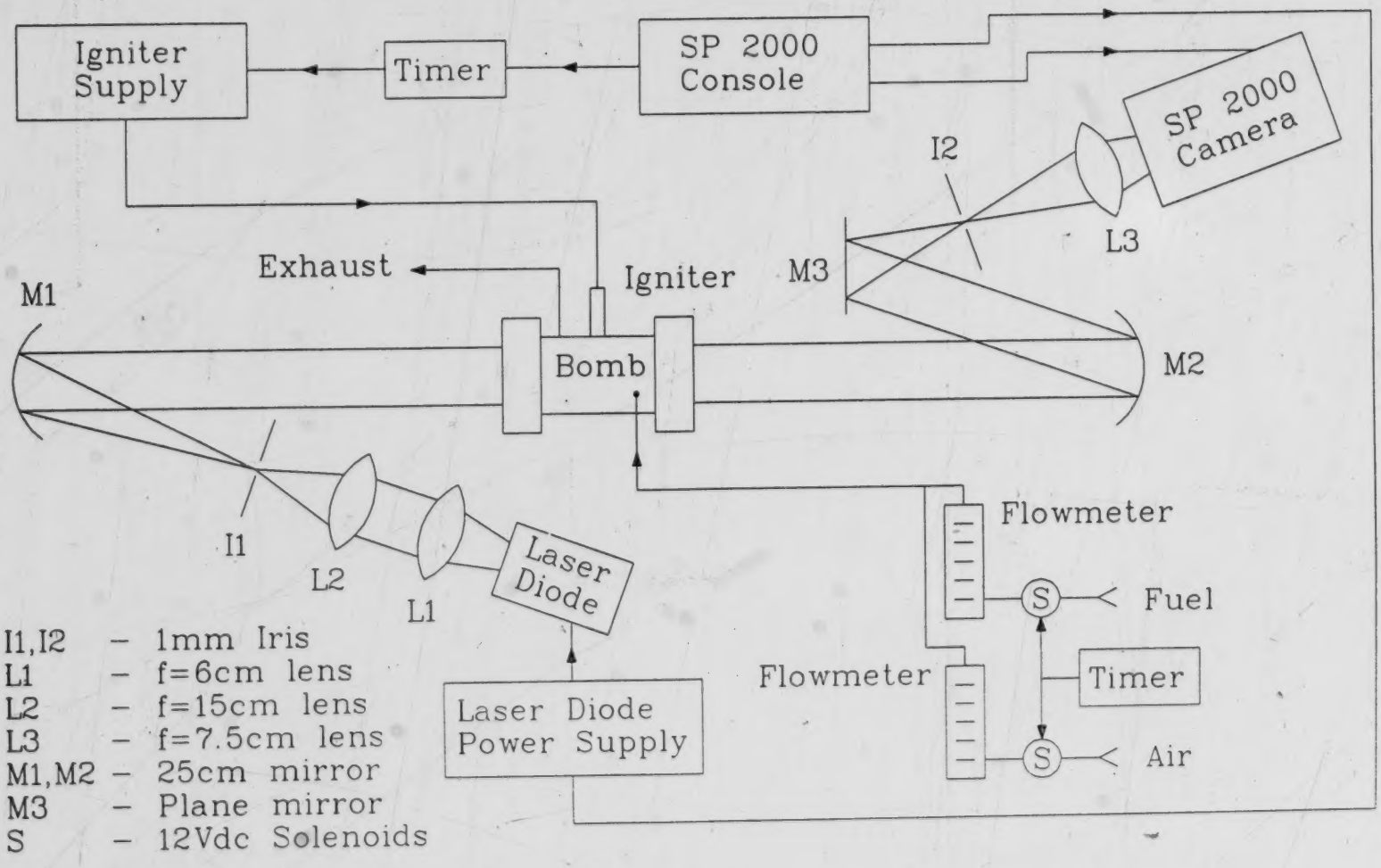

Figure 3.3 Schlieren Cinematography Experiment

The entire layout (Figure 3.3) was set in the shape of a "Z" so that distortions such as spherical aberrations, astigmatisms and coma, caused by angled reflections, would cancel each other out. Schlieren cinematography works in a similar manner to laser schlieren. Both are refractive index methods of measurements obeying equation 3.1, except cinematography is 2-dimensional in space and consists of consecutive images in time.

3.3 LANGMUIR PROBE

Electrostatic probes are one of the fundamental techniques in plasma diagnostics. In 1924 Langmuir developed the electrostatic probe technique, which produces good spatial resolution over a wide range of conditions (Chung et al, 1975). A Langmuir probe is simply a metallic wire inserted into a plasma. The wire can be biased positively or negatively with respect to the plasma by a power supply or battery. The current and voltage characteristics provide information about the ionization condition of the plasma. For a wide range of conditions the presence of the probe does not perturb the plasma, so that the probe has a negligible effect on the quantities being measured (Smy, 1976).

In Chapter 4, the Langmuir probe is used for two types of measurements: floating ionization in Section 3, and biased ionization in Section 5. Floating voltage measurements are taken to determine if a region of elevated

electron/ion temperature ($T_e = T_i$) exists in a wavefront. An elevated electron/ion temperature indicates the presence of a reaction zone. Floating voltage measurements are taken by monitoring the absolute potential of an unbiased Langmuir probe; however, oscilloscope probe loading of the electrostatic probe is of concern.

Biased ionization measurements are taken to determine where ionization occurs in the flame front. As the electron and ion species encounter the Langmuir probe, a voltage difference is applied across the probe and the return rod. This potential difference causes a current I to flow through a series resistor between the probe and the return rod. This current is directly related to the electron/ion density ($n_e = n_i$) and so the magnitude of the electron/ion density can be obtained.

Although a probe is very easy to construct, the interpretation of the results is not so simple (Smy, 1976). Difficulty arises because probes are boundaries to the plasma. The equations of motion of the charged particles in the plasma do not hold in the boundary region. The condition of quasineutrality, which is defined as "charged and neutral particles which exhibit collective [neutral] behavior [in a plasma]" (Chen, 1974), is not valid near the boundary, which is known as the "sheath", where the electron and ion density differ.

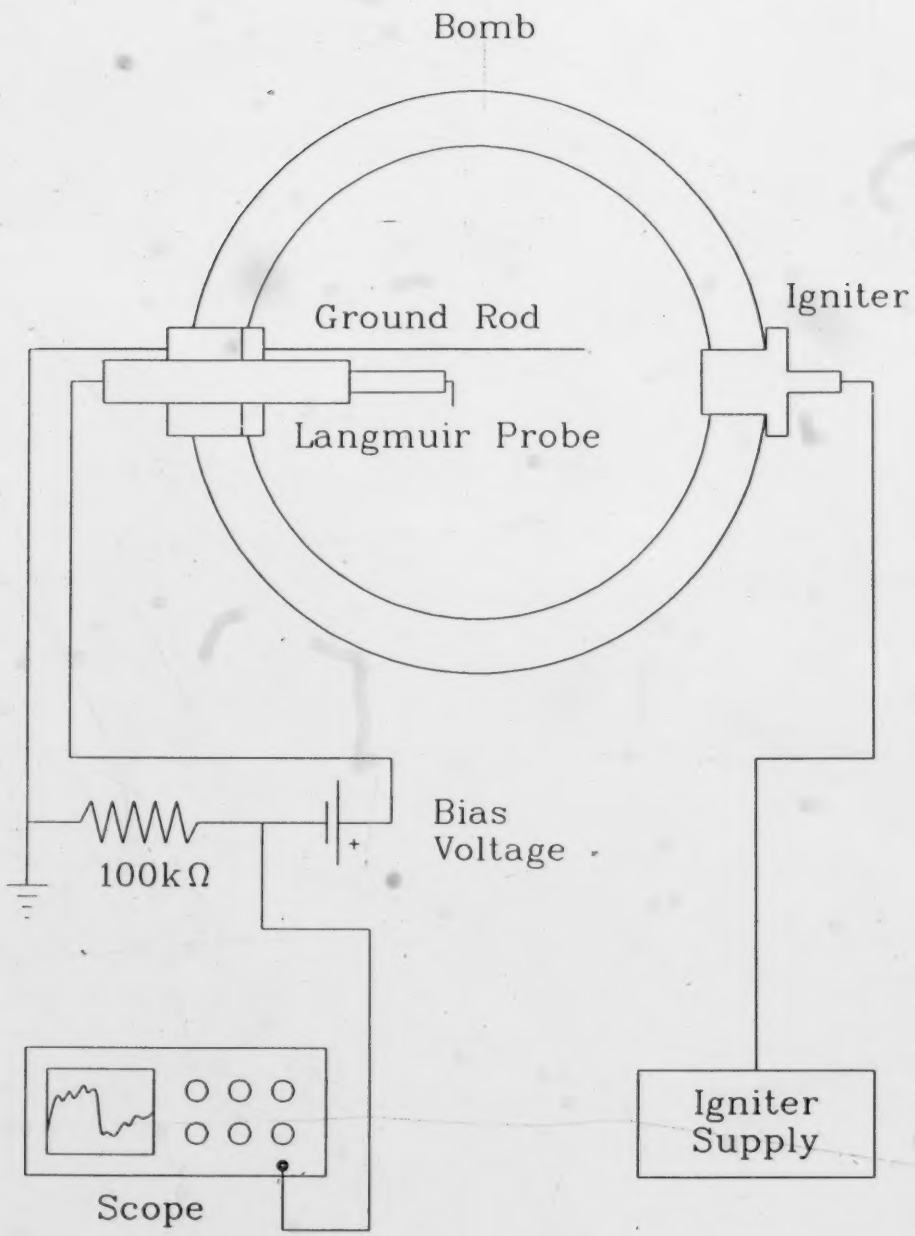

Figure 3.4 Langmuir Probe Setup

The Langmuir electrostatic probe (Figure 3.4) used in these experiments consisted of a seventy-five micrometer diameter spring steel wire, four millimeters in length, mounted at a ninety degree angle on the tip of a 3.175 mm (1/8 inch) ceramic tube. This ceramic tube was in turn housed with one centimeter of its length protruding from a 6.35 mm (1/4 inch) ceramic tube. A brass Swage-Lock fitting held the probe in place, mounted directly opposed to the igniter in the cylinder wall. The Swage-Lock connector allowed the probe to be set at various distances from the igniter. A grounding rod extended from the wall, mounted immediately beside the ceramic housing, across the diameter of the cylinder. This rod was permanently mounted as a return lead for the electrostatic probe. As was mentioned, the probe could be biased for any negative or positive offset voltage. Voltage offset was supplied by batteries, because of their low noise and stable voltage. To reduce the effects of ambient electrical noise, the battery pack, resistor, laser and photomultipliers were enclosed in shielding and grounded.

The probe circuitry (Figure 3.4) for the biased probe consisted of a series loop between the battery pack, electrostatic probe, ground rod, and resistor. When the bomb was refueled and at rest, no neutral plasma was present to bridge the electrical path between the probe wire and the ground rod. With the gaseous mixture as a

series infinite resistance, no current could flow through the resistor and generate a signal. After ignition, though, the plasma within the ensuing wave encountered the probe and made electrical conduction possible. Monitoring the voltage drop across the in-line resistor allowed a plasma density profile of the flame front to be captured and stored as a voltage versus time plot on the digital oscilloscope. From analysis of this plasma density profile information concerning the flame front thickness and velocity could be obtained.

Changing the polarity of the offset voltage selected the plasma species to be observed, and changing the magnitude selected the amplification at which it was measured. With the Langmuir probe negatively biased, the positive ion species of the neutral plasma was sensed. However, with positive biasing, the electrostatic probe observed electrons. If the magnitude of the biasing voltage is sufficient then the probe current will saturate. Sufficient positive biasing causes electron saturation current, and sufficient negative biasing causes ion saturation current.

For the purpose of these experiments, where a determination of electron/ion current density rise time and flame front travel time was desired, either biasing polarity could have been used. To obtain reliable meaningful single event observations using an oscilloscope,

the positively biased probe was more desirable because it provided a larger current signal. The larger electronic current is described by the following expression from Chung et al (1975) which equates the ratio between ionic and electronic currents to the square root of the ratio between their respective temperatures and also inversely to their respective masses:

$$\frac{I_i}{I_e} = \left[\frac{m_e\ T_i}{m_i\ T_e}\right]^{1/2} \qquad (3.2)$$

When dissociation occurred, as the reactant reached a plasma state, the theoretically calculated ratio of negative electron current to positive ion current was approximately three hundred to one from equation 3.2. The actual ratio of negative electron to positive ion current was determined experimentally to be seventy to one. With the positive biased probe signal seventy times larger, and with the amplification provided by the magnitude of the offset voltage, a clean noise-free signal could be collected by the storage oscilloscope.

3.4 DISCUSSION ON PROBES

Langmuir and optical probe techniques are discussed, particularly with respect to considerations for achieving meaningful observations by avoiding probe influences on the measurements. The Langmuir probe is considered in terms of its physical dimensions and its biasing of polarity and

magnitude. With a similar concern for its effect, the optical probe is discussed in terms of its physical dimensions, focused laser beam diameter, and photomultiplier sensing apparatus.

Two different methods of determining the flame front thickness were used to rule out the influences of experimental processes, apparatus, components and physical probe effects. One concern was that with the electrostatic probe biased with an offset voltage, an ionic sheath could increase the effective dimensions of the Langmuir probe, making it appear larger electrostatically than physically. This effect would have made the probe sense the plasma of the wavefront prematurely. In effect, the wavefront would have appeared to be thicker than it actually was. The experiments were repeated with a constant stoichiometric mixture, constant igniter-probe distance (4 cm), and constant probe dimensions (4 mm length, 75 μm diameter) for varying probe bias voltages of -41.2 to 114 volts DC. The results, as seen in the flame front thickness versus probe voltage graph of Figure 3.5, clearly show that bias voltage had little or no effect on the experimentally determined flame front thicknesses taken. Thus, biasing the Langmuir probe anywhere in the voltage range of 9 volts to 114 volts produced an insignificant electrostatic sheath extending around the physical probe. Biasing at -41.2 volts, caused ionic saturation to influence the results, as outlined in

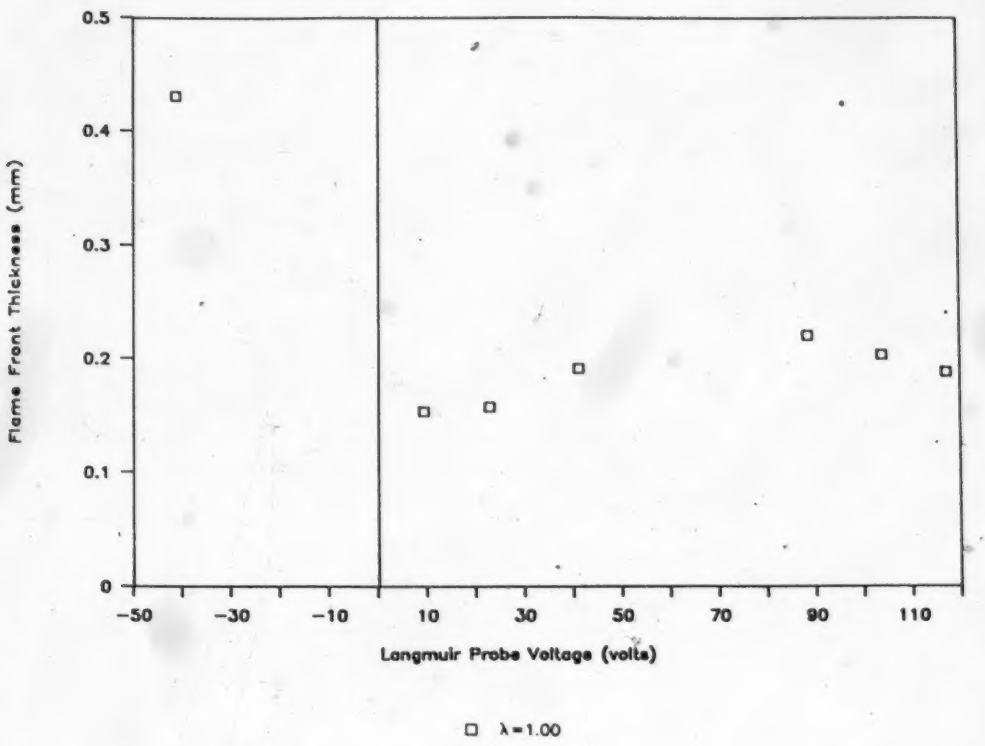

Figure 3.5 Apparent Flame Front Thickness Graph

section 3.3 on Langmuir probes.

The physical dimensions of the probe were also a concern, because if the diameter of the probe was greater than that of the actual flame front thickness, the effect would be that of simply measuring the thickness of the Langmuir probe instead of the flame front thickness. This was found to occur for many larger sizes of electrostatic probes. It was not until a wire 75 micrometers in diameter was used, three times less in thickness than the flame front, that observations and measurements could be taken with confidence.

It was also imperative that the laser beam diameter be less than that of the flame front thickness for the optical probe. Unfortunately, beam divergence became a problem as the one millimeter diameter Helium-Neon laser beam could only be focused to an observation point of 0.1 millimeters. As the beam continued on to the photomultiplier, its beam diameter increased linearly with distance toward the photomultiplier knife edge arrangement. This has the effect of lowering the sensitivity and resolution of index refraction deflections. As a result, the rise time of the deflection could appear greater than it actually was, and the flame front thickness would also appear to be larger.

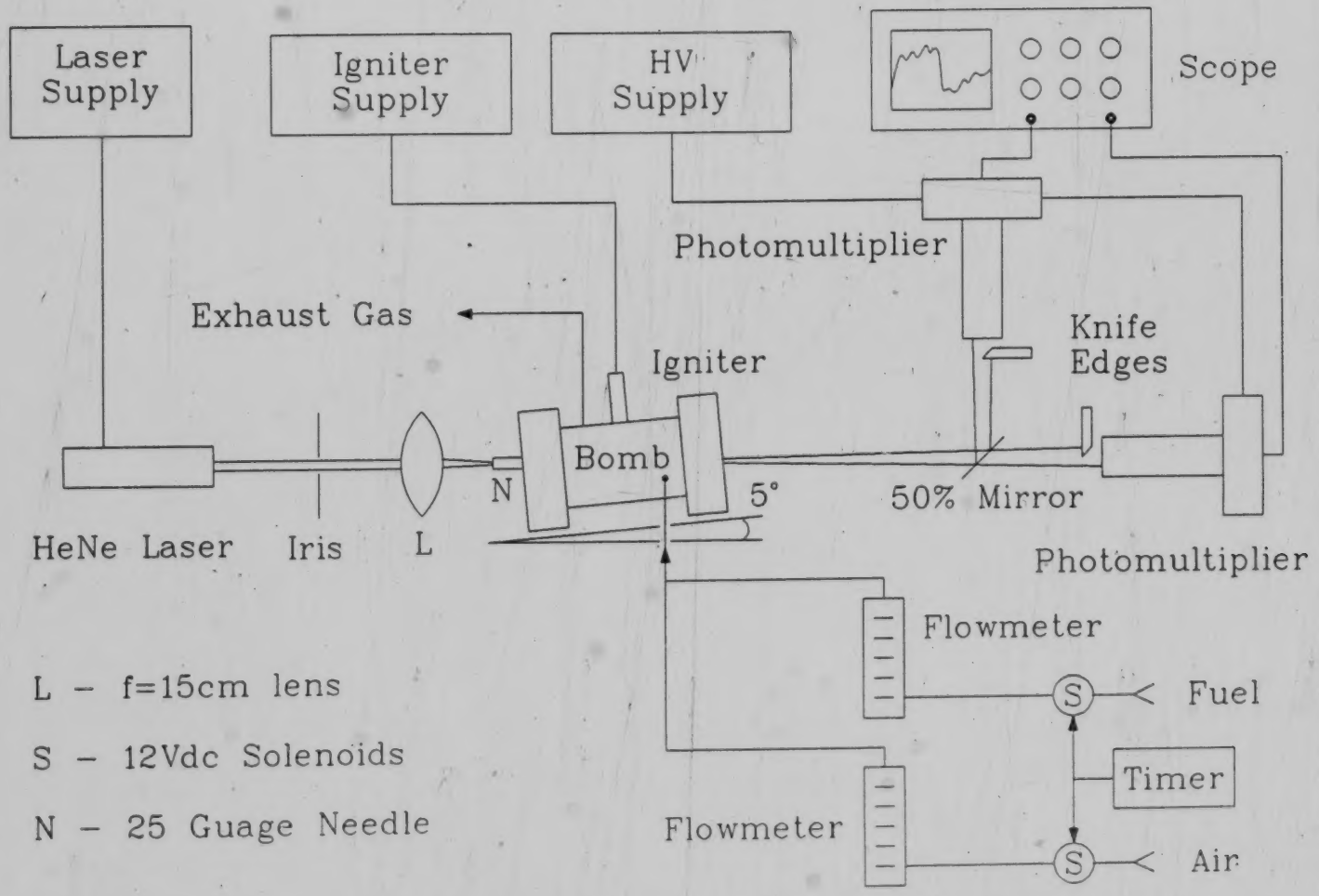

Figure 3.6 Laser Schlieren Dual Photomultiplier Experiment

In order to resolve this problem a discriminating dual photomultiplier-knife-edge arrangement was developed. As seen in Figure 3.6, the laser was focused into a hypodermic needle and allowed to pass through the combustion chamber. Upon exiting, it continued onto a fifty-percent reflective mirror oriented at a forty-five degree angle. Half of the light beam was passed straight on to the first photomultiplier knife-edge, while the remaining light was reflected ninety degrees onto the second photomultiplier knife-edge. Vertical knife edges were situated on the photomultipliers so that half of the sensor opening was blocked. Consequently, the laser beam fell half on the knife edge and half on the photomultiplier. When the beam emanating from the bomb was deflected, the light falling on the first knife edge moved partially off the razor blade and onto the light sensor, while the light falling on the second sensor arrangement moved further onto the razor blade. The signals from these two photomultipliers were then subtracted. The resultant waveform was free from the effects of beam absorption and devoid of any apparatus vibrations.

An additional problem which contributed to divergence was the effect of the diameter of the hypodermic needle used to position and contain the laser beam. Since the beam pierced the bomb at an angle of five degrees with respect to the igniter wall, it had to be isolated from the ensuing

combustion reaction prior to its observational point of interest. Ideally, the use of a fine gauge needle was desired so that its presence would not disturb the ensuing flame front. Also, because a 3 mm diameter Pyrex window was mounted over one end of the needle, between the shaft of the needle and one end of the 3.175 mm brass tube, random divergence of the laser beam from within the shaft of the needle, caused by varying indices of refraction within the region, did not occur. With the needle sealed at one end with a window, no gaseous mixtures could flow through the needle, and consequently a temperature profile could not develop within the shaft of the needle to cause diffraction.

One thing common to both probe techniques was that the use of a fine diameter probe gave good observational resolution, and thus greater accuracy in experimental measurements. The experimentally determined flame front thickness of both optical and electrostatic methods have been found to be in good agreement -- within 10 percent, as will be mentioned in Chapter 4. Therefore, these two methods support and complement each other.

3.5 PHOTOMULTIPLIER

The photomultiplier is a light sensing device utilizing the photoelectric effect first described by Einstein in 1905. When a photon of light falls on a plate carrying a high negative potential, electrons are emitted

which in turn fall upon additional plates causing an exponential emission of electrons. These electrons flow from the negative plates to a (positive) ground plate. This current is applied across a known resistance (100 k-ohms) and the voltage drop is monitored by an oscilloscope. As seen in Figure 3.7, a record of light intensity versus time is stored and plotted.

The photomultiplier's sensitivity is dependent upon the magnitude of the voltage energizing the negatively biased emission plates. If the voltage is low, the photomultiplier will be insensitive to low levels of light irradiating the emitter. If, on the other hand, the voltage is high, over-sensitivity can create numerous electronic "noise" problems that mask the experimental results. Another problem with high energizing voltage is that electrons emitted upon illumination may saturate the energized plate. (This can cause serious irreversible damage to the photomultiplier.) Results from the photomultiplier appear to be best for a moderate-to-high sensitivity in the voltage range of 800 V to 1200 V DC.

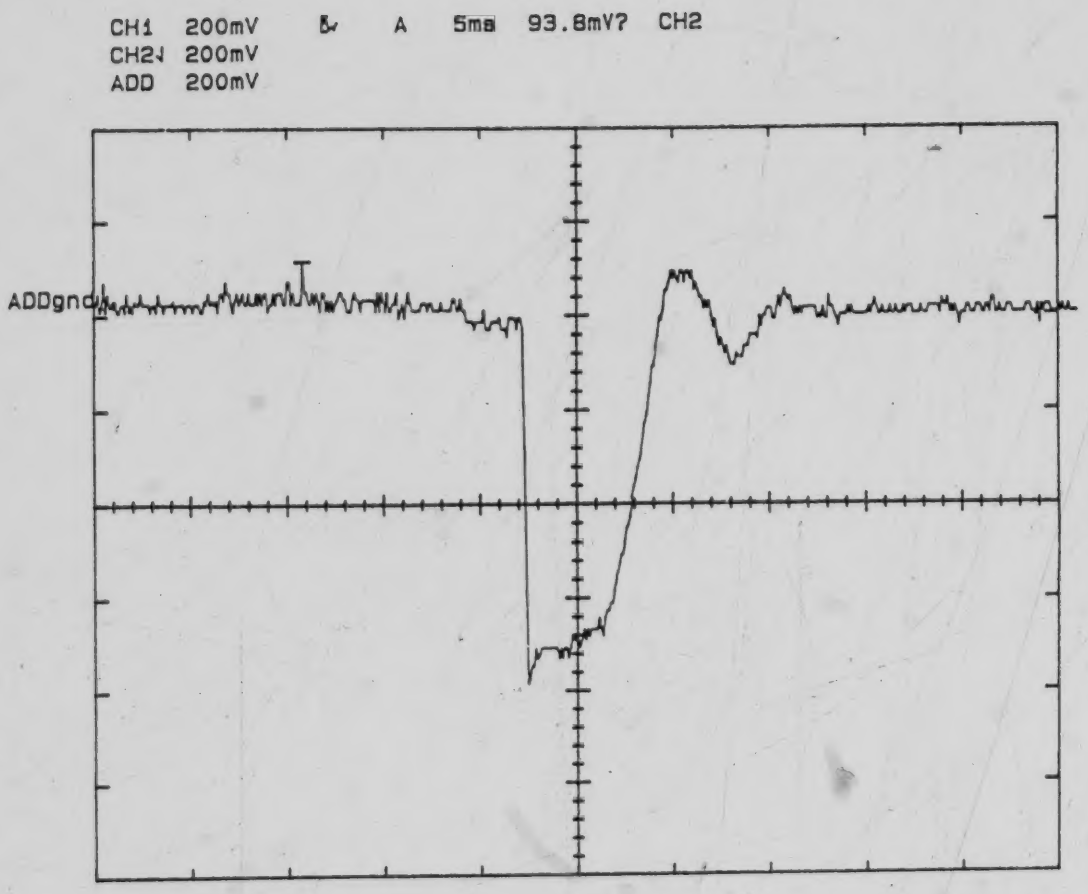

Figure 3.7 Typical Photomultiplier Oscillogram of Light Intensity from a Flame Front

4. EXPERIMENTAL STUDIES

The experimental results are presented in a single chapter. They were obtained using conventional still photography together with the diagnostic techniques described in Chapter 3. The underlying objective of the measurements was to determine the relative effects of igniter generated turbulence and plasma radicals (chemical) upon flame dynamics (e.g. front thickness and flame speed).

The initial plates from luminosity measurements revealed that luminosity (radicals) extended further from the igniter and existed longer then was previously thought (Weinberg, 1983). As a result, chemical plasma effects might significantly influence flame dynamics for milliseconds rather than tens of microseconds. Because of the importance of this discovery, a streak image intensifier was designed and used to obtain more information on this phenomena. Additionally, ionization measurements were conducted to support photographic chemical findings.

With the possibility of further penetration and longer existence established, the diagnostic measurements of electronic rise time and wavefront travel time were used to calculate flame front thickness (i.e. probe and schlieren), thermal conductivity, and turbulent radical diffusion. These measurements were used to determine the central influence of plasma radicals upon flame dynamics.

4.1 LUMINOSITY MEASUREMENTS

In this set of experiments, the plasma plug was discharged in pure nitrogen and the resulting plume photographed. The purpose of studying the plasma plug in a nitrogen environment is to determine if energy transfer at the wavefront is partially due to excited nitrogen species. A further objective is to study one method of tracking particles from the plume to the wavefront.

The initial stage of the experiment was to determine if any excitation existed in the plasma plume. After detecting luminosity, which could only arise from such excitation, an effort was made to determine the relative levels of luminosity as a function of distance beyond the plume and of time. It was also important to relate the plasma plug's behavior in nitrogen to that in air. To do this, the experiment was repeated with low concentrations of oxygen added to the nitrogen.

4.1.1 EXPERIMENT DESIGN

The plasma plug was installed in the combustion chamber, and the chamber adapted so that either nitrogen or oxygen could be admitted (Figure 4.1). A pure nitrogen environment was achieved by extended purging of the chamber with nitrogen. Low oxygen concentrations were achieved by first placing the system under vacuum, then adding measured amounts of oxygen. The chamber was then brought to atmospheric pressure with nitrogen (all runs were begun at

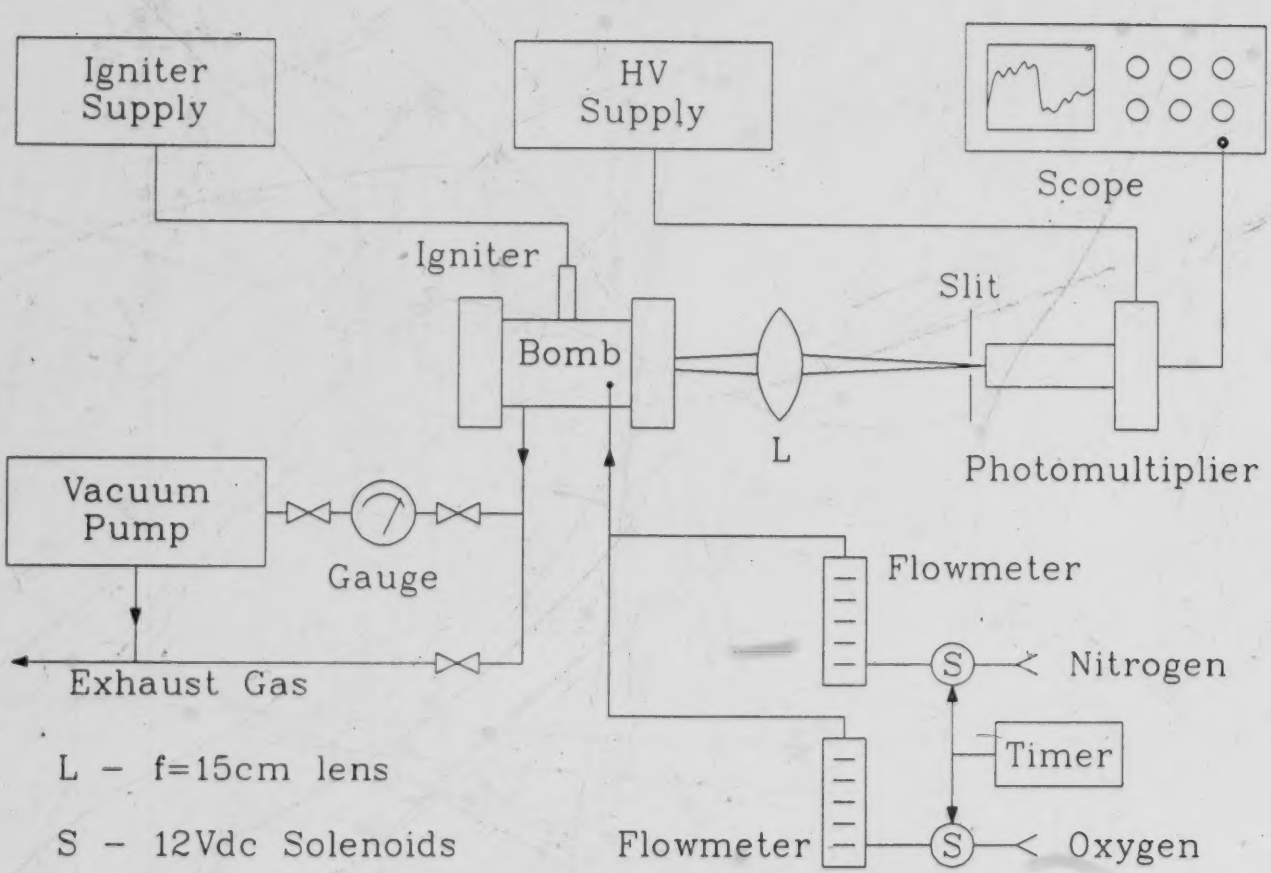

Figure 4.1 Luminosity Measurement Experiment

atmospheric pressure).

A lens was focused at various distances below the plug; the lens image was directed to a photomultiplier. A slit (a pinhole was also used) was placed in front of the photomultiplier so that the only light admitted to the photomultiplier would be from a specified line or point below the plug. It proved possible to track the illuminated nitrogen ions further with the slit configuration because the slit provided maximum sensitivity, and so the slit was used in the final design of the experiment.

The photomultiplier was run at 1.2 kV for the duration of the experiment to give high sensitivity, as described in Chapter 3. An oscilloscope picked up the photomultiplier signal through a 100 k-ohm terminal resistor placed in series with the line to the scope. This resistance maximized the sensitivity of the signal while minimally affecting the rise time. High sensitivity was necessary because of the low luminosity of the nitrogen ions. Sharp rise times, actually sharp deflections, were desired to determine the speed of the luminosity front.

The plasma plug power supply was measured at 1190 volts. The supply was fitted with a 6 μF capacitor, so that the electrical energy delivered to the plug was calculated to be 4.25 Joules. A 4 ohm resistor was placed in the line from the power supply to the plug to reduce any persistence in the discharge current which could be picked up by the

scope and which would mask the luminosity signal.

4.1.2 RESULTS

When the plasma plug is fired in a pure nitrogen environment at atmospheric pressure (760 Torr), there is a visible orange glow that extends from the plume. This luminosity was recorded on Polaroid 3000 ASA film, as seen in Plate 4.1. In an environment at atmospheric pressure, where 5 Torr of the pressure is oxygen and 755 Torr is nitrogen, the glow is only faintly visible to the naked eye. These results were recorded on Polaroid 20,000 ASA film, as seen in Plate 4.2.

Using the photomultiplier it was possible to track the glowing nitrogen ions to a distance 4 centimeters from the plug. Beyond this distance, the equipment used in this experiment was not sensitive enough to detect any luminosity. In a nitrogen environment, at oxygen concentrations of 5 Torr and 10 Torr it was possible to track the glow to a distance 3 cm below the plug. At higher oxygen concentrations up to 150 Torr it was possible to detect the glow only to 2.5 cm below the plug. A typical oscillogram is presented in Plate 4.3.

Plate 4.1 3000 ASA Polaroid Photograph of Plasma Plume

Plate 4.2 20,000 ASA Polaroid Photograph of Plasma Plume

Plate 4.3 Typical Photomultiplier Luminosity Oscillogram

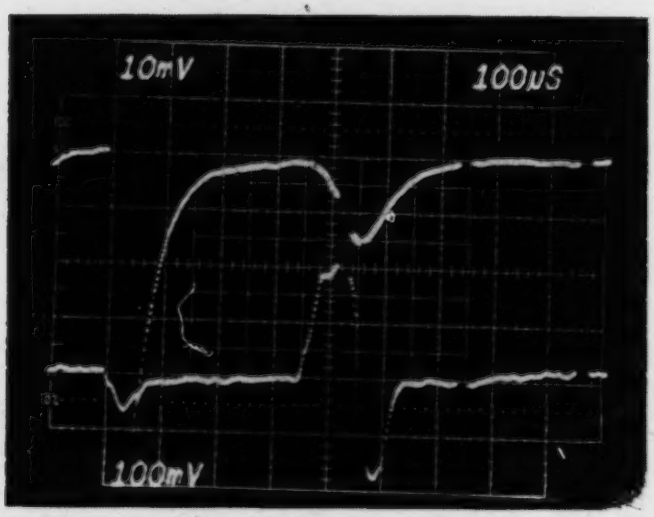

Plate 4.4 Oscillogram of Simultaneous Schlieren and Photomultiplier Outputs

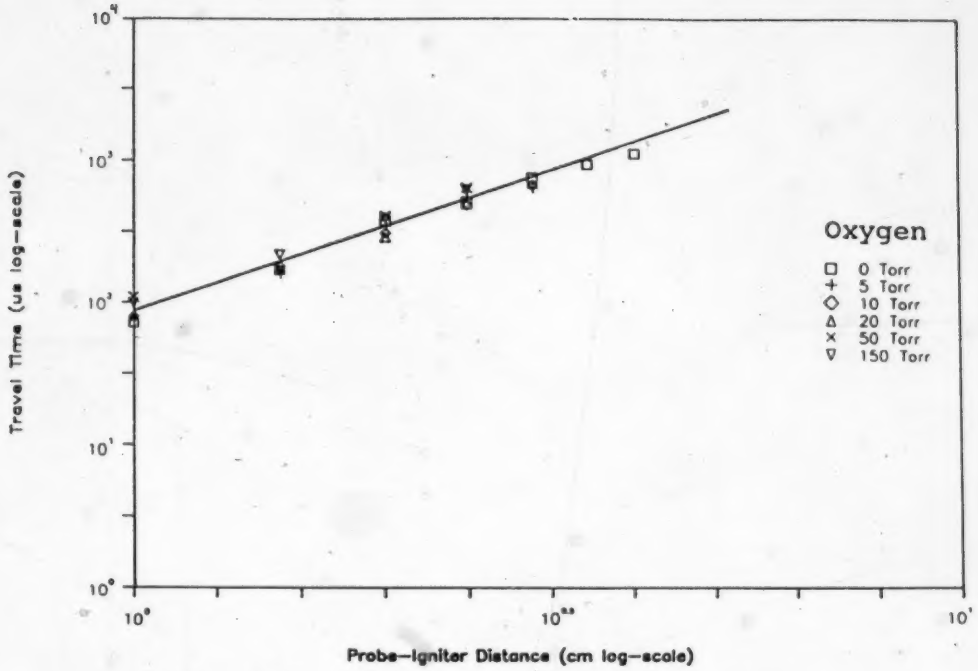

Figure 4.2 Luminosity Travel Time Graph

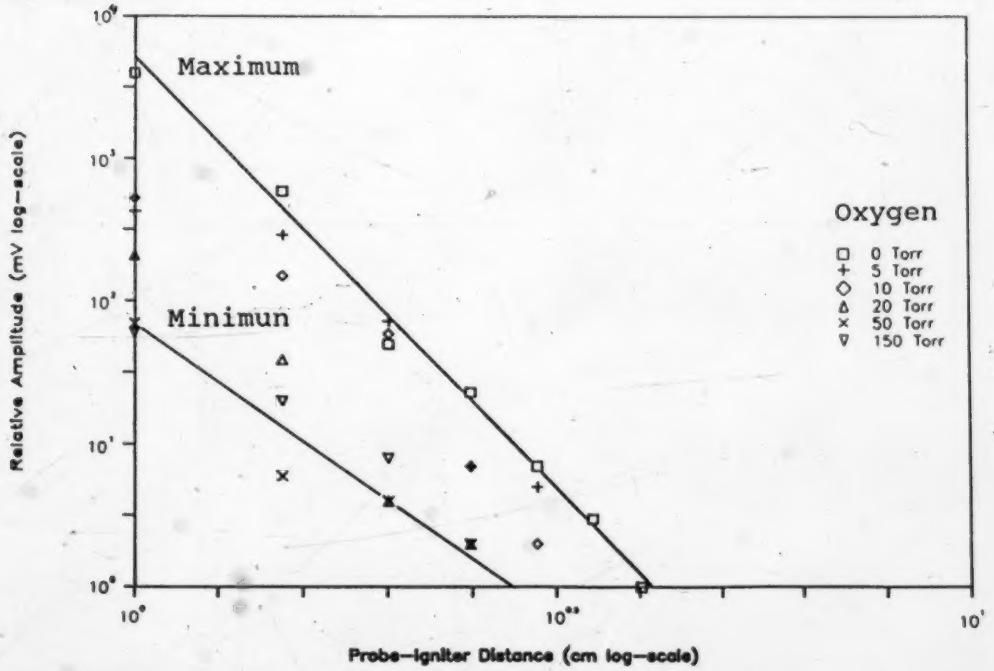

Figure 4.3 Luminosity Relative Amplitude Graph

The oscilloscope signals gave information on travel time and relative amplitude (optical intensity) of the wavefront. Travel time versus the corresponding distance below the plug resulted in a single straight line (positive slope) in the log-log graph of Figure 4.2 for all nitrogen-oxygen concentrations. The resulting single straight slope indicated that the velocity of the wavefront did not change (decelerate) with distance below the igniter for varied nitrogen-oxygen mixtures; that is, the presence of oxygen in a mixture with nitrogen does not have the effect of decreasing the velocity of the ensuing plasma wavefront. Therefore, the presence of illumination at decreased distances below the igniter, with increased concentrations of oxygen, cannot be caused by a reduction in wavefront velocity. A reduction in wavefront velocity would decrease the distance illumination can be seen for a given excited nitrogen state lifetime. Instead, the observation of luminance at decreased distances below the igniter can only be caused by the presence and effect of oxygen.

Additionally, the slope of the line in Figure 4.2 indicates that the distance, d, of the wavefront varies with travel time, t, approximately as:

$$d \propto t^{1/4} \qquad (4.1)$$

This relation was first introduced by Scorer (1978) and is consistent with existing work done by Topham et al (1982),

in which the progression of a plasma plume is that of a hydrodynamic species known as a "puff".

In Figure 4.3, relative amplitude (optical intensity) versus distance below the plug (at fixed concentrations) resulted in straight lines (negative slopes) in the log-log graph. The slopes of the lines in this graph are all of the same magnitude, ranging from approximately -1 mV/cm at an oxygen concentration of 150 Torr to -7 mV/cm for pure nitrogen. As the content of oxygen increased in the nitrogen-oxygen mixture, the intensity of light emitted from the wavefront decreased in a logarithmic manner over all igniter distances. It is believed that the presence of oxygen results in less luminosity because of oxygen's ability to quench excitation.

A final check was performed to confirm the relationship between luminosity and excitation. A laser beam was directed through the same point that the photomultiplier/lens configuration was focused on, in a manner such that both the laser beam and the focal point of the lens were at the same distance below the plug. The resulting scope signals, as seen in Plate 4.4, are simultaneous. Luminosity (top waveform) and laser schlieren (bottom waveform) observations of plasma in pure nitrogen both change at the same instant. The inverted luminosity waveform is directly related to the magnitude of luminosity emitted, whereas the laser schlieren waveform is directly

related to the differential refractive index term of Equation 3.1, induced by changes in temperature in the luminous region. Comparing the proportional and differential waveforms, both are found to be closely related. In the proportional waveform, luminosity begins to appear and increase in magnitude with the positive value and maximum of the differential waveform. Next, as the luminosity waveform stops changing and becomes a maximum, the differential waveform corresponds with a zero crossing. As the luminosity decreases in magnitude to zero, the differential schlieren waveform shows a negative value which reaches a minimum. Finally, the differential waveform returns to zero with the luminosity waveform. The proportional luminosity waveform and the differential waveform are found to be coincidental within 10 microseconds. Thus, a close relationship exists between the luminous region and the ionization zone produced by a plasma plume. This luminous region is a characteristic of activated nitrogen and is evidence of the transporting of radicals to the flame front, a concept which is investigated further in following sections.

4.1.3 CONCLUSION

From Polaroid photographs, luminosity was observed beyond the extent of the plasma plume in pure nitrogen. Since only pure nitrogen was present, luminosity must have

been caused by excited nitrogen states.

Light intensity data from the photomultiplier for nitrogen-oxygen mixtures showed that the relationship between plume travel time and distance below the igniter was identical for all mixture concentrations ranging from pure nitrogen to air. This made it clear that the velocity of the expelled plume and wavefront were the same for all mixture concentrations. For a given radical lifetime (time of excitation to recombination) and a known nitrogen-oxygen concentration, the distance to which illumination could be observed was independent of wavefront velocity.

However, a relationship was found to exist between the presence of oxygen in the mixture and the level of luminosity. As the oxygen concentration increased, the observable illumination distance decreased from 4 cm in pure nitrogen to 2.5 cm in air. From this relation, it was evident that oxygen had a thermal energy absorbing effect. As a result, insufficient energy was present to excite nitrogen molecules.

In a mixture with a sufficient concentration (density) of radicals, transportation of these radicals from the plasma plume to the wavefront, or from the reaction zone to the (cold) pre-heat zone of the flame front, is believed to play an important role in the enhancement of flame propagation (Weinberg, 1983).

A laser schlieren technique provided evidence that

radicals at the wavefront are generated at the same time, for a given distance below the igniter, as the observed luminosity from the front. This served as a check to verify that radical density and luminosity are in fact caused by the same excited molecular states.

The results of this experiment indicate that further study is required to both track particles from the plume to the wavefront and to determine the lifetime of luminosity produced by molecular activation. A more comprehensive device was desired to further the investigation, one which would monitor luminosity at all points simultaneously, and so acquire all the desired information on a single shot. For this reason, the image intensified streak camera was developed.

4.2 IMAGE INTENSIFIED STREAK PHOTOGRAPHY

The purpose of this study was to produce enhanced luminosity photographs of excited molecular species from a plasma jet igniter operating in an environment of nitrogen, air, and various propane-air mixtures. The photographs were taken with the aid of an image intensified streak camera. A conventional surface gap igniter was used as a basis for comparison. A further purpose of the experiment was to observe wavefront penetration, and wavefront velocity in the form of distance versus time streak photographs.

4.2.1 EXPERIMENTAL DESIGN

The plasma plug was installed in the combustion chamber and the chamber was filled with either nitrogen, air, or a propane-air mixture (Figure 4.4). Propane-air mixtures varied from trace propane volume concentrations of 0.5%, 1.0%, 2.0%, and 2.5%, to a combustible stoichiometric mixture of 4.02%. The plasma plug power supply was energized by a 4 μF capacitor charged to 813V. The energy to the plug was thus 1.32 Joules.

A 50 mm lens focused the image from the region covering one to three centimeters below the plug onto the slit/shutter arrangement of the image intensified streak camera. The slit only admitted light into the camera in the form of a specified line from the focused region. Thus the streak area provided a record of luminosity along a line as a function of time. A velocity profile of the luminosity

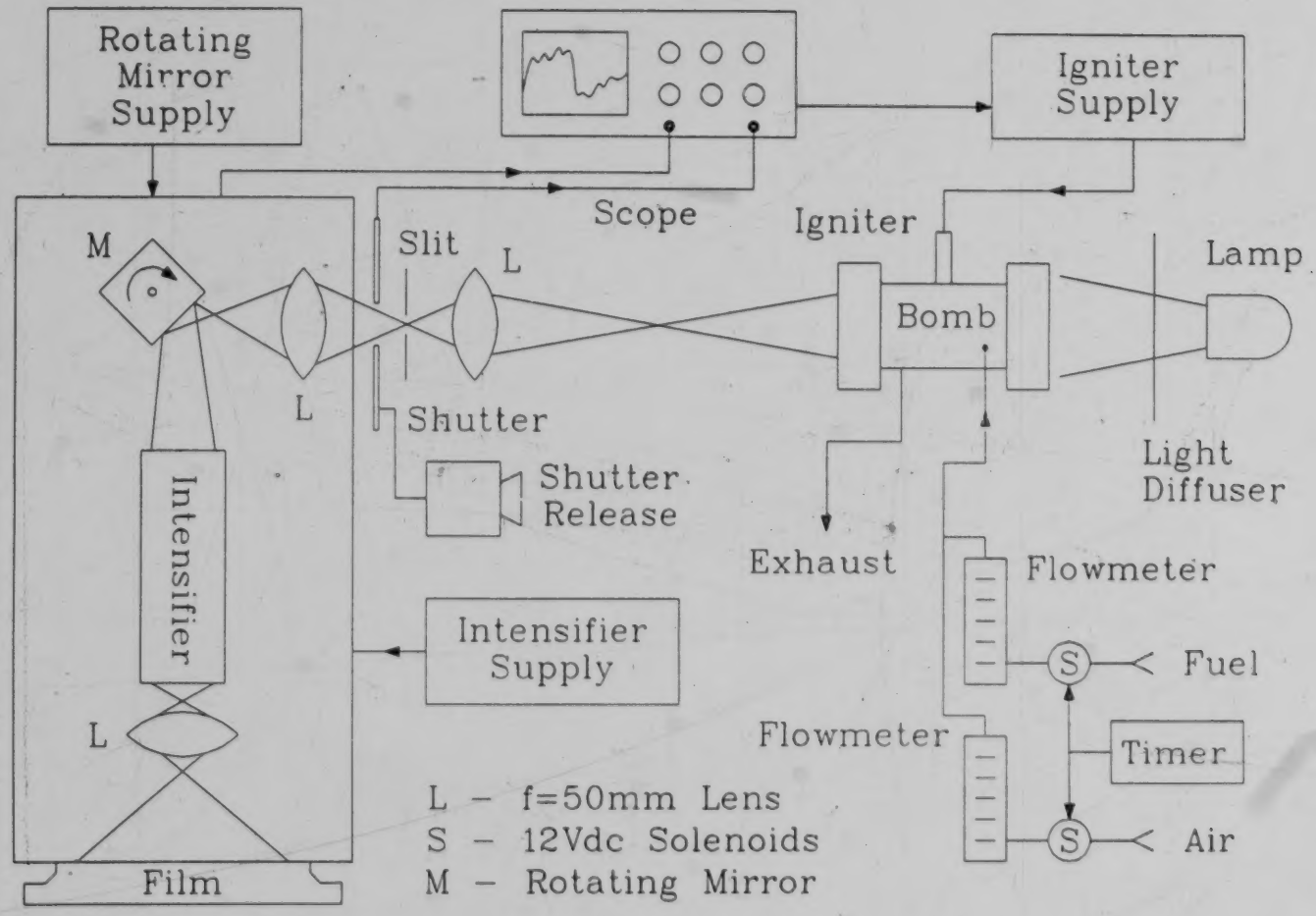

Figure 4.4 Image Intensified Streak Camera Experiment

front can thus be deduced from such a photograph. Instantaneous velocity can be determined by measuring the slope of a line tangent to the luminosity curve on the photograph.

4.2.2 RESULTS

Image intensified streak photographs for nitrogen, air, and propane-air mixtures are presented in Plates 4.5 through 4.8. In a typical photograph, it is observed that luminosity from the igniter is initially present and can be seen to exist for extended periods of time (up to 3 ms) and for extended distances (up to 1 cm) from the igniter. As time progresses, luminosity fades with time. The luminous region closest to the igniter fades first while luminosity still exists at greater distances. Finally, even distant luminous regions are exhausted.

Comparing Plates 4.5 and 4.6, it is found that the luminosity present in pure nitrogen endures for a substantially longer period (one millisecond rather than tens of microseconds) of time than for air. Also, luminosity is found to extent a greater distance from the plasma jet igniter, to about 1 cm beyond the actual plasma plume. From these observations it is evident that excited molecular species are responsible for the presence of luminosity beyond the plasma plume in a pure nitrogen environment. When a nitrogen-oxygen environment is present,

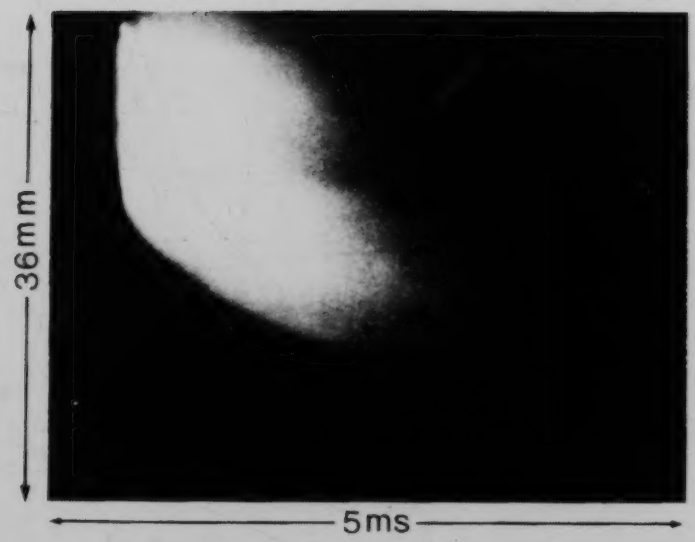

Plate 4.5 Polaroid of Plasma Jet Igniter in Nitrogen

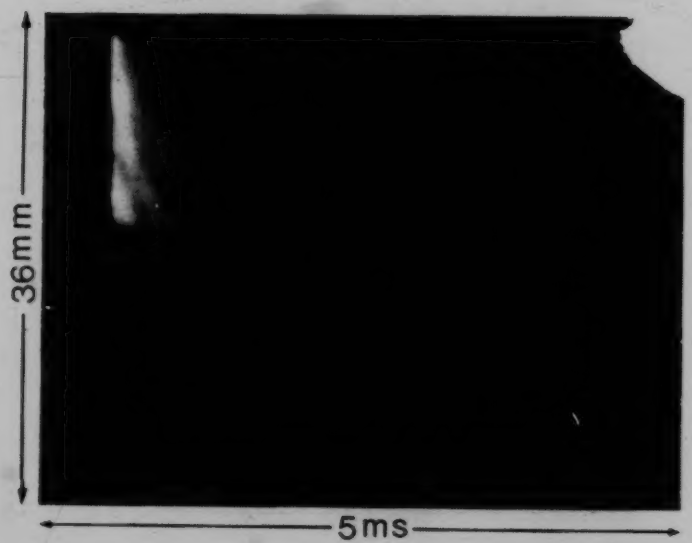

Plate 4.6 Polaroid of Plasma Jet Igniter in Air

as is the case for air (with proportions of 79% nitrogen and 21% oxygen), the presence of oxygen within the mixture is responsible for quenching excitation in the plasma plume, as discussed in Section 4.1. Consequently, quenching causes early recombination of species in nitrogen and the resulting luminosity is reduced. These results support the findings of section 4.1 for a nitrogen-oxygen environment.

In the case of propane-air environments, it was found that as propane content increased from 0% (pure air) to 2.5%, as seen in Plates 4.7a to 4.7d respectively, luminosity from the plasma plume was observed to have increasingly longer durations of up to 3 ms, and to extend greater distances of up to 1 cm beyond the plasma plume. This indicates that the presence of propane causes activated species to persist longer. The consequence of this characteristic is that thermal energy within the plume is transported beyond the plume into cold (300 K) gaseous mixture.

When the percentage of propane in air is increased to that of a stoichiometric mixture (4.02%), the streak photograph of Plate 4.7e shows the existence of multiple flames extending from within the plume to the flame front beyond the plume. Also, the flames can be seen to exist for several milliseconds. As noted above, the extended duration of the flame kernels at early times, and the increased consumption of reactants as the combustion process

Plate 4.7 (a) Polaroid Photographs of Plasma Jet Igniter in Propane-Air Mixtures 0.5% Propane

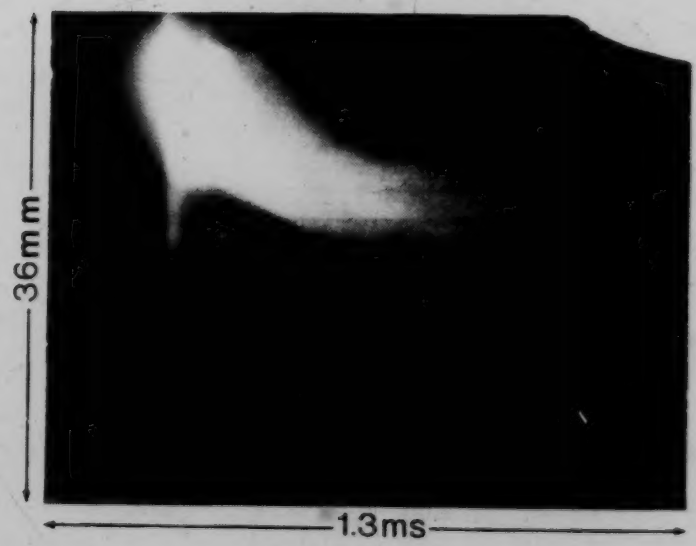

Plate 4.7 (b) 1.0% Propane

Plate 4.7 (c) 2.0% Propane

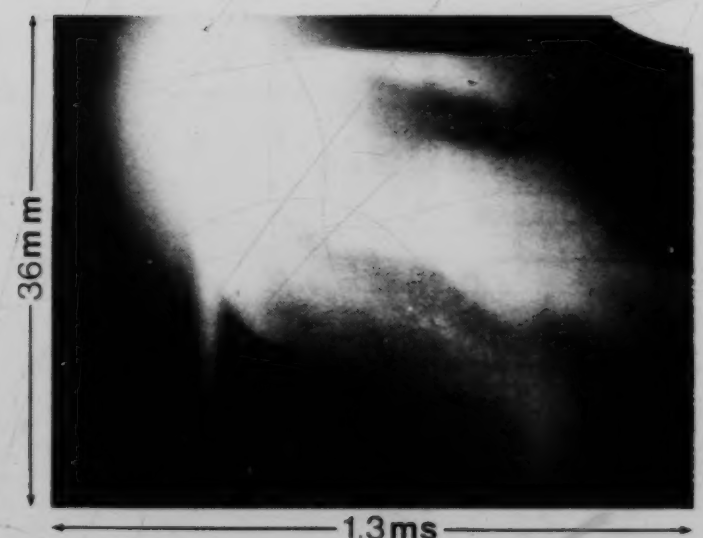

Plate 4.7 (d) 2.5% Propane

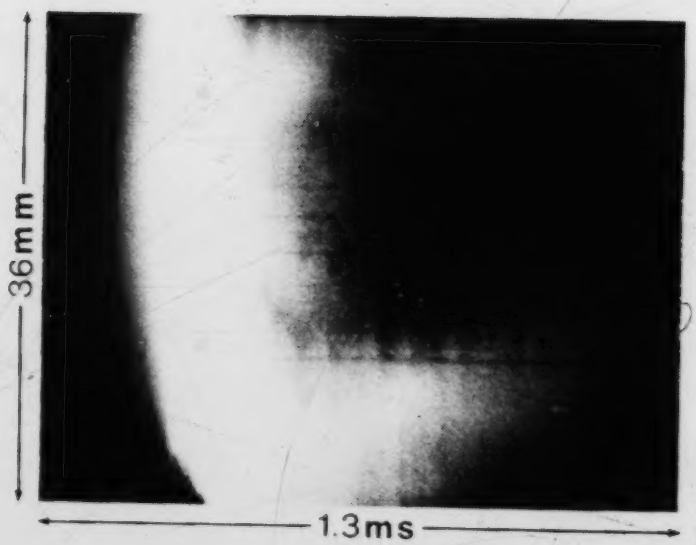

Plate 4.7 (e) 4.02% Propane

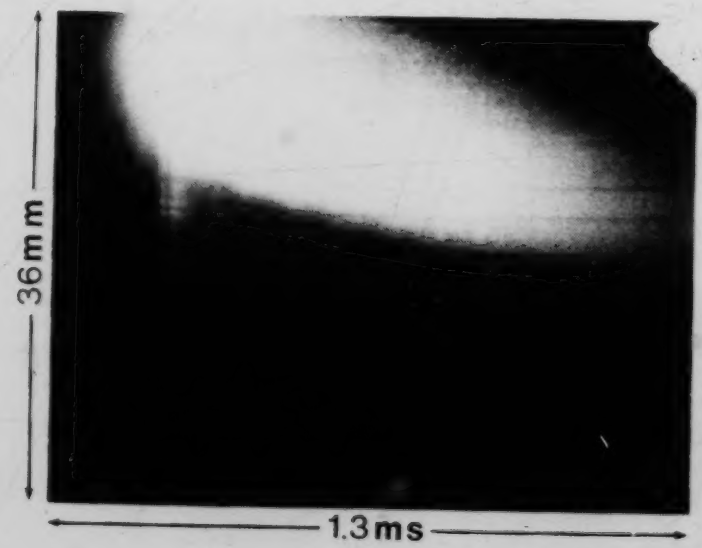

Plate 4.8 Polaroid of Surface Gap Igniter in Stoichiometric Mixture of Propane-Air

continues, are caused by the transport of activated species (radicals) from the reaction zone to the cold gas within the turbulent flame front. The region where cold gas is heated before combustion occurs is known as the pre-heat zone (Weinberg, 1986), and the diffusion mechanism in which radicals are transported across its width, accounts for one aspect of enhanced combustion from a plasma jet igniter as compared to a conventional igniter.

In Plate 4.8, the surface gap igniter is notably different from the plasma jet igniter for the stoichiometric combustion case. The difference is that a single flame kernel is created which forms into a flame wavefront that propagates in a laminar manner. Also, it was found that instantaneous velocities of the activated luminous region were much faster for the plasma jet igniter at 4 m/s compared to the surface gap igniter at 2 m/s. Mixture penetration of the plasma jet was twice that of the surface gap and transportation beyond the plume was not observed for the surface gap igniter.

4.2.3 CONCLUSION

The intensified streak photographs served to show the presence and persistence of activated nitrogen beyond the boundaries of the plasma plume. It was also observed that oxygen has the ability to quench excited nitrogen species.

As the propane content of propane-air mixtures was increased, activation luminance was again found to be

present at extended distances and durations from the igniter. This indicated an increase in the mechanism of transporting activated species (radicals) from the plasma plume to the cold mixture. When the propane content was increased closer to that of a stoichiometric mixture, combustion streak photographs showed that multiple flames existed and combustion was promoted by the transport of activated species from the reaction zone to the pre-heat zone of the flame front. In comparison to the plasma jet igniter, the surface gap igniter was found to have the different characteristics of a single flame kernel, and a laminar flame front. Also, flame propagation into the gaseous mixture was much slower for the surface gap compared with the plasma jet igniter.

4.3 IONIZATION MEASUREMENTS

The purpose of this study was to calculate the resistivity of the plasma within the flame front and to determine if the impedance of the oscilloscope probe, used to take signals from the Langmuir probe, caused loading and thus a reduction in magnitude of floating voltage waveform measurements. It was shown that probe measurements were reliable, since the oscilloscope probe loading of the plasma could be compensated for by increasing the magnitude of current density by a measurable compensating factor.

An additional purpose of this study was to observe flame structure in terms of the ionization region preceding, during, and following the passage of the flame front. Floating voltage observations were made with the use of an unbiased Langmuir probe.

4.3.1 EXPERIMENTAL DESIGN

For both parts of this study, the same experimental set-up and operating conditions were used (Figure 4.5). The plasma plug was installed in the combustion chamber and the chamber purged with either nitrogen, air, or a propane-air mixture. The plug's power supply was energized by a 4 μF capacitor charged to 813V, corresponding to a stored energy of 1.32 Joules. Floating voltage measurements were also repeated using the surface gap igniter in nitrogen.

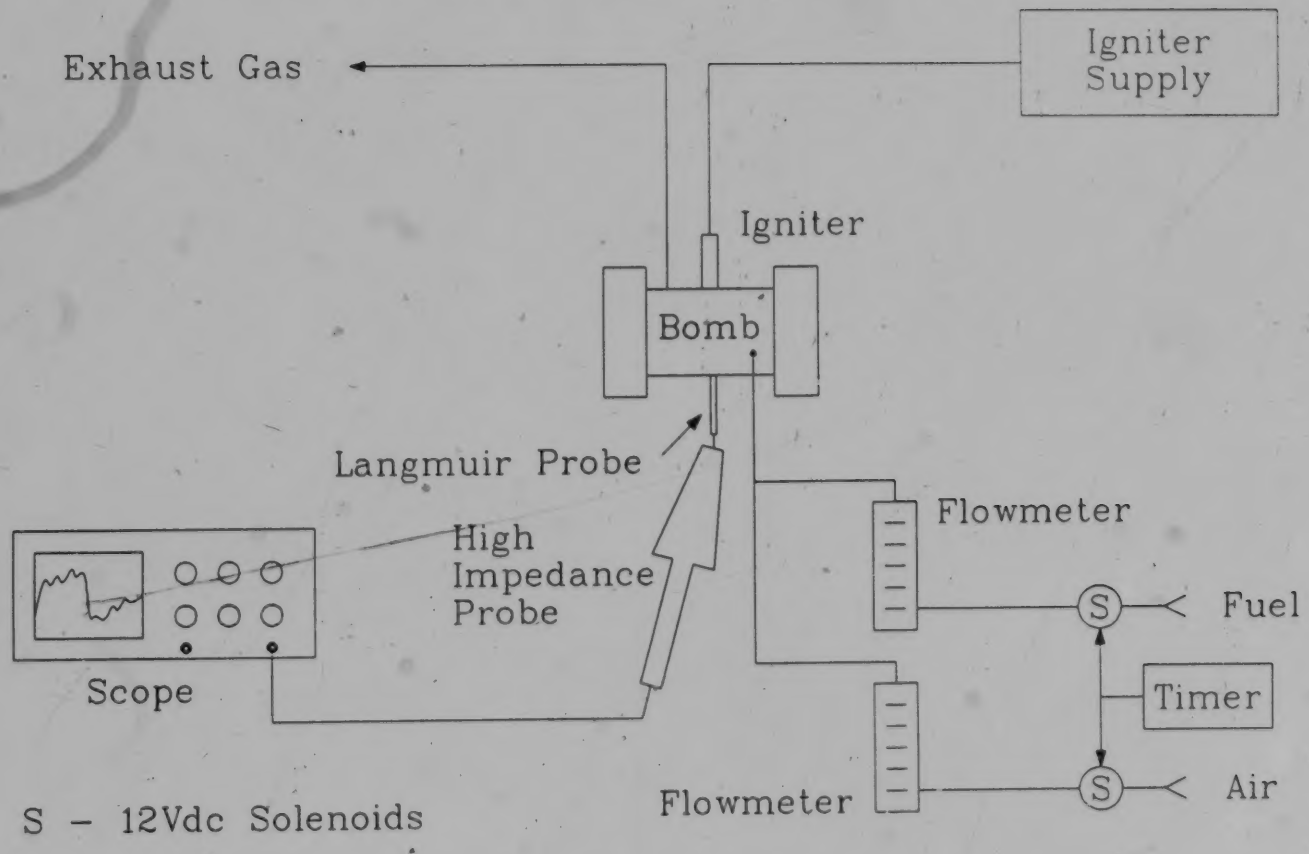

Figure 4.5 Langmuir Probe Ionization Experiment

The igniter was fired in the gaseous environment. As the expelled plume passed the unbiased Langmuir probe, voltage versus time measurements were recorded on the Tektronics 2430A digital storage oscilloscope. This information was then saved permanently in the form of oscillogram photographs for reference. The experiment was repeated for various probe-igniter distances, mixtures, and oscilloscope probes of different impedances.

The highest impedance oscilloscope probe available for experimentation was the 100 meg-ohm (MΩ) probe. In order to determine if the 100 MΩ probe loaded the plasma within the flame front, the impedance of the scope probe needed to be compared with that of the plasma. To calculate the impedance of the plasma, two scope probe arrangements, each with a different impedance, were used to take floating voltage measurements from the unbiased Langmuir probe. First, the 100 MΩ scope probe was used on its own for one set of measurements. Next, a second 100 MΩ probe was added in parallel with the first to give a 50 MΩ net impedance. By determining the decrease in waveform magnitude when the voltage waveform from the 100 MΩ probe was compared with the voltage waveform from the 50 MΩ probe combination, a reduction factor or ratio results which can be used to calculate loading and wavefront impedance.

In equation 4.2, this quantity is labeled "r", and is the ratio of the 50 MΩ probe readings to the 100 MΩ

readings. r is less than one (i.e. r<1) when the plasma impedance is large enough to load the 50 MΩ probe arrangement more than the 100 MΩ probe. The ratio is equal to one (i.e. r=1) when loading does not occur for the lesser impedance of the 50 MΩ probe arrangement, as compared to the 100 MΩ probe. Once the ratio term, r, is calculated from equation 4.2, the question of probe loading can be determined by comparison of this value with unity.

$$r = \frac{|V_{\text{floating, 50 M}\Omega\text{ probe}}|}{|V_{\text{floating, 100 M}\Omega\text{ probe}}|} \qquad (4.2)$$

In equation 4.3, r is the ratio of the plasma impedance, R_{plasma}, in parallel with the 50 MΩ scope impedance all over the plasma impedance, R_{plasma}, in parallel with the 100 MΩ scope impedance. Equation 4.2 and 4.3 are equivalent since there is a direct relationship between the reduction in magnitude of the floating voltage waveforms and the reduction in magnitude of the net impedance of the wavefront-scope-probe arrangement.

$$r = \frac{R_{plasma} \;//\; 50\ \text{M}\Omega}{R_{plasma} \;//\; 100\ \text{M}\Omega} \qquad (4.3)$$

Consequently, equation 4.4 was derived for the wavefront plasma impedance by rearranging expression 4.3 in terms of the ratio term, r.

$$R_{flame}(\text{M}\Omega) = 100\ \frac{1-r}{2r-1} \qquad (4.4)$$

The procedure to determine the resistivity of the plasma within the wavefront was accomplished in the following manner. Firstly, the Langmuir probe, positioned 4 centimeters from the igniter, was connected to the oscilloscope by a 100 MΩ probe. When combustion occurred, a record of the floating voltage was stored on the oscilloscope. Observations were taken for 15 runs. Next, another 100 MΩ probe was added in parallel with the first scope probe. As mentioned above, the resultant probe combination had a net impedance of 50 MΩ. When combustion occurred for the same combustible conditions, the floating voltage waveforms of each individual probe of the parallel probe arrangement were stored in the oscilloscope. Since the two probes were in parallel, each waveform was identical in magnitude and signature. Observations were also taken for 15 runs.

4.3.2 RESULTS

For the determination of flame front plasma resistivity, and thus, probe loading, the results were as follows: the floating voltage waveform of the 100 MΩ probe was compared with the waveform from the 50 MΩ probe combination, and it was found that both were identical in signature shape. However, from equation 4.2, the magnitude of the 50 MΩ probe waveform was 81% (i.e. r = 0.81) of the waveform magnitude observed from the 100 MΩ probe. From

these observations, the 50 MΩ probe combination, as compared to the 100 MΩ probe, loaded the impedance of the flame to a small degree. Also, the resistivity of the plasma ionization was calculated to be 30 ±3 MΩ from equation 4.4. By comparing the impedance magnitude of the 30 ±3 MΩ flame to the 100 MΩ probe, the flame impedance was found to be (30 ±3 MΩ/100 MΩ) 30% ±3% of the probe impedance. A 30% factor indicates that probe loading does slightly reduce the magnitude of the oscilloscope waveforms. Thus, by monitoring the Langmuir probe with this 100 MΩ oscilloscope probe, a reduction of 30% in the floating voltage signal was observed. However, this reduction can be corrected for by increasing the observed floating voltage signals by 30% in magnitude.

As the flame front boundary region encountered the unbiased electrostatic probe, positive ions and electrons within the flame front were sensed by the probe. As the flame front swept over the probe, a sharp initial positive deflection occurred as a dense region of positive ions was observed. This indicated that no reaction was present. Plate 4.9 shows this in the form of a voltage versus time oscillogram. The head of the flame front was well defined between the combustible mixture and the actual combustion area. Continuing on, the positive ion density peaked and rolled off exponentially to a negative potential (electron density) as the wavefront passed. The magnitude of the

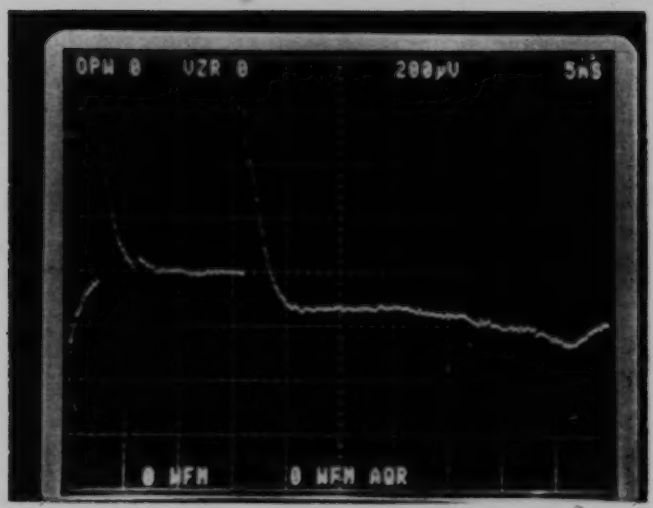

Plate 4.9 Oscillogram of Ion Density

positive deflection was found to be 3 times that of the negative deflection, whereas the duration of the negative region was found to be greater than 5 times the duration of the positive region. When dissociation occurred in the reaction zone, the concentration of ions was greater than that of electrons; however, quasineutrality was intact. As the distance from the probe to the igniter increased, the magnitude of the negative floating voltage slowly decreased. A slow decrease in voltage indicated that dissociation (i.e. temperature) was maintained before the recombination of radicals could occur. Maintained dissociation implies substantial radical mixing over a long period (Simeoni et al, 1986).

Results obtained with the plasma jet igniter in a nitrogen environment were corrected for by the 30% error and are presented in the log-log graph of Figure 4.6 as a line slope of relative floating voltage amplitude (charge density n_e) versus probe-igniter distance. Comparing this line to the line slope of relative luminosity amplitude versus distance below the igniter, which is a subset of the nitrogen data from Figure 4.3, it can be seen that the slope of the nitrogen line is similar in magnitude for both instances. This indicates that the presence of ions in the wavefront decreases at the same rate with distance from the igniter as the emission of light. From this evidence, the ionization must in fact be linked with the source of light,

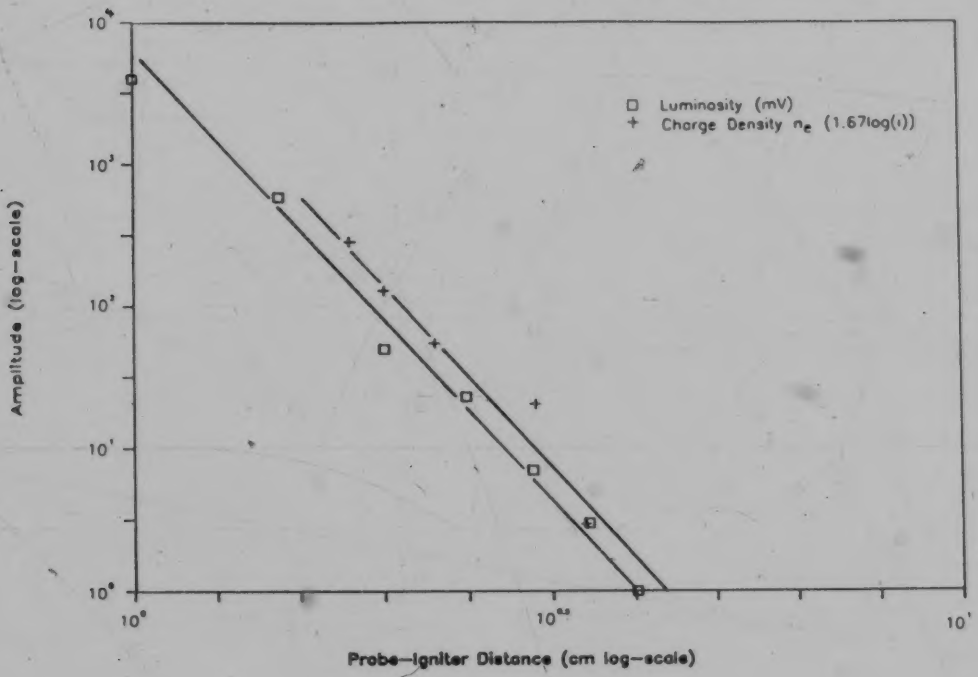

Figure 4.6 Langmuir Probe - Luminosity Comparison

N.B. The fact that the absolute values of luminosity and charge density (n_e), as plotted, are identical is a coincidence. The significant point (regarding the text) is that the slopes are the same.

and this fact further supports the possibility that illumination is caused by the activation of molecular species, as previously stated in Section 4.1.

4.3.3 CONCLUSION

In this study, the resistivity of plasma at a distance of 4 centimeters from the plasma jet igniter was determined to be 30 MΩ. In relation to the 100 MΩ oscilloscope probe, which was used as a sensory device for the Langmuir probe, the plasma impedance was found to be moderately loaded by the impedance of the oscilloscope probe. This caused a reduction in the magnitude of floating voltage versus time waveforms by a factor of 30%. It was also recognized that this reduction could be compensated for by increasing the observed measurements by the same 30% amount.

The dissociated structure of the wavefront had the characteristics of a well defined concentration of positive ion rich plasma, followed by a persistent electron rich plasma. Comparing the decrease in magnitude of dissociated ions to the decrease in intensity of luminosity from the wavefront shows that both change at the same rate over the same distance from the igniter. Consequently, it is likely that luminosity is associated in some way with the presence of dissociated particles. This further supports the findings of Section 4.1 on radical luminosity.

4.4 RELATIVE BURNING VELOCITY

Relative burning velocity is the speed at which the flame front is moving with respect to the unburnt gas ahead of it. This is different from the instantaneous velocity of the flame front, which is the rate at which the flame moves away from the ignition source. In the instantaneous case, the unburnt gas ahead of the flame front is put in motion by the induced pressures of the combustion itself. The purpose of this study was to determine the relative speed of the flame front with respect to its instantaneous velocity, since it is this velocity which is used to calculate flame front parameters from the measured flame thickness (later).

4.4.1 EXPERIMENTAL DESIGN

As described in Chapter 3, the schlieren cinematography system consisted of the Kodak Spin Physics SP2000 camera, a laser diode illumination source, two concave spherical mirrors, two irises, various convex lenses, and a single flat monochromatic mirror. Figure 4.7 shows the Z-shaped layout of this system.

The combustion chamber was positioned in the parallel beam viewing area of the schlieren layout. In this infinite focus location, varying degrees of refraction from a combusting mixture could be observed and recorded on magnetic tape by the SP2000 camera. This schlieren photographic image was used to observe the flame front

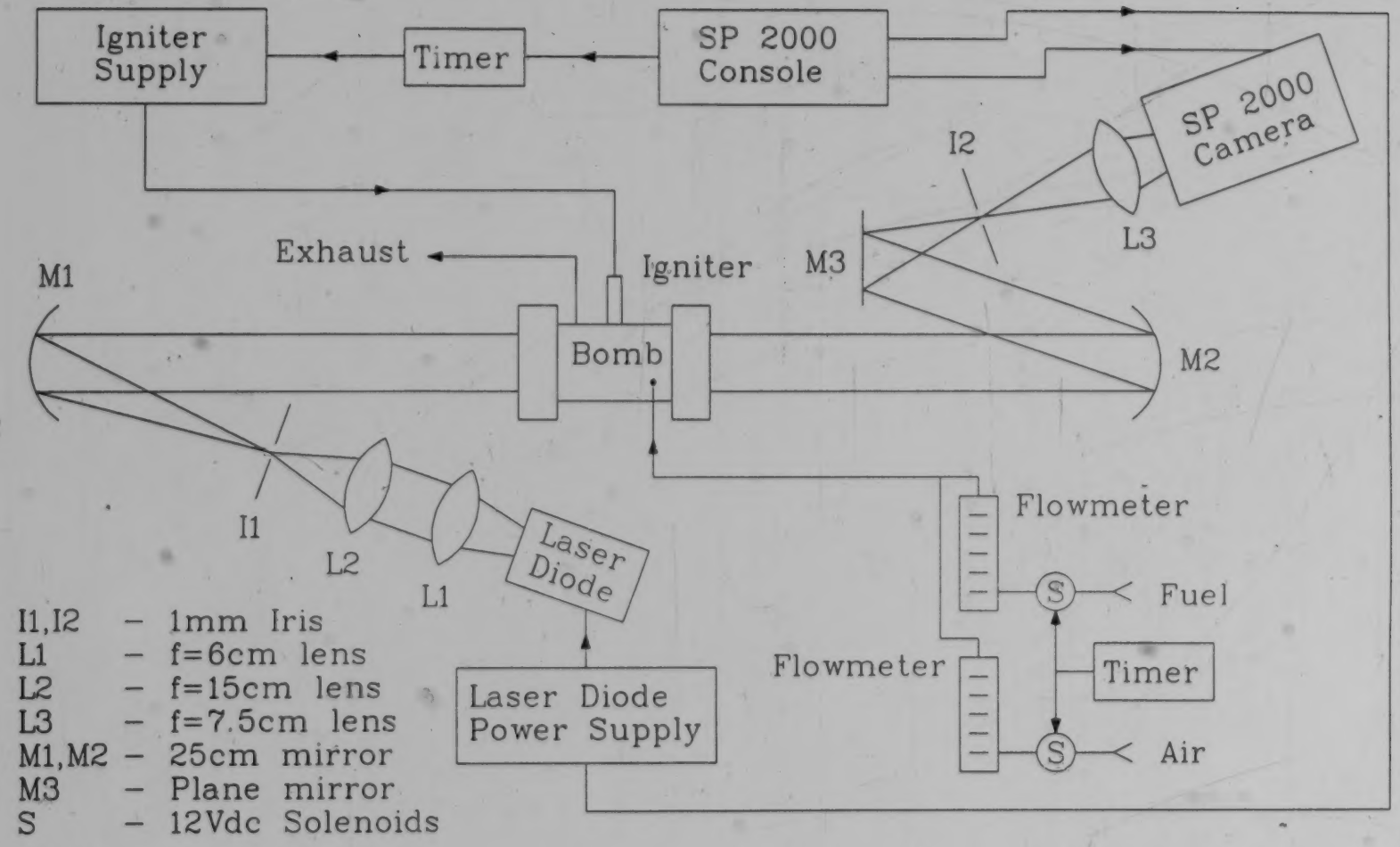

Figure 4.7 Schlieren Cinematography Experiment

velocity of a premixed burn within the combustion chamber.

A rectangular glass tube with one open end (cup) having dimensions of 25 millimeters in width, 50 mm in length, and 52 mm in depth was centered in the bomb. It was placed lengthwise along the path of the optical beam, across from the igniter such that the distance of the igniter to the cup-opening was 2 centimeters. The bomb was filled with a stoichiometric mixture of methane and air and then ignited. As part of a mixture was allowed to burn down the rectangular tube, the adjacent unconfined flame front burned freely across the diameter of the cylinder on either side of the cup. This can be seen in Plate 4.10. The cup stopped the absolute movement of gas ahead of the propagating flame within the cup by confining the flame and isolating it from the rest of the bomb volume. The experiment was repeated for a conventional spark plug, a surface gap plug, and a pulsed plasma jet igniter.

4.4.2 RESULTS

After the flame kernel developed into a laminar flame front at the mouth of the cup (2 centimeters from the igniter), the flame front velocity within the cup was found to be slower than the velocity external to the cup. This can be seen in Plate 4.10, and is confirmed by a graph of distance versus time in Figure 4.8, where the internal and external flame fronts have different slopes (i.e.

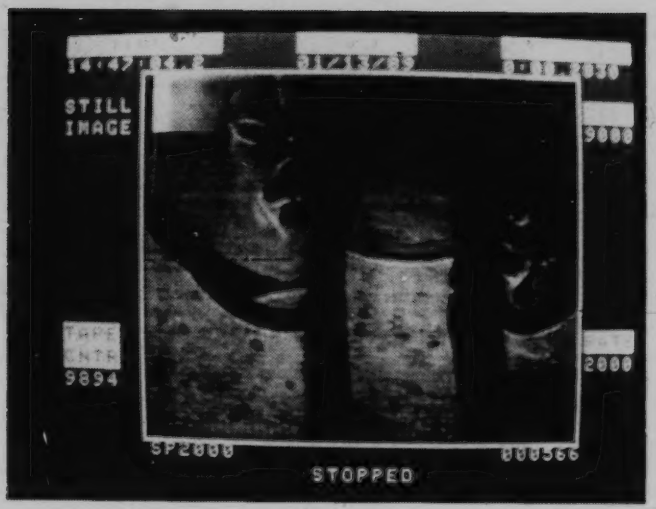

Plate 4.10 Schlieren Photograph of Relative Burning Velocity

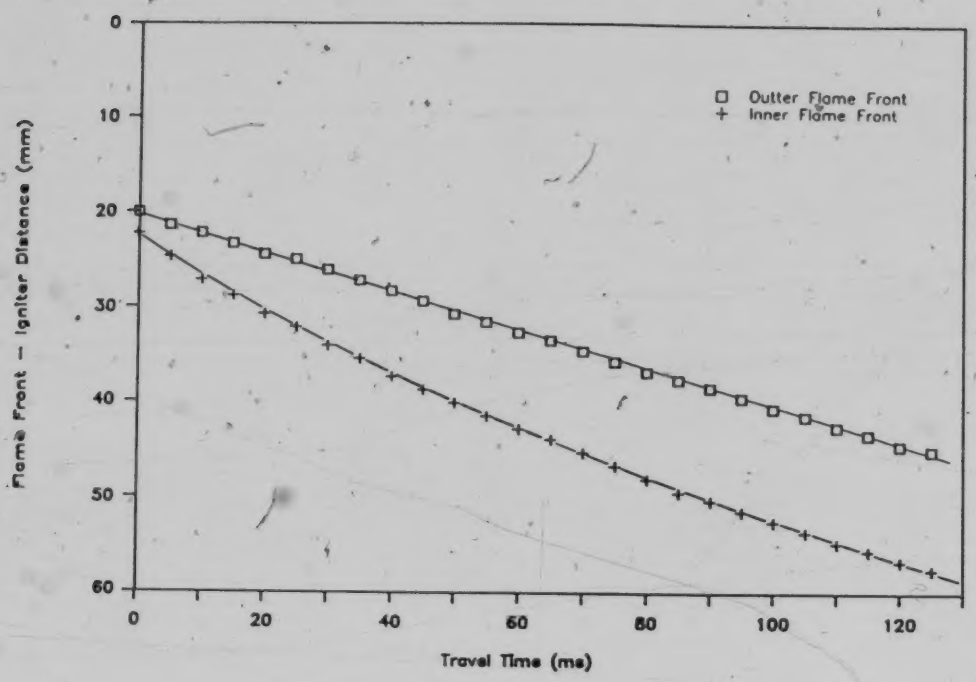

Figure 4.8 Flame Front Distance Graph

velocities). However, the external velocity was found to be constant by the linearity of its slope, while the internal velocity, being quite linear in nature, experienced a slight deceleration from the fluid boundary layer along the interior walls of the cup.

These results showed that the instantaneous velocity of the confined flame front was 70% of the instantaneous velocity of the unconfined flame front. This percentage indicates that the relative burning velocity of the flame front, with respect to the unburnt gas ahead of it, is approximately 70% of the instantaneous flame front velocity of the normal unconfined flame. Since pressure equilibrium existed throughout the bomb and cup, and since the flame speed was relatively slow in comparison to the speed of sound, a difference in flame speed between the exterior and interior flames can not be attributed to compression within the bomb and cup.

This 70% value was found to be relatively constant for each of the igniters used. A variation of only ±5% was found to exist between different igniters. This was because the individual flame fronts created by each igniter took on similar burning characteristics with increased distance from the igniter; that is, the flame became less dependent upon the device as distance from the igniter increased.

4.4.3 CONCLUSION

Relative burning velocity, which is defined as the velocity of a flame front with respect to unburnt gas ahead of it, was approximately 70% of the instantaneous igniter-flame velocity of unconfined premixed combustion. The effect was found to be the same for various types of igniters. Burning velocity is important when considering how turbulence is related to flame speed, in the following section on flame structure, because heat conduction is directly related to burning velocity and not to instantaneous velocity.

4.5 FLAME STRUCTURE MECHANISMS

The object of this experiment was to determine the influence of electrically induced turbulence upon flame structure. In order to do so, Langmuir probe measurements of the flame front generated by surface gap and plasma jet igniters were taken at various probe-igniter distances for various methane-air mixtures. For these experiments, methane was used because it is known to have a thicker flame front than propane (Jarosinski, 1984). A thicker flame front was desirable because it had a greater spatial resolution to observe radicals within the wavefront.

Measurements of the electron density rise time and the flame front travel time provided information to calculate instantaneous velocity and flame front thickness, which were then combined in a derived relation to give thermal conductivity. The experiment was repeated to observe the effect of elevated ambient temperatures on velocity and flame front thickness. Optical probe measurements were conducted to verify the flame front thickness results.

Instantaneous velocity and probe-igniter distance were combined in a derived relation to give turbulent (fluid) diffusion. A quantity which indicates dispersion based on the distance particles (radicals as opposed to molecules) are transported while mixing occurs and their local velocity.

Comparison of probe-igniter distance, mixture strength, and igniter type with instantaneous velocity, flame front thickness, thermal conductivity, and particle diffusion allows a determination of how the latter characteristics are affected by varied conditions. By comparing these observations, characteristics of enhanced flame structure caused by the electrically induced turbulence of a plasma jet igniter are revealed.

4.5.1 THEORY

From Clements et al (1984), it is known that radicals can be expected to exist within the plume (about 1 cm in extent) ejected from a plasma jet igniter. However, on the basis of molecular diffusive transport alone, they cannot be expected to survive for a transverse distance of more than approximately 1 mm before recombination occurs (at the end of their excitation lifetime). Consequently, an additional mechanism must be responsible for the increased flame speed observed beyond the igniter. A logical explanation is the convective or turbulent transport of particles beyond the plume to the wavefront.

Clements has suggested that transport of radicals from anywhere within the plasma jet cavity to the plume front boundary could be accomplished in a manner similar to the transport of particles in atmospheric thermals (See equation 4.1). Therefore, radicals could be rapidly swept from the cavity to the plume front boundary. Also, since

the velocity of the plume (13.5 m/s at 1 cm from the igniter orifice) is greater than the flame velocity (about 1 m/s at 7 cm), it is conceivable that a similar transport process could be capable of transporting radicals into the combustible mixture ahead of the flame.

Particles diffuse at a speed determined by the local gas diffusion constant D, and heat flows at a rate determined by the thermal conductivity k. The diffusion constant is a measure of particle transport-mixing and thermal conductivity can be augmented by turbulent heat transfer within the wavefront (Batchelor, 1976; Kadomtsev, 1965).

An expression for heat conductivity can be derived from a combination of relation 4.5 (Lewis and von Elbe, 1961) which governs an adiabatic plane combustion wave and also from a relation which expresses the width of the pre-heat zone, preceding the reaction zone, in terms of flame front thickness.

$$\frac{d}{dx}\left(k \frac{dT}{dx}\right) - S_u \rho_u c_p \frac{dT}{dx} = Q \qquad (4.5)$$

where

T is temperature;
k is thermal conductivity;
S_u is relative burning velocity;
ρ_u is density of the mixture;
c_p is specific heat of the mixture;
Q is chemical energy per unit mass of the mixture in the x-plane.

Integrating expression 4.5 with respect to x between the

temperature limits of the pre-heat boundary T_1 to the cold boundary T_u, where the reaction rate is zero, we obtain:

$$S_u \rho_u c_p (T_1 - T_u) = k(\frac{dT}{dx})_1 \qquad (4.6)$$

In order to express equation 4.6 meaningfully in terms of wave dimensions, d is defined as a thickness related to the width of the pre-heat zone. As illustrated in Figure 4.9, the slope of the temperature profile at the boundary between the pre-heat zone and the reaction zone is taken as temperature gradient dT_1/dx. As a slope, this quantity can be expressed in terms of a rise in temperature from the cold boundary T_u, to the pre-heat boundary limit T_1, while transversing a distance, d, in the pre-heat zone.

$$(\frac{dT}{dx})_1 = \frac{T_1 - T_u}{d} \qquad (4.7)$$

By combining and rearranging equations 4.6 and 4.7, expression 4.8 is obtain expressing thermal conductivity, k, in terms of flame front thickness, relative burning velocity, and mixture constants of density and specific heat. Resulting observations of instantaneous velocity can be converted to burning velocity by the 70% ratio of Section 4.4. This quantity is used with flame front thickness in equation 4.8 to determine heat conductivity, and thus, the role of convective heat transfer in combustion can be revealed.

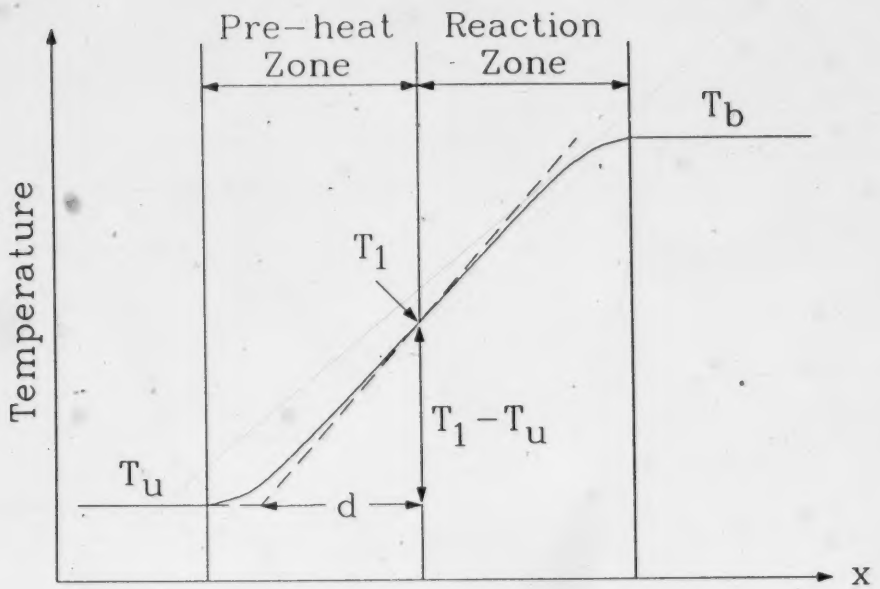

Figure 4.9 Temperature Profile of Wavefront

$$k = d\ S_u\ c_p\ \rho_u \tag{4.8}$$

From Simeoni et al (1986), kinetic theory gives the molecular propagation speed of both particles (diffusion) and heat (conduction) in equation 4.9. This expression relates propagation speed in terms of root-mean-square molecular velocity (υ), and molecular mean free path (λ), all over length L. L is the length in which both density and temperature gradients of diffusion and heat conduction, respectively, are quantified (assuming that both have the same length).

$$v \sim \frac{\upsilon\ \lambda}{L} \tag{4.9}$$

From propagation speed in equation 4.9, a conventional diffusion-constant (D_m) defined in equation 4.10 can be expressed in terms of two of the same molecular parameters: root-mean-square velocity and mean free path. This constant gives the diffusion rate on a molecular level; however, for the purpose of studying the effect of turbulence upon transport processes, a relation which gives diffusion on the more appropriate fluid level was required.

$$D_m \sim \upsilon\ \lambda \tag{4.10}$$

Equation 4.11 for turbulent diffusion can be derived as an analogy to molecular diffusion. In a similar manner

that molecular velocity and mean free path relate to molecular diffusion, local turbulent velocity (v_t) and "mixing length" (l) relate to the turbulent diffusion constant D. This constant readily describes diffusion activity of particles (and their associated temperature) based on turbulent mixing effects.

$$D \sim \frac{v_t \, l}{3} \tag{4.11}$$

Since turbulent velocity is of dimensions appropriate to turbulent eddies within the wavefront (Simeoni et al, 1986), it can be expected to be less in magnitude than the full convective velocity. Here it is assumed that a factor of one-third scales convective velocity to turbulent velocity.

4.5.2 EXPERIMENTAL DESIGN

The experimental apparatus was set up as shown in Figure 4.10. It consists of the combustion cell, associated gas line plumbing, a timed gas mixture control unit, igniter, igniter power supply, optical probe, Langmuir probe, and oscilloscope.

Methane gas and air were used as the combustion reagents, and were allowed to flow through the bomb for fifty five seconds. (Longer flow periods showed no change in the results.) This elapsed purge time is equivalent to exchanging the bomb cavity with twenty bomb volumes of gas.

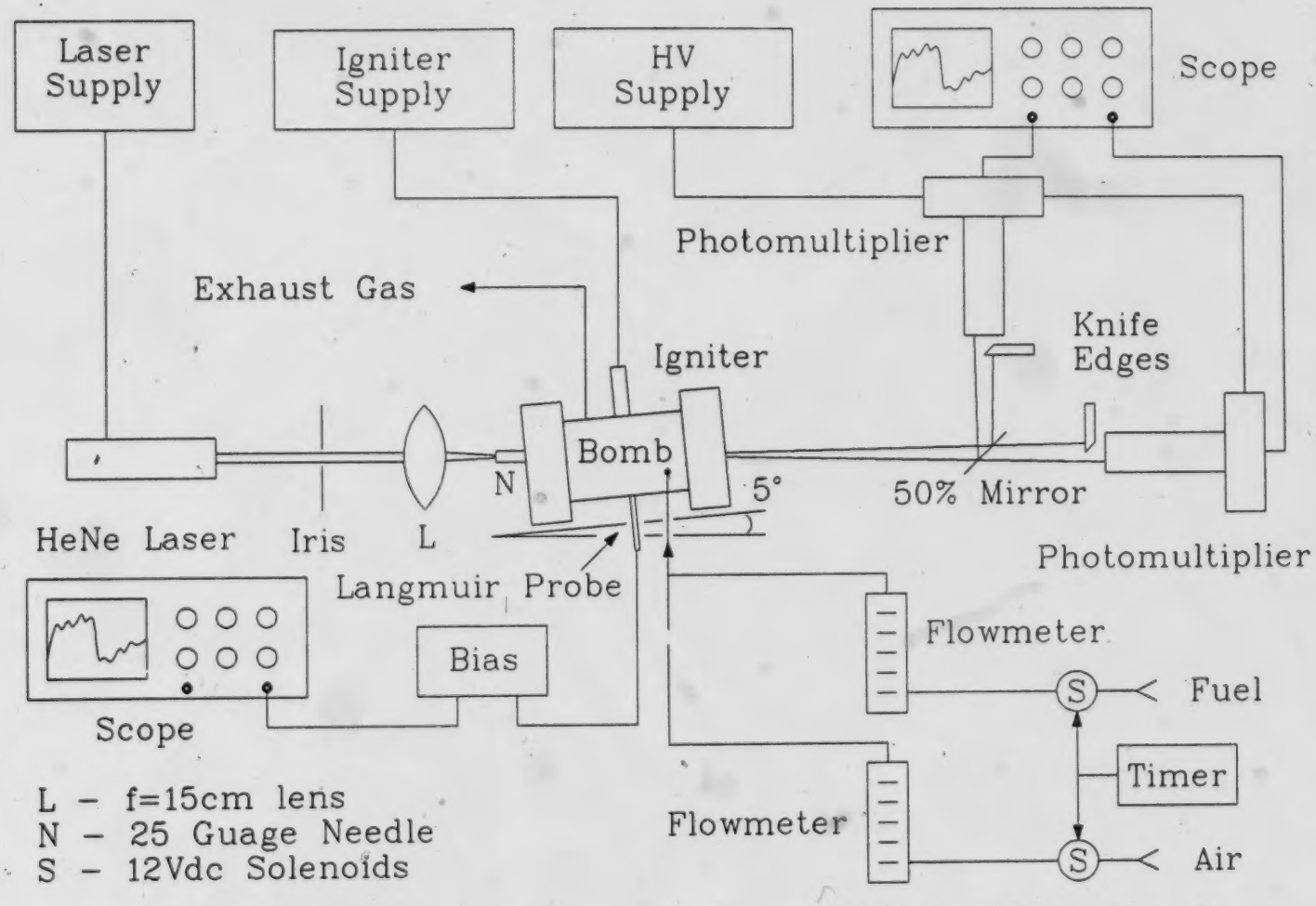

Figure 4.10 Langmuir Probe and Laser Schlieren Experiment

Consequently, all exhaust gases and vapor were flushed as new fuel and air were allowed to mix within the combustion cylinder. Next, with the oscilloscope reset to trigger on an impulse from the igniter, the power supply was set to discharge through the igniter. The fuel-air mixture burned in the manner of an expanding balloon, outwards to the surrounding chamber walls. For both types of igniter, the combustion process was initiated and the volume of reagents burned to completion.

The above procedure was repeated for elevated ambient temperatures. This was accomplished by wrapping an electrical heat belt around the exterior of the bomb, which heated the combustion cylinder to the following temperatures: 50, 75, 100, and 138 degrees Celsius. The heat belt was powered by a Variac connected to the mains. The mixture within the bomb was then allowed to stand for 5 minutes before combustion, while the internal mixture was heated to the same temperature. External and internal temperatures were monitored with a high temperature thermometer.

As the boundary of the expanding flame between the burnt and unburnt mixture, known as the flame front, passed the experimental Langmuir probe, current versus time measurements were recorded on the digital storage oscilloscope. This information was then saved for reference in the form of plotted graphs generated by an Hewlett

Packard ColorPro plotter connected to the data bus of the oscilloscope.

In order to formulate a theory of enhanced flame front propagation, a study with several experimental variables had to be conducted. Therefore, the experiment was varied independently for probe-to-igniter distances of up to 7 centimeters, electrostatic probe bias voltages of -41.2 to 113 volts, mixture strength ratios of 1.00 to 1.50, and ambient temperatures of 20 to 138 degrees Celsius. The firing procedure was repeated at least twelve times for each change in conditions to eliminate scatter. This produced a good set of experimental data for a given variable. With this reliable data, a solid foundation for the theory presented below was obtained.

4.5.3 RESULTS

As the flame front boundary region encountered the positively biased Langmuir electrostatic probe, electrons within the wavefront were attracted to the probe. This attraction, as has been mentioned, allowed an electric current to flow from the battery through the plasma and series resistance. Taking voltage drop readings from the resistor gave a voltage versus time graph of electron density on the oscilloscope (Figure 4.11). While the probe was swept by the flame front, the density measurement of the electron population initially showed a significantly sharp deflection, as seen in Figure 4.11. The head of the

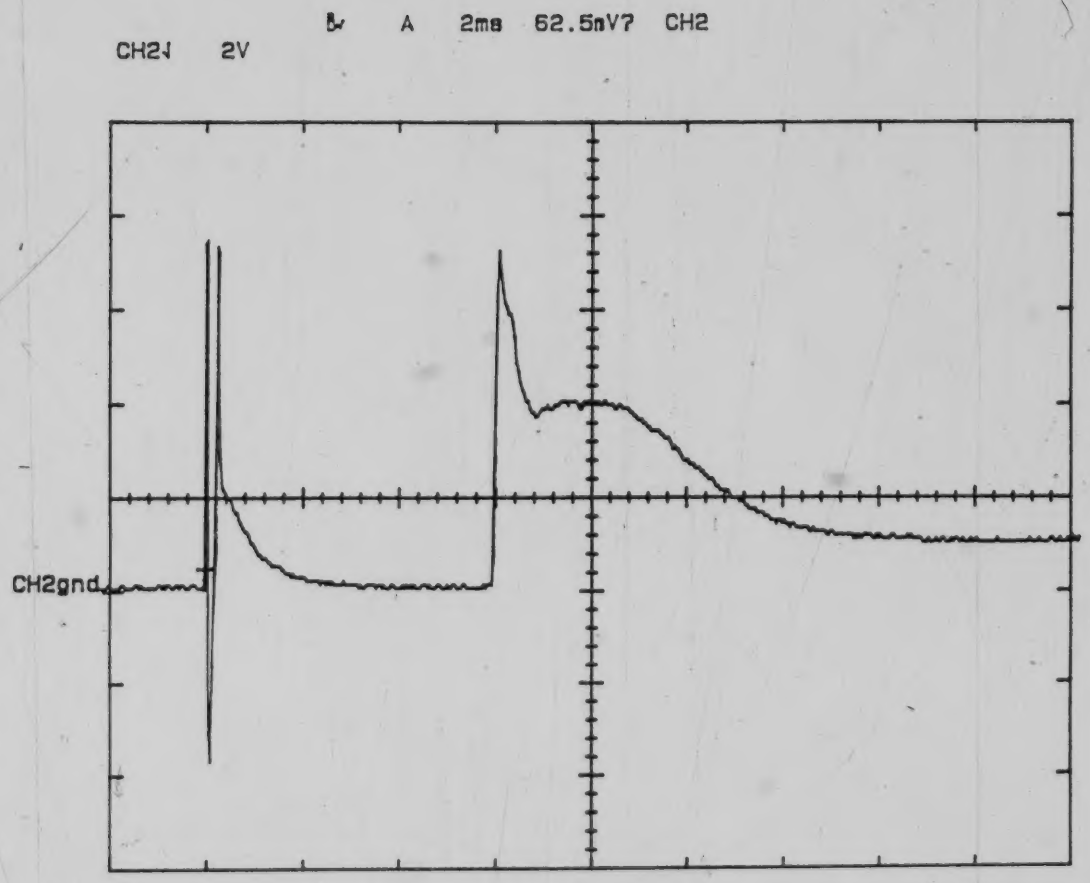

Figure 4.11 Typical Photomultiplier Output Oscillogram of Langmuir Probe

flame front, between the combustible mixture and the actual combustion area, was well defined. The electron density then peaked and rolled off modestly to exhaustion as the combustion process continued.

The electron density front, as measured by the Langmuir probe, appears to be coincidental with the gas temperature front, from schlieren optical measurements (i.e. both occur at the same time, and have the same rise time). The 10% to 90% (Jarosinski, 1984) rise time of the electronic (density/temperature) deflection was used because it spans the width of the pre-heat zone between the cold (ambient) temperature, T_u (298 K), and the pre-heated ignition temperature, T_1 (978 K) (Weast, 1970), of the mixture. Also, the ionization rate of change is approximately constant within the 10% to 90% region. Prior to 10%, electron diffusion from the reaction zone of the flame front tends to be observed. After 90%, ignition occurs at the combustion temperature T_b (2191 K) (Weast, 1970), and the rate of ionization slows as all reactants become ionized.

The flame front 10% to 90% rise time is presented in Table 4.1a for the surface gap igniter, and in Table 4.1b for the plasma jet igniter. The rise times of Table 4.1 vary with an instrumentation error of approximately 1%; however, a deviation in the measurement of rise time is also present. This deviation primarily arises in the probe

detection of the flame front because of the nature of the wavefront having a non-uniform (turbulent) surface. The standard deviations of this data indicated that the wavefront initiated from the plasma jet was much more turbulent than the laminar wavefront initiated from the surface gap igniter.

TABLE 4.1

FLAME FRONT 10% TO 90% RISE TIME (μs)

(a) SURFACE GAP IGNITER

Mixture Strength	Probe-Igniter Distance					
	2cm	3cm	4cm	5cm	6cm	7cm
λ=1.00	92	121	113	115	127	222
λ=1.10	65	122	123	123	140	245
λ=1.25	123	191	187	176	179	253
λ=1.50	617	540	387	407	478	611

(b) PLASMA JET IGNITER

Mixture Strength	Probe-Igniter Distance				
	3cm	4cm	5cm	6cm	7cm
λ=1.00	43	66	70	139	144
λ=1.25	68	75	105	152	251
λ=1.50	109	154	171	398	533

The instantaneous velocity of the flame front was determined by repeating the experiment for different

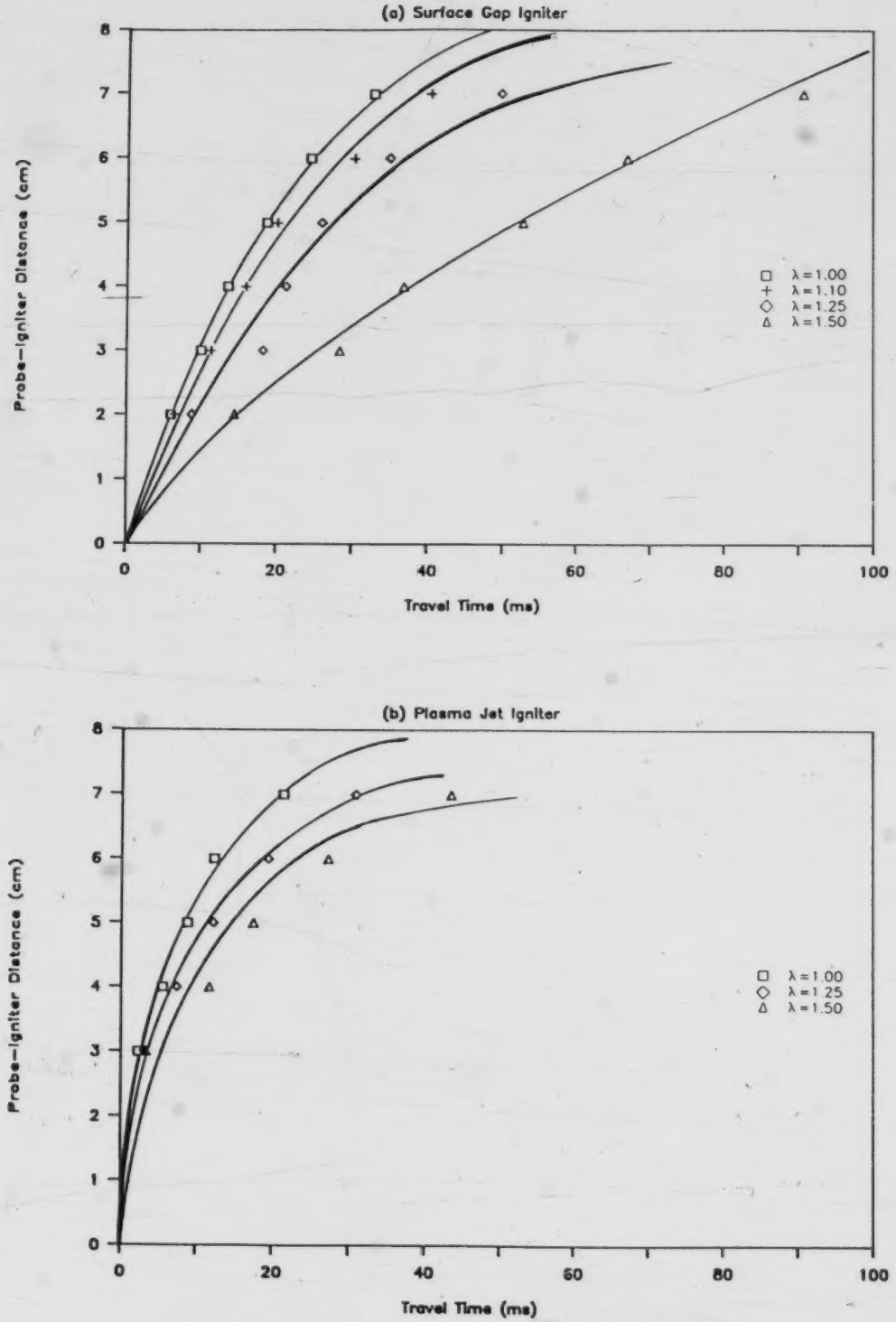

Figure 4.12 Wavefront Distance Graph

Langmuir probe-igniter distances. Plotting travel time versus probe distance produced a velocity profile of the flame front as it expanded to the bomb walls. Graphs of travel time versus probe-igniter distance are presented in Figures 4.12a and 4.12b for the surface gap and plasma jet igniters, respectively. The instantaneous velocity was then found by taking tangents to the profile curve. In this way, the instantaneous velocity could be determined for any distance between the Langmuir probe and igniter. The resultant instantaneous flame front velocities for the surface gap and plasma jet igniters are tabulated in Tables 4.2a and 4.2b, respectively.

When a comparison was made between the instantaneous velocities of the plasma jet and the conventional surface gap igniter, the magnitude of the initial velocity for the plasma jet igniter was found to be about 5 times that of the conventional for a stoichiometric mixture. The flame from the plasma jet achieves a velocity of 4.9 m/s at 3 cm from the plug, whereas the flame from the surface gap igniter has already experienced a decrease in velocity to 2.3 m/s for a stoichiometric mixture. It is not until the 7 centimeters probe-igniter distance that the two velocities from each igniter are the same at about 1 m/s.

The instantaneous velocities of Table 4.2 vary with a maximum error of ±5% for all mixture strengths. Velocity error primarily arises from probe detection of the

turbulent flame front, curve fitting the data of Table 4.2, and achieving an accurate tangent line measurement of instantaneous velocity.

TABLE 4.2

FLAME FRONT INSTANTANEOUS VELOCITY (m/s)

(a) SURFACE GAP IGNITER

Mixture Strength	Probe-Igniter Distance						
	1cm	2cm	3cm	4cm	5cm	6cm	7cm
λ=1.00	4.14	2.90	2.32	1.96	1.74	1.39	1.12
λ=1.10	3.86	2.59	1.94	1.69	1.30	1.08	0.91
λ=1.25	3.73	2.22	1.60	1.31	1.04	0.83	0.69
λ=1.50	1.49	1.05	0.82	0.70	0.60	0.53	0.41

(b) PLASMA JET IGNITER

Mixture Strength	Probe-Igniter Distance						
	1cm	2cm	3cm	4cm	5cm	6cm	7cm
λ=1.00	14.54	7.70	4.87	3.37	2.71	1.64	1.03
λ=1.25	11.33	5.73	3.70	2.21	1.55	1.12	0.75
λ=1.50	7.11	3.76	2.37	1.65	1.31	0.84	0.46

By measuring the 10% to 90% rise time of the electron density front, and multiplying this time by the instantaneous velocity at that location, the flame front thickness could be determined. The flame front thicknesses are tabulated by mixture strength and probe-igniter distance in Table 4.3a for the surface gap igniter, and in

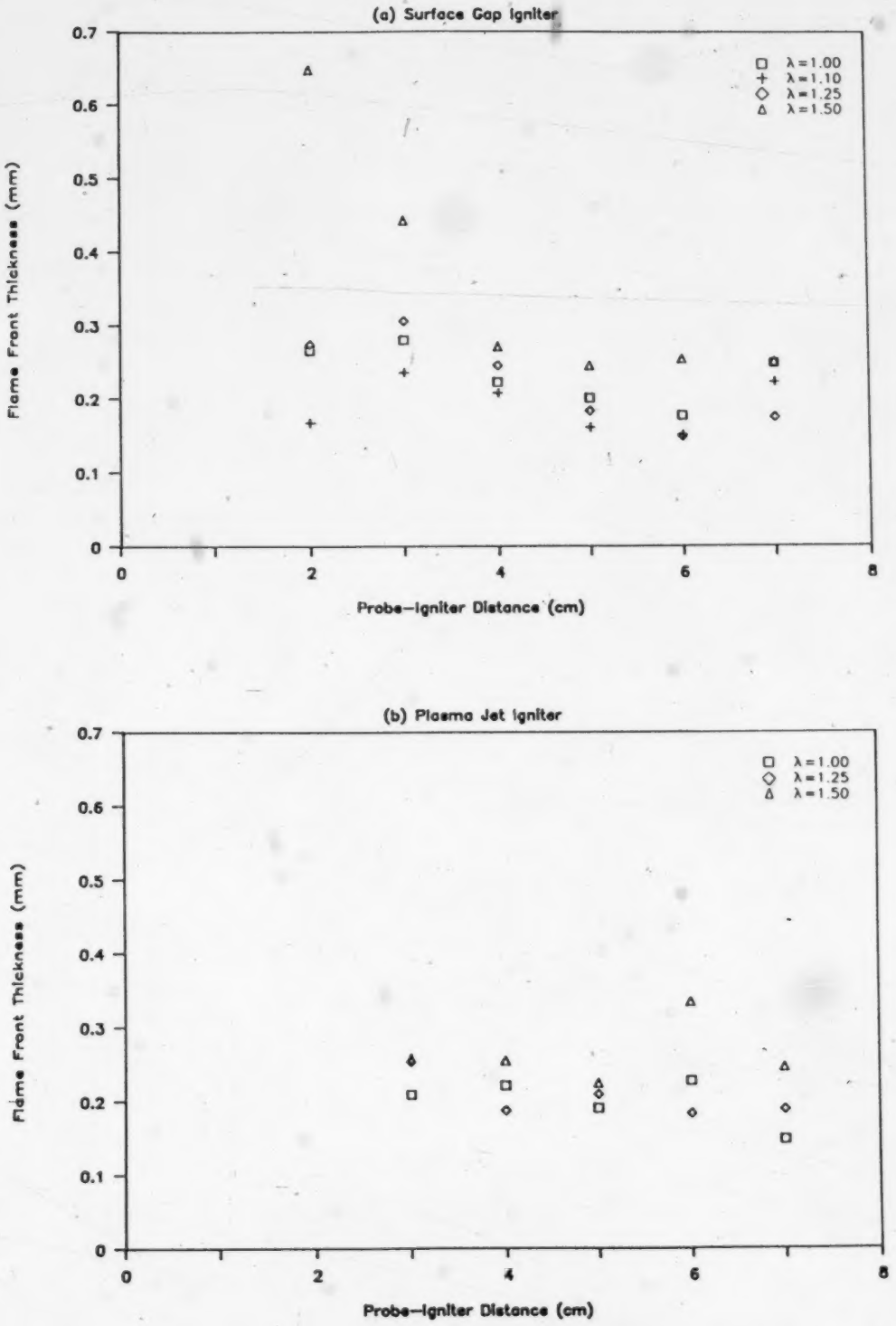

Figure 4.13 Flame Front Thickness Graph

Table 4.3b for the plasma jet igniter. This data is also graphed as flame front thickness versus probe-igniter distance in Figure 4.13a and 4.13b, respectively. Both graphs show that the flame front thickness does not change for mixture strength or for probe-igniter distance. This is because the flame front instantaneous velocity decreases in magnitude at the same rate that the rise time of negative ionization (electron) density increases in magnitude. Thus, as the flame front propagates away from the igniter, the thickness of the flame front stays essentially constant. Averaging all of the data from Table 4.3a gives the thickness of the flame front created by the surface gap igniter as 0.22 millimeters. Similarly, the flame front thickness created by the plasma jet igniter was found to be 0.25 millimeters for the averaged data of Table 4.3b. These two measurements only differ by 13 percent and therefore are in good agreement of each other.

The flame front thicknesses of Table 4.3 vary with an error of ±6%, for all mixture strengths. Deviation in flame front thickness arises from the errors introduced into the 10% to 90% rise times and the instantaneous velocities.

TABLE 4.3

FLAME FRONT THICKNESS (mm)

(a) SURFACE GAP IGNITER

Mixture Strength	Probe-Igniter Distance					
	2cm	3cm	4cm	5cm	6cm	7cm
λ=1.00	0.266	0.280	0.222	0.201	0.177	0.248
λ=1.10	0.167	0.236	0.207	0.160	0.151	0.223
λ=1.25	0.274	0.306	0.245	0.183	0.148	0.174
λ=1.50	0.648	0.443	0.271	0.244	0.253	0.251

(b) PLASMA JET IGNITER

Mixture Strength	Probe-Igniter Distance				
	3cm	4cm	5cm	6cm	7cm
λ=1.00	0.209	0.211	0.191	0.227	0.148
λ=1.25	0.253	0.165	0.162	0.171	0.188
λ=1.50	0.258	0.255	0.224	0.334	0.245

Flame front thickness measurements were repeated for elevated ambient temperatures, in order to determine if thickness and instantaneous velocity have a dependence upon the increased chemical activity induced by temperature. Langmuir probe measurements were taken with a constant stoichiometric mixture, constant igniter-probe distance (4 centimeters), constant probe bias voltage (+41.2V), and with ambient temperatures varied from 20 to 138 degrees centigrade.

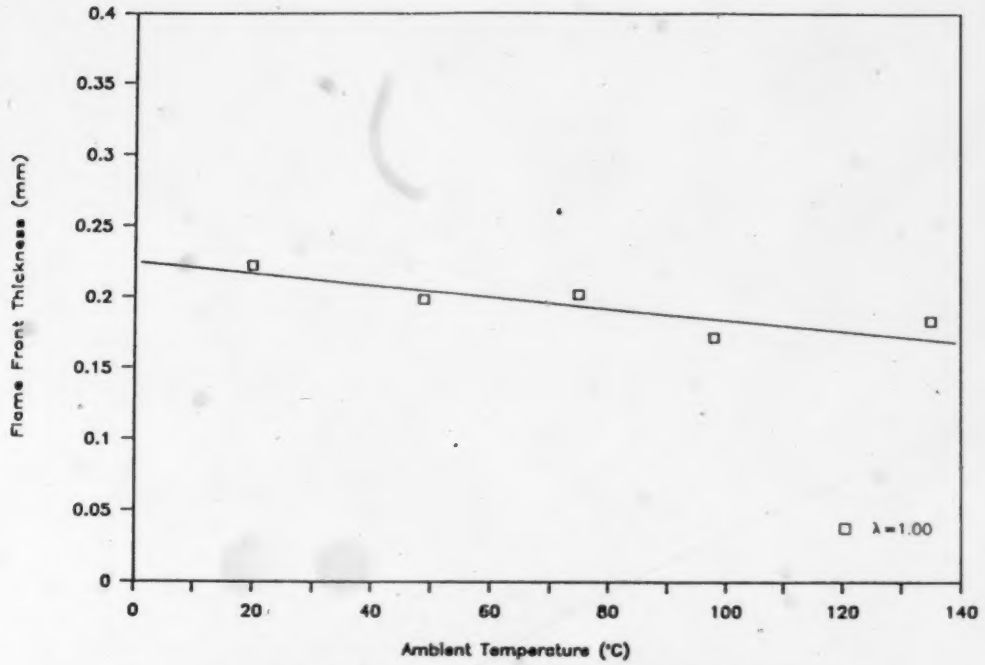

Figure 4.14 Ambient Temperature Flame Front Thickness Graph

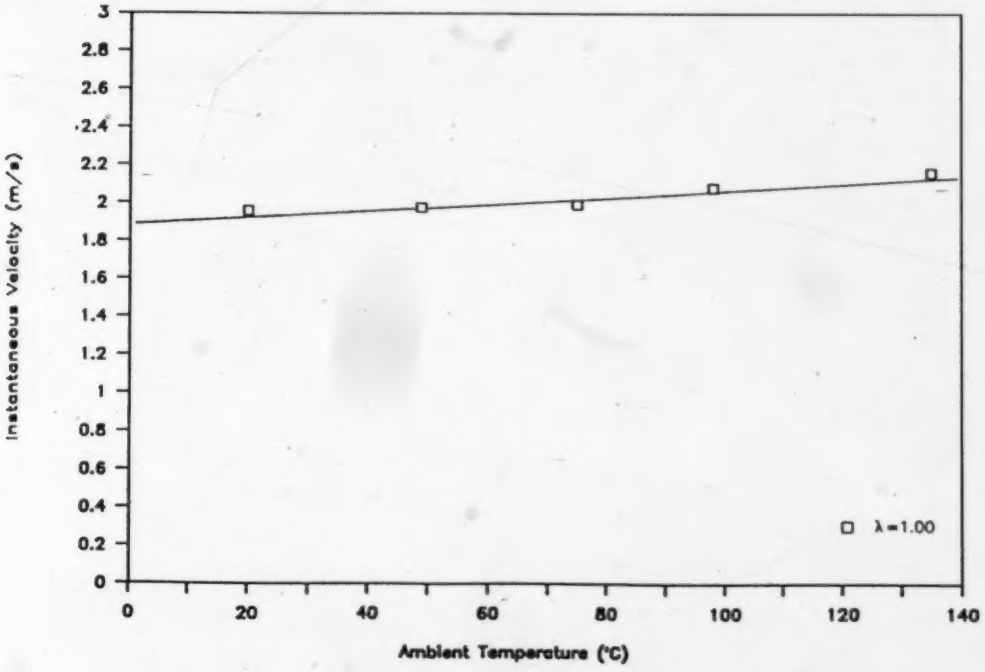

Figure 4.15 Ambient Temperature Instantaneous Velocity Graph

The results, as seen in the flame front thickness versus ambient temperature graph of Figure 4.14, clearly show that elevated temperature had only a minute diminishing effect on the experimentally determined flame front thicknesses. As the ambient temperature, T_u, of the mixture is increased from 293 K to 411 K (20 to 138 °C), the boundary temperature T_1 (978 K) (Weast, 1970), where combustion first initiates between the reaction zone and the pre-heat zone of the flame front, is more easily met with pre-heating from the reaction zone. Regardless of the mechanism behind pre-heating, the thickness of the pre-heat zone decreases because of the lower temperature gradient to be transversed from T_u to T_1. In this case, the change in ambient temperature is small in comparison with the boundary temperature, and as a result, only a minute change in flame front thickness was observed. If the ambient temperature was elevated to a high level - say 800 K - comparable to the boundary temperature, the thickness of the pre-heat zone would be observed to have decreased significantly.

Also, the results, as seen in the instantaneous velocity versus ambient temperature graph of Figure 4.15, clearly show that elevated temperature had only a minute effect on increasing the experimentally determined instantaneous velocity. In a similar manner that thickness is effected by elevated ambient temperature, the velocity

of the front will increase because less time is required to transverse the temperature gradient from T_u to T_l. As in the thickness case, if the ambient temperature was elevated to a very high level, the velocity would be observed to have increased significantly.

Thus, experimenting anywhere in the temperature range 20 to 138 degrees centigrade caused only a minor effect on the flame front thickness and instantaneous velocity. From these results, it is inconclusive whether a chemical activity mechanism enhances combustion; however, it seems unlikely that a chemical effect such as diffusion is responsible for flame speed.

In the case of the optical probe, as the flame front region encountered the focused laser beam, the decreased index of refraction from the heated dense plasma caused the laser beam to bend off of the photomultiplier knife edge arrangement and onto the photomultiplier. A deflection from the knife edge onto the light sensor can be observed on the voltage versus time graph of Figure 4.16. As the flame front initially deflected the laser beam, a sharp boundary was encountered between the combustion mixture and the peak of the flame front. Following this, the laser exhibited many deflections as it encountered varying degrees of refraction from changing combustion reaction temperatures and by-products (e.g. water vapour). This initial sharp deflection, seen in Figure 4.16, gave information about the

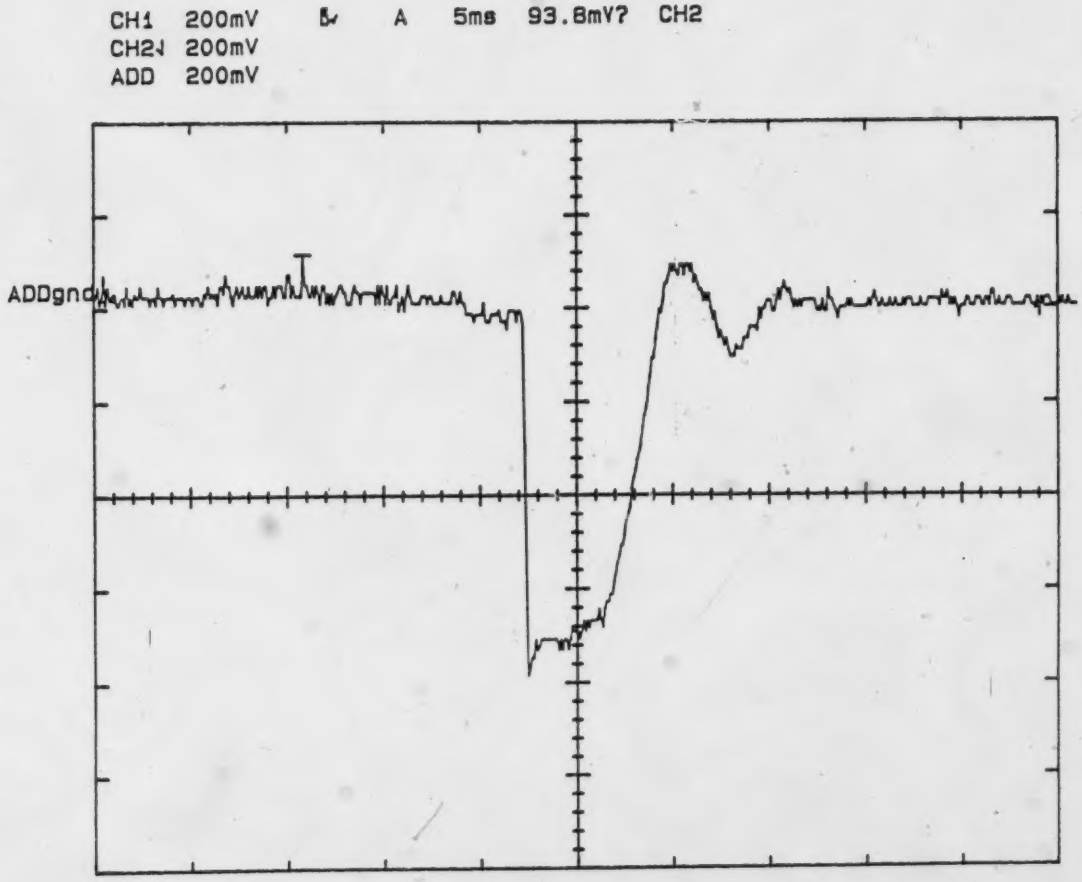

Figure 4.16 Typical Oscillogram of Optical Probe, Voltage vs Time Graph

flame front thickness. As with the Langmuir probe, the instantaneous velocity was determined at a probe-igniter distance of 4 centimeters then multiplied by the 10% to 90% rise time to obtain the flame front thickness. The flame front thicknesses determined by the optical probe are presented in Table 4.4 by mixture strength and igniter type. Averaging the thicknesses by mixture type for each igniter gives values of 0.20 millimeters for the surface gap, and 0.23 millimeters for the plasma jet. These optical probe values are in good agreement with the Langmuir probe measurements determined above, since they only differ by less than 10 percent.

TABLE 4.4

FLAME FRONT THICKNESS BY OPTICAL PROBE

Mixture Strength	Surface Gap Igniter	Plasma Jet Igniter
λ=1.00	0.218 mm	0.270 mm
λ=1.50	0.180 mm	0.198 mm

Thermal conductivity is tabulated by mixture strength and probe-igniter distance in Table 4.5 for the igniters. This data was scaled by division of the thermal conductivity of air ($2.59 * 10^{-2}$ W / m K) (Weast, 1970) and graphed as thermal conductivity with respect to air versus probe-igniter distance in Figures 4.17a and 4.17b, respectively for the surface gap and plasma jet igniters. As can be seen from these graphs, the thermal conductivity

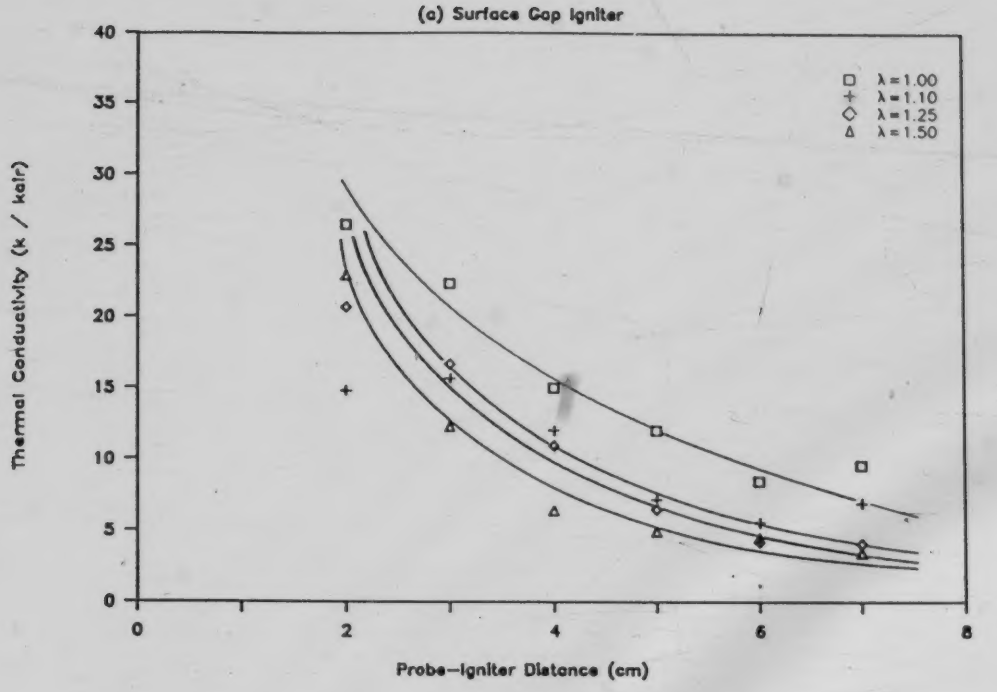

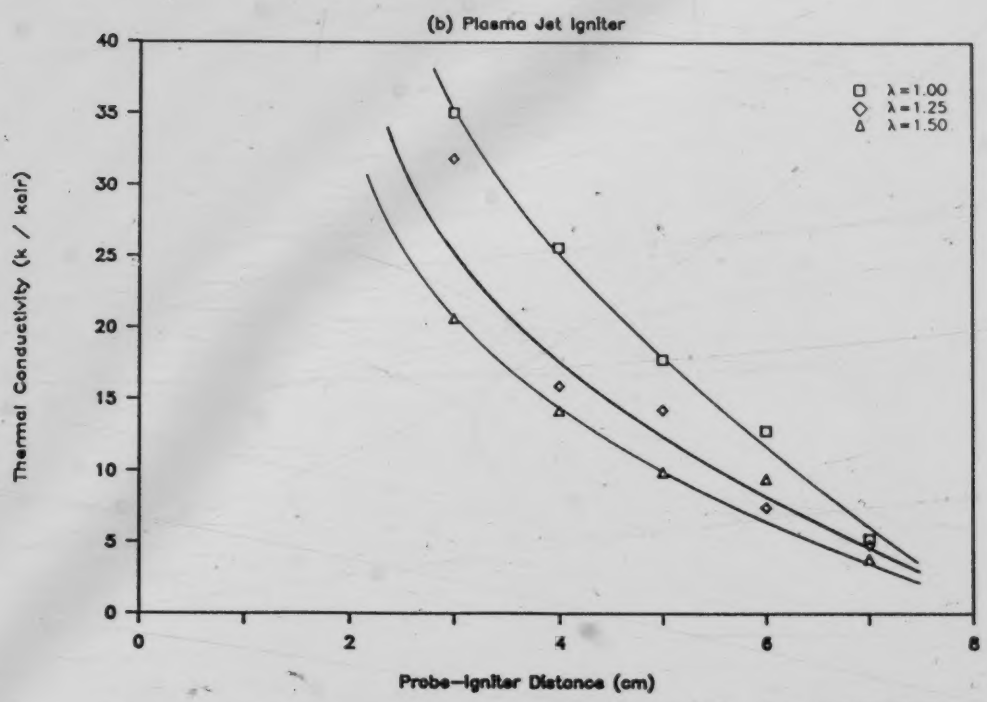

Figure 4.17 Thermal Conductivity with respect to Air Graph

from the igniters is much more than a factor of one times the thermal conductivity of air. In fact, the igniters generate up to 35 times more thermal conductivity than does air. This is a significant difference. Also, thermal conductivity steadily decreases with distance from the igniter. This is true for all mixture strengths, and for both igniters. Once a flame is initiated from the igniter, its velocity (and thus its consumption rate) is greatly influenced by turbulence induced heat conductivity from within the flame kernel. As the flame increases in distance from the igniter, combustion enhancement caused by turbulent activity is diminished. Figures 4.17a and 4.17b, show that the thermal conductivity is a major result of the turbulent activity up to about 7 centimeters from the igniter.

The thermal conductivity values of Table 4.5 vary with an error of ±11%, for all mixture strengths. Deviation in the measurement of thermal conductivity arises from the errors introduced into the flame front thickness, and relative burning velocity.

TABLE 4.5

WAVEFRONT THERMAL CONDUCTIVITY (mJ / m s K)

(a) SURFACE GAP IGNITER

Mixture Strength	Probe-Igniter Distance					
	2cm	3cm	4cm	5cm	6cm	7cm
λ=1.00	687	578	388	311	219	248
λ=1.10	384	406	311	185	144	180
λ=1.25	536	431	283	168	109	106
λ=1.50	595	318	166	128	117	090

(b) PLASMA JET IGNITER

Mixture Strength	Probe-Igniter Distance				
	3cm	4cm	5cm	6cm	7cm
λ=1.00	908	664	460	332	136
λ=1.25	825	322	221	168	124
λ=1.50	535	367	256	245	99

The thermal conductivity data for both igniters is also graphed as thermal conductivity with respect to a stoichiometric mixture versus probe-igniter distance in Figures 4.18a and 4.18b. A stoichiometric mixture was used in both cases. As can be seen in both figures, all data points are less than unity, indicating that thermal conductivity for lean mixtures is less than that of stoichiometric mixtures. Thus, as the mixture is leaned out, the ability for the mixture to conduct heat decreases.

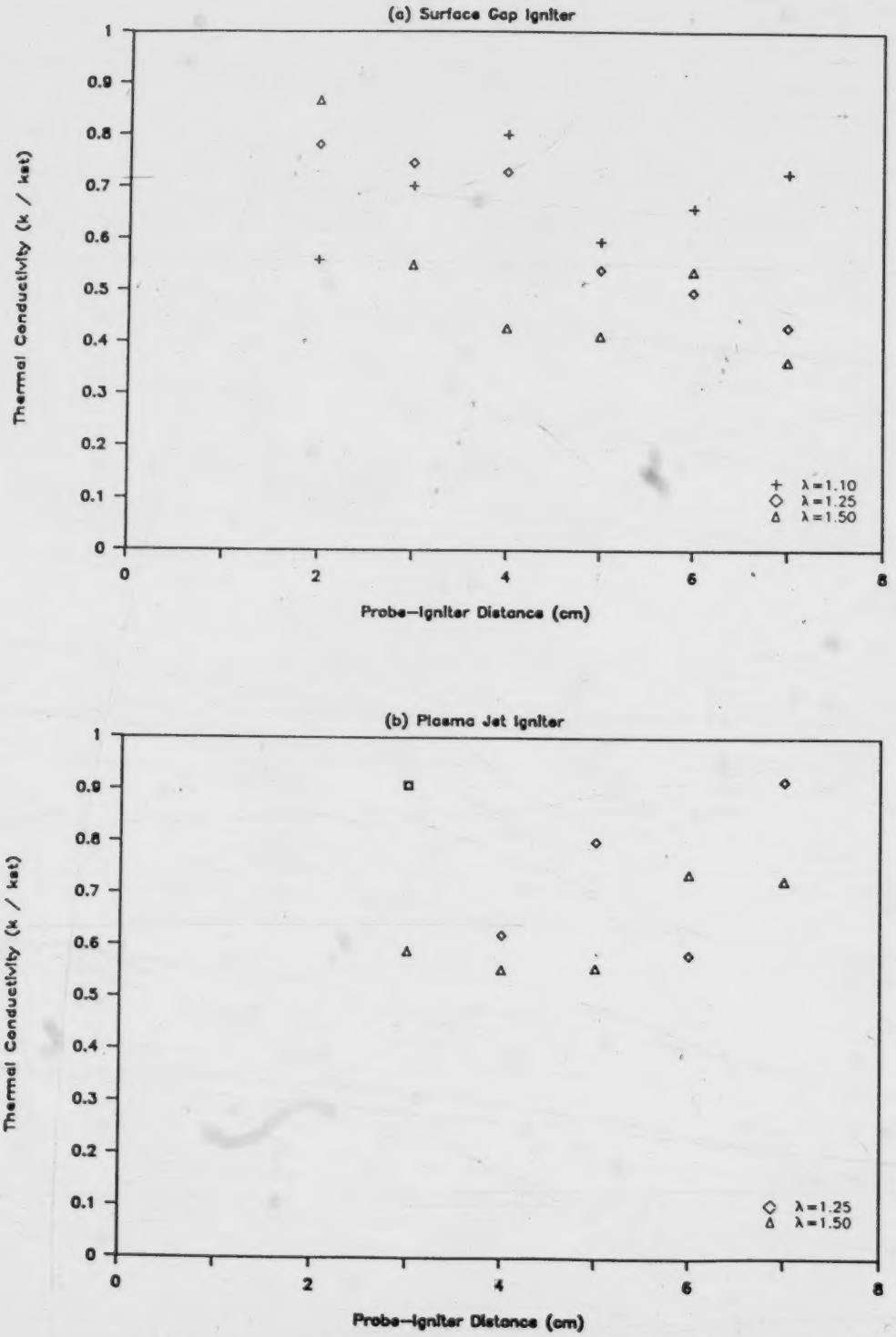

Figure 4.18 Thermal Conductivity with respect to Stoichiometric Ratio Graph

This evidence indicates that leaner mixtures have less turbulent activity in the flame than richer mixture strengths. Therefore, the possibility of enhanced combustion from turbulent activity and thus heat conduction is decreased with leaned mixtures.

A thermal conductivity comparison of the plasma jet igniter to the surface gap igniter (k_{pj}/k_{sg}) is presented in Figure 4.19, as a function of probe-igniter distance. For the majority of the data shown, it is evident that the thermal conductivity of the plasma jet igniter is from 1.2 to 2.2 times greater than that of the surface gap igniter. For lean mixture strengths, there is a greater difference in the thermal conductivity of the plasma jet to that of the surface gap than for richer mixtures. Thus, the plasma jet igniter has a greater ability to create turbulence beyond the extent of its plume, and also the characteristic of allowing the turbulence to maintain its intensity up to 7 centimeters from the igniter. Therefore, the plasma jet igniter has a greater ability to promote combustion within the first 7 cm, based on its turbulent nature, than does the surface gap igniter. For the test conditions beyond a 7 cm distance from the igniter, the flame loses all enhancement characteristics induced by the plasma jet igniter. As propagation continues, flames produced from either type of igniter become indistinguishable, and thus have the same combustion

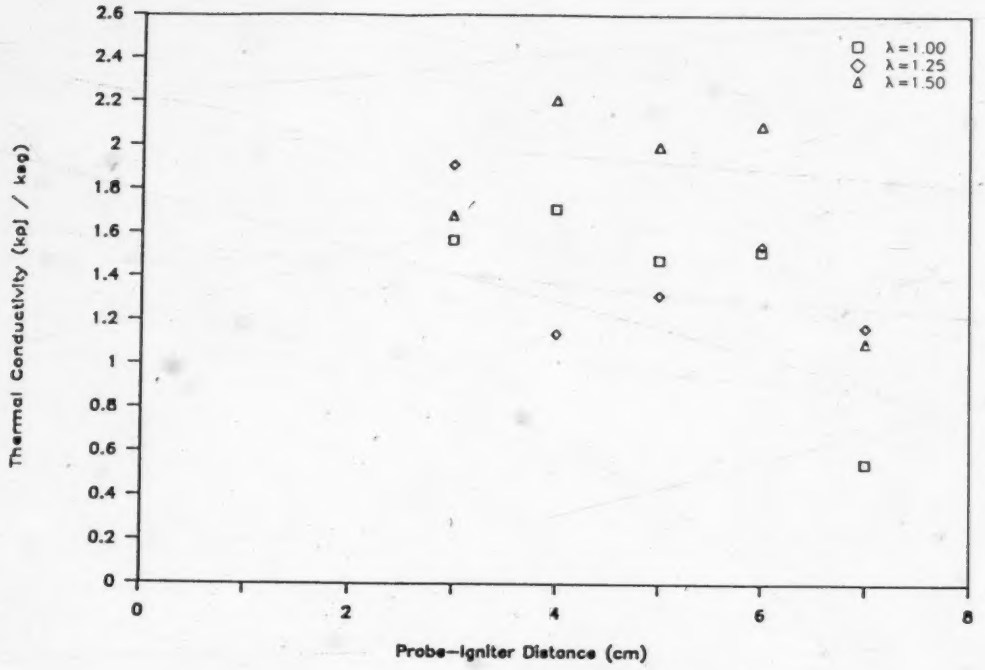

Figure 4.19 Igniter Comparison of Thermal Conductivity

characteristics.

Turbulent diffusion is tabulated by mixture strength and probe-igniter distance in Table 4.6 for the igniters. This data has been scaled by division of the diffusion coefficient for air ($2.46 * 10^{-5}$ m^2/s) (Weast, 1970) and graphed as diffusion with respect to air versus probe-igniter distance in Figures 4.20a and 4.20b, respectively for the surface gap and plasma jet igniters As can be seen from these figures, the turbulent diffusion from these igniters is much more than a factor of one times the turbulent diffusion of air. In fact, the igniters generate up to 2100 times more turbulent diffusion than does air. This is a very significant difference. Also, diffusion from the surface gap igniter increases in magnitude to about 4 cm distance from the igniter. It then remains essentially constant until it begins to decrease at about 7 cm distance for all mixture strengths. The surface gap igniter created little diffusion upon ignition. As the flame became less dependent upon the igniter with distance, mixing activity within the flame front could have developed as a natural characteristic of the flame itself. On the other hand, diffusion from the plasma jet igniter was initially created in a larger volume (of approximately 4 times greater for a stoichiometric mixture), and stayed essentially constant for the first 5cm distance from the igniter, for all mixture strengths. After this point, it then quickly

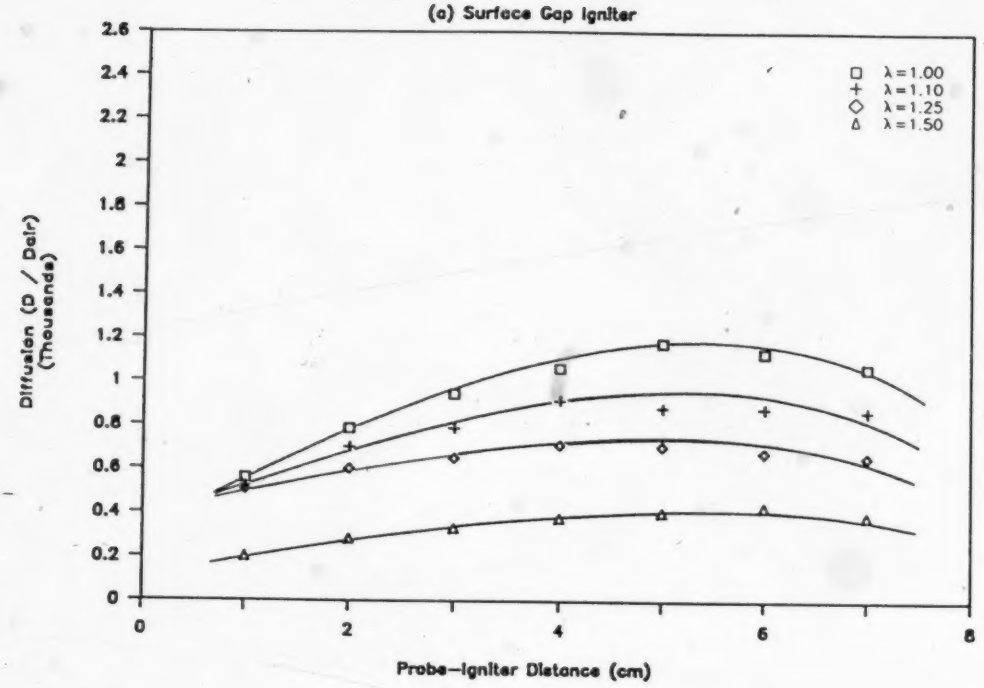

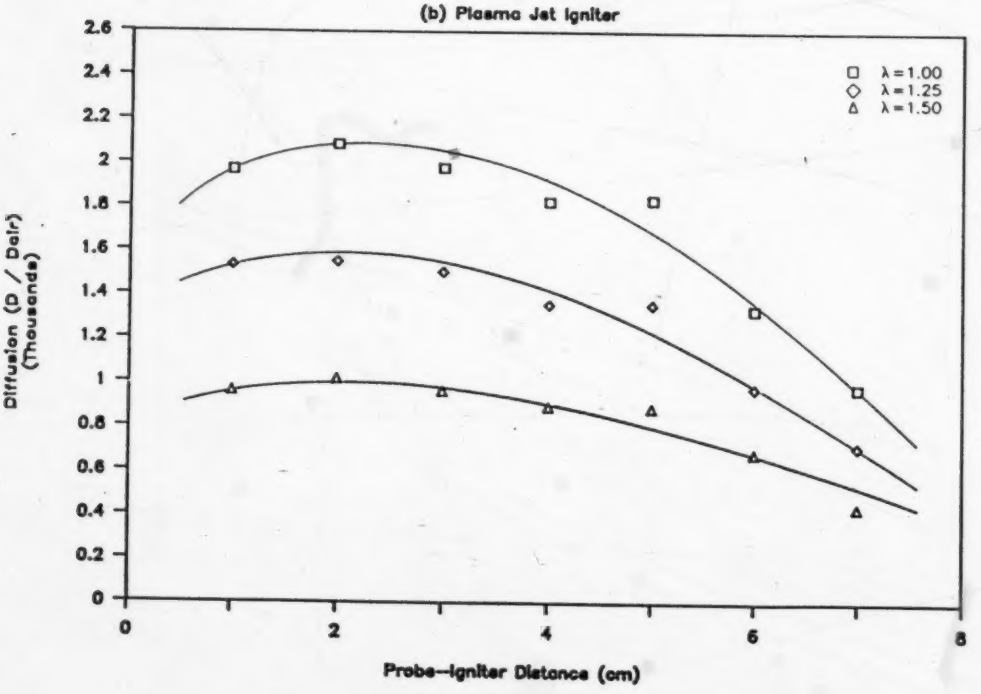

Figure 4.20 Diffusion with respect to Air Graph

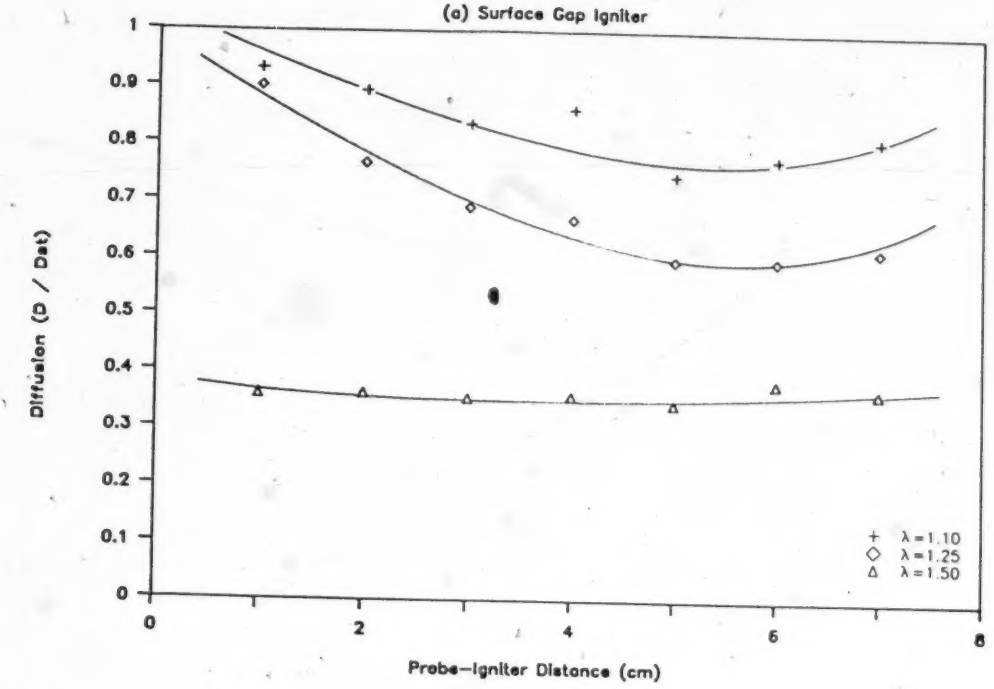

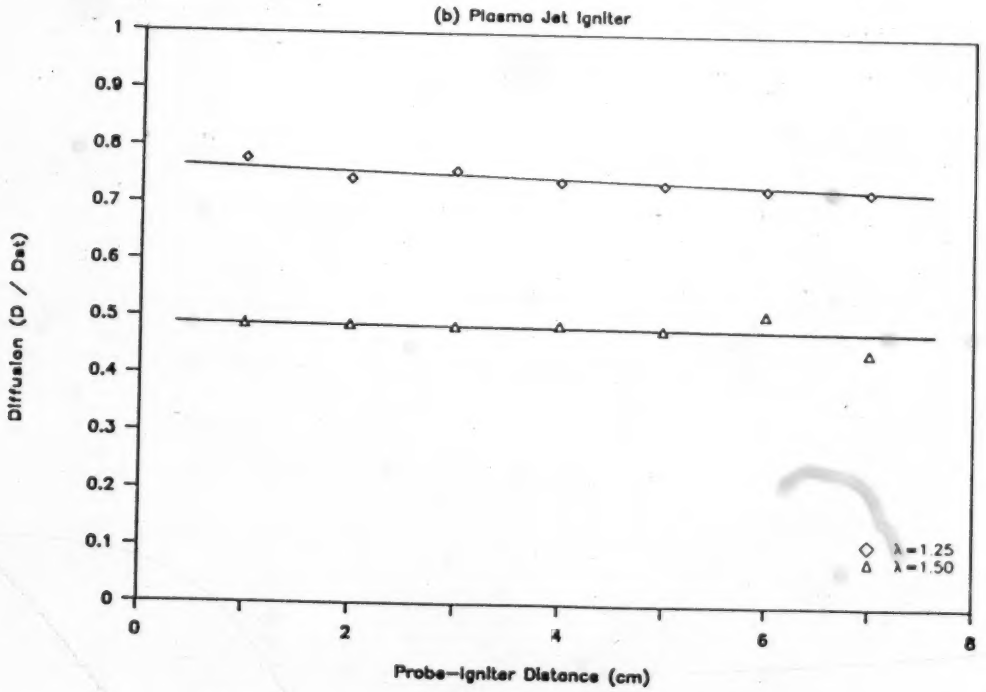

Figure 4.21 Diffusion with respect to Stoichiometric Ratio Graph

decreased in magnitude between 5 and 7 cm distance.

Once a flame is initiated from the plasma jet, its velocity and thus consumption rate is influenced by diffusion induced mixing from within the flame kernel. As the flame increases in distance from the igniter, its enhanced combustion characteristic caused by diffusion is diminished. Also shown in Figures 4.20a and 4.20b, diffusion is a major influence of mixing activity up to about 7 centimeters from the igniter.

The data is also graphed as turbulent diffusion with respect to a stoichiometric mixture versus probe-igniter distance in Figures 4.21a and 4.21b for their respective igniters. As can be seen in these figures, all data points are less than unity, indicating that diffusion for lean mixtures is less than that of stoichiometric mixtures, for both igniters. As the mixture is leaned out, the ability of the mixture to diffuse particles (radicals) decreases. This evidence indicates that leaner mixtures have less diffusive activity in the flame than do richer mixture strengths. Therefore, the ability of the flame to enhance combustion by way of particle mixing activity, otherwise known as diffusion, is decreased with leaned mixtures.

A diffusion comparison of the plasma jet igniter to the surface gap igniter (D_{pj}/D_{sg}) is presented in Figure 4.22, as a function of probe-igniter distance. It is evident from this graph that the diffusion of the plasma

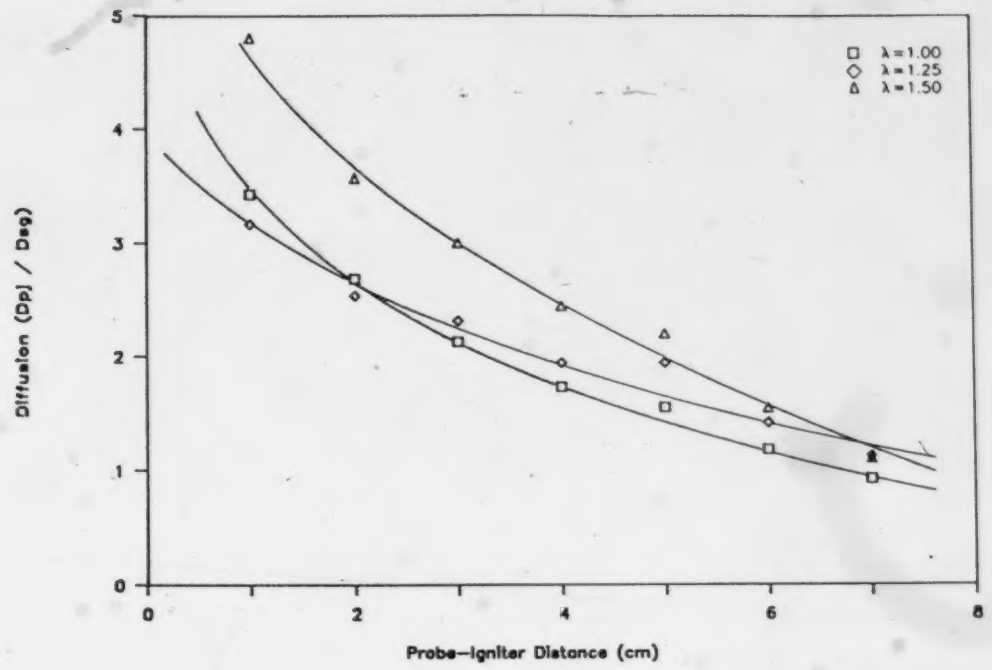

Figure 4.22 Igniter Comparison of Diffusion Graph

jet igniter is from 1 to 5 times greater than that of the surface gap igniter and that it is more dominant for lean mixtures than for near stoichiometric mixtures. This shows that the plasma jet igniter has a greater ability to transport and mix particles (associated to temperature) beyond the extent of its plume. It also demonstrates a diffusive persistence characteristic which allows the diffusion to maintain its intensity up to 7 centimeters from the igniter, which is not present when using the surface gap igniter. This 7 cm limit supports the findings of the 7 cm limit in the heat conduction case. However, since diffusion in the plasma jet case is essentially constant for the first 5 cm distance, it can be defined as the appropriate "mixing length" (l) and combined with the instantaneous velocity at that point to give a turbulent diffusion constant of $4.5 * 10^{-2}$ m^2/s for a stoichiometric mixture, from equation 4.11. This constant is nearly double that of diffusion in the surface gap case ($2.6 * 10^{-2}$ m^2/s) at the same location.

The turbulent diffusion values of Table 4.6 vary with a maximum error of ±5%, for all mixture strengths. Deviation in the measurements of turbulent diffusion arises from the errors introduced into the instantaneous velocities.

TABLE 4.6

TURBULENT DIFFUSION (m^2/s)

(a) SURFACE GAP IGNITER

Mixture Strength	Probe-Igniter Distance						
	1cm	2cm	3cm	4cm	5cm	6cm	7cm
λ=1.00	0.014	0.019	0.023	0.026	0.029	0.028	0.026
λ=1.10	0.013	0.017	0.019	0.023	0.022	0.022	0.021
λ=1.25	0.012	0.015	0.016	0.017	0.017	0.017	0.016
λ=1.50	0.005	0.007	0.008	0.009	0.010	0.011	0.010

(b) PLASMA JET IGNITER

Mixture Strength	Probe-Igniter Distance						
	1cm	2cm	3cm	4cm	5cm	6cm	7cm
λ=1.00	0.048	0.051	0.049	0.045	0.045	0.033	0.024
λ=1.25	0.038	0.038	0.037	0.033	0.033	0.024	0.018
λ=1.50	0.024	0.025	0.024	0.022	0.022	0.017	0.011

4.5.4 CONCLUSIONS

This study showed that as flame propagation occurred, the velocities of flame fronts from both igniters decreased with distance until they were similar in magnitude at a distance of 7 centimeters from the igniter. The magnitude of the initial velocity for the plasma jet igniter was found to be about 5 times that of the conventional surface gap igniter.

Once the flame front thicknesses were calculated from the electron density rise time and the instantaneous velocity, they were found to be essentially constant for mixture strength, and probe-igniter distance. The results were found to be only minutely changed by varied ambient temperature increases, which suggests that the flame has little dependence on diffusion activity. In terms of igniter type, the flame thickness produced by the plasma jet was found to be in good agreement with the flame thickness produced by the surface gap. The average flame front thickness was approximately 0.2 millimeters for both igniters. This value is also in good agreement with that given by schlieren optical probe measurements.

Thermal conductivity was calculated from a derived expression which related the relative burning velocity, the flame front thickness, and the mixture constants of specific heat and density. Thermal conductivity for both igniters was found to be initially up to 35 times greater than that of air then decreased steadily over the first 7 centimeter distance from the igniter. Also, thermal conductivity decreased with lean mixture strengths for both igniters. A comparison of thermal conductivity magnitudes indicated that the thermal conductivity of the plasma jet was up to 2.2 times greater than that of the conventional igniter. This gave evidence that the flame front was enhanced by turbulent activity initially created by the

plasma jet igniter. After the 7 cm limit, flame propagation produced by the plasma jet igniter was devoid of any combustion enhancement effects from heat conduction and was indistinguishable from the flame produced by the conventional igniter.

The turbulent diffusion coefficient was calculated from a derived expression which related the instantaneous relative flame velocity, the probe-igniter distance, and a scaling constant. The surface gap igniter created little diffusion upon ignition. As the flame propagated, mixing activity within the flame front developed as a natural characteristic of the flame itself. Diffusion from the plasma jet igniter was initially larger, and remained almost constant for the first 5 cm distance from the igniter, before quickly decreasing in magnitude. Diffusion was up to 2100 times greater than that of air and decreased with lean mixture strengths for both igniters. A comparison of magnitudes indicated that the diffusion of the plasma jet was up to 5 times greater than that of the conventional igniter, and was more dominant for leaner mixtures than for near stoichiometric mixtures. This gave evidence that the flame front was enhanced by mixing activity of radicals which were initially transported by the plasma jet igniter, especially for leaner mixtures. Since diffusion was consistent for a 5 centimeter distance, it was defined as the "mixing length" l and combined with the instantaneous

velocity at that point to give a turbulent diffusion constant ($4.5 * 10^{-2}$ m^2/s) double that of the surface gap igniter. As in the heat conduction case, after the 7 cm limit, flame propagation produced by the plasma jet igniter was devoid of any combustion enhancement effects and was indistinguishable from the flame produced by the conventional igniter.

5. SUMMARY OF RESULTS FROM ALL EXPERIMENTAL STUDIES

Luminosity produced upon pulsing an igniter in a homogeneous mixture was found to be caused by excited molecular states, otherwise known as radicals, and this conclusion is supported by tests using three different experimental methods. Luminosity (i.e. radicals) extended further from the igniter and existed longer than was previously thought (Clements et al, 1984) for a plasma jet igniter. These findings are characteristics of the heavy radical concentration from the igniter up to the wavefront and must be attributed to some mechanism of transport from their origin within the igniter. A diffusion mechanism called turbulent diffusion (Batchelor, 1967; Kadomtsev, 1965) was proposed to transport these radical "hot pockets" created by electrically induced turbulent eddies upon ignition (Haley et al, 1989).

Relative burning velocity (the true velocity of the wavefront), which is the velocity of the flame front with respect to the unburnt gaseous mixture ahead of it, was found to be 70% of the apparent velocity of the flame front. This figure was independent of igniter type. Burning velocity is much more significant than instantaneous velocity, because it indicates the actual consumption rate of reactants, a quantity which is of consequence when flame speed is considered to be increased.

In a comparison of instantaneous velocities, the flame front created from the plasma jet igniter had a higher velocity over the first 7 cm distance from the igniter, a velocity which was initially 5 times greater than that from the surface gap igniter. Also, in an ignition comparison of different mixture strengths, velocities from the plasma jet were significantly larger for lean mixtures than for near stoichiometric mixtures. These findings indicate that, in general, the plasma jet igniter enhances combustion.

Flame front thickness, a width measurement of the the flame front, was approximately 0.2 millimeters. This value did not vary substantially with mixture strength, distance from the igniter, or igniter type; characteristics which indicate the independence of flame front thickness from turbulent activity. However, elevated ambient temperature caused a minute increase in the burning velocity and a minute decrease in the flame front thickness for a stoichiometric mixture. These characteristics indicate that the thickness of the reaction zone has little dependence upon chemical diffusive activity in the reaction zone.

Two mechanisms have been found to enhance combustion at the flame front: heat conduction and turbulent diffusion. Heat conduction has been found to be a consequence of turbulent activity within the flame front, while transversing the first 7 cm distance from the

igniter, for each type of igniter. This mechanism has the effect of transferring thermal energy by way of physical molecular flow (conduction) activity from the hot reaction zone to the cold pre-heat zone. Pre-heating the mixture to be burned allows the mixture to ignite faster, thus increasing the burning velocity. Heat conduction becomes the dominant burning enhancement mechanism for near stoichiometric mixtures. In a comparison of igniters, the plasma jet igniter has an ability to conduct heat up to 2.2 times greater than that of the surface gap igniter. After a 7 cm igniter distance, the flame front initiated by the plasma jet approaches heat conduction abilities similar to that of the surface gap igniter.

The mechanism termed turbulent diffusion is analogous to molecular diffusion. It is the result of particle (as opposed to molecular) mixing while transversing a "mixing length" distance. Diffusion of this sort transports radicals from their origin within the igniter cavity to the wavefront. Since, on the basis of molecular diffusion, radicals can only exist for a transverse distance of 1 mm (Clements et al, 1984), turbulent diffusion could be accountable for transporting radicals up to distances of 7 centimeters from the igniter. Diffusion becomes the dominant enhancement mechanism for mixtures near the lean flammability limit.

In a comparison of igniters, the plasma jet igniter creates up to 5 times more diffusion than does the surface gap igniter. Diffusion within the flame front initiated by the conventional igniter tends to develop as a natural characteristic of the flame itself. On the other hand, diffusion initiated by the plasma jet igniter is initially present in a greater quantity and stays essentially constant with distances up to 5 cm from the igniter. This distance becomes the characteristic "mixing length" of turbulent diffusion. After this point, the flame front initiated by the plasma jet becomes similar to that from the surface gap igniter in its diffusion characteristics.

A major part of this study was an in-depth investigation of the role of turbulence enhanced combustion resulting from electric sparks. Since results are in good agreement with theory, and support the findings of other researchers, experimentation with pulsed plasma jets and conventional igniters resulted in an accurate explanation of observable increases in flame speed. Such an increase in flame speed would, of course, offer more reliable ignition of leaner fuel-air ratios, and more complete burning of these mixtures. The practical benefits to society in a commercial application of these techniques would be reduced pollutant emissions and more efficient and effective use of fuels.

REFERENCES

Andrews, G. E., Bradley, D. and Lwakabamba, S. B. "Turbulence and Turbulent Flame Propagation - A Critical Appraisal" Combustion and Flame, Vol. 24, p. 285, 1975.

Batchelor, G. K. An Introduction to Fluid Dynamics Cambridge University Press, Cambridge, London, pp. 28-36, 1967.

Cetegen, B., Teichman, K. Y., Weinberg, F. J. and Oppenheim, A. K. "Performance of a Plasma Jet Igniter" Society of Automotive Engineers (SAE), Technical Paper Series 800042, p. 14, 1980.

Chen, F. F. Introduction to Plasma Physics Plenum Press, New York, p. 3, 1974.

Chung, P. M. Electric Probes in Stationary and Flowing Plasmas: Theory and Application Springer-Verlag, New York, p. 6, 1975.

Clements, R. M., Smy, P. R., Topham, D., Vince, I. M., Vovelle, C., and Weinberg, F. J. "Chemical Activity and Transport Processes in the Vicinity of a Plasma Jet Igniter" Combustion and Flame, Vol. 57, No. 3, pp. 265-274, 1984.

Dale, J. D., and Oppenheim, A. K. "Enhanced Ignition for I. C. Engines with Premixed Gases" Society of Automotive Engineers (SAE), Technical Paper Series 810146, 1981.

Dale, J. D., Smy, P. R., and Clements R. M. "The Effects of a Coaxial Spark Igniter on the Performance of and the Emissions from an Internal Combustion Engine" Combustion and Flame, Vol. 31, No. 2, pp. 173-185, 1978.

Edwards, C. F., Oppenhiem, A. K., and Dale, J. D. "A Comparative Study of Plasma Ignition Systems" Society of Automotive Engineers (SAE), Technical Paper Series 830479, 1983.

England Electric Valve Company Ltd. (EEV) Night Vision Pamphlet May 1987.

Grant, J. F., Marram, E. P., and McIlwain, M. E. "Optimization of Plasma Jet Ignition Properties: Ignition of lean-quiescent mixtures of propane" Combustion Science and Technology, Vol. 30, pp. 171-184, 1983.

Haley, R. F. and Smy, P. R. "Electrically Induced Turbulence - The Short Duration Spark" Journal of Physics D: Applied Physics, Vol. 22, pp. 258-265, 1989.

Jarosinski, J. "The Thickness of Laminar Flames" Combustion and Flame, Vol. 56, pp. 337-342, 1984.

Kadomtsev, B. B. Plasma Turbulence Academic Press Inc., New York, New York, p. 106, 1965.

Keck, J. C. "Turbulent Flame Structure and Speed in Spark Ignition Engines" Nineteenth Symposium (International) on Combustion, The Combustion Institute, Pittsburgh, pp. 1451-1466, 1982.

Lewis, B., and von Elbe, G. Combustion, Flames and Explosions of Gases Academic Press, second edition, p. 226, 1961.

Motorola Optoelectronic Device Data Motorola Inc., pp. 3-23, 1981.

Orrin, J. E., Vince, I. M. and Weinberg, F. J. "A Study of Plasma Jet Ignition Mechanisms" Eighteenth Symposium (International) on Combustion, The Combustion Institute, Pittsburgh, p. 1755, 1981.

Scorer, R. S. Environmental Aerodynamics Ellis Horwood Limited, John Wiley & Sons, New York, p. 60, 1978.

Simeoni, D. and Smy, P. R. "Diffusion and Heat Conduction in the Vicinity of Plasma Plug Igniters" Combustion and Flame, Vol. 64, pp. 285-297, 1986.

Smy, P. R. "The Use of Langmuir Probes in the Study of High Pressure Plasmas" Advances in Physics, Vol. 25, No. 5, pp. 517-553, 1976.

Smy, P. R., Clements, R. M., Simeoni, D. and Topham, D. R. "Plasma Expulsion from the Plasma Jet Igniter" Journal of Physics D: Applied Physics, Vol. 15, pp. 2227-2239, 1982.

Topham, D. R., Smy, P. R. and Clements, R. M. "An Investigation of a Coaxial Spark Igniter with Emphasis on its Practical Use" Combustion and Flame, Vol. 25, p. 187, 1975.

Topham, D. R., Zhang, J. X., Clements, R. M., and Smy, P. R. "Turbulent Mixing Induced by a high-energy ignition device" Journal of Physics D: Applied Physics, Vol. 15, pp. 65-67, 1982.

Tozzi, L. and Dabora, E. K. "Plasma Jet Ignition in a Lean-Burn CFR Engine" Nineteenth Symposium (International) on Combustion, The Combustion Institute, Pittsburgh, pp. 1467-1474, p. 1523, 1982.

Weast, R. C. Handbook of Tables for Applied Engineering Science The Chemical Rubber Company, Cleveland, p.9, p. 303, p. 453, 1970.

Webster's Seventh New Collegiate Dictionary Toronto: Thomas Allen and Son Ltd., 1973.

Weinberg, F. J. Advanced Combustion Methods Academic Press, London, pp. 277-330, 1986.

Weinberg, F. J. "Plasma Jets in Combustion" Institute of Mechanical Engineering Symposium, Combustion in Engineering, Oxford, April, p. 65, 1983.

Weinberg, F. J., and Lee, A. J. J., "A Novel Ignition Device for the Internal Combustion Engine" Nature, Vol. 311, pp. 738-740, 1984.

Zhang, J. X., Clements, R. M., and Smy, P. R. "An Experimental Investigation of the Effect of a Plasma Jet on a Freely Expanding Methane-Air Flame" Combustion and Flame, Vol. 50, pp. 99-106, 1982.

APPENDIX I

1. INTRODUCTION

This section investigates the operating nature of the English Electric Value (EEV) P8079DC First Generation 25 millimeter Cascade Image Intensifier and qualifies its use as part of the major optics within the millisecond streak camera to enhance that camera's light sensitivity. Controlled experiments were performed to study the transient and steady state response of the image intensifier. This study involved utilizing experimental evidence to derive a real time system transfer function. The objective was to prove that the device was capable of linear light amplification with respect to time exposure.

It is known from the manufacturer, EEV that the intensifier incorporates an internal automatic gain/brightness control (England, 1987). To justify using the image intensifier as an integral part of the streak camera requires an understanding of this automatic control in relation to system response. By incorporating the image intensifier's characteristics into the camera, enhanced experimental data can be collected reliably.

2. EXPERIMENTAL DESIGN

The apparatus illustrated in Figure I.1 was set up to perform controlled experiments on the P8079DC Image Intensifier. This apparatus consists of two photomultipliers, a 1% neutral density filter, a 50%

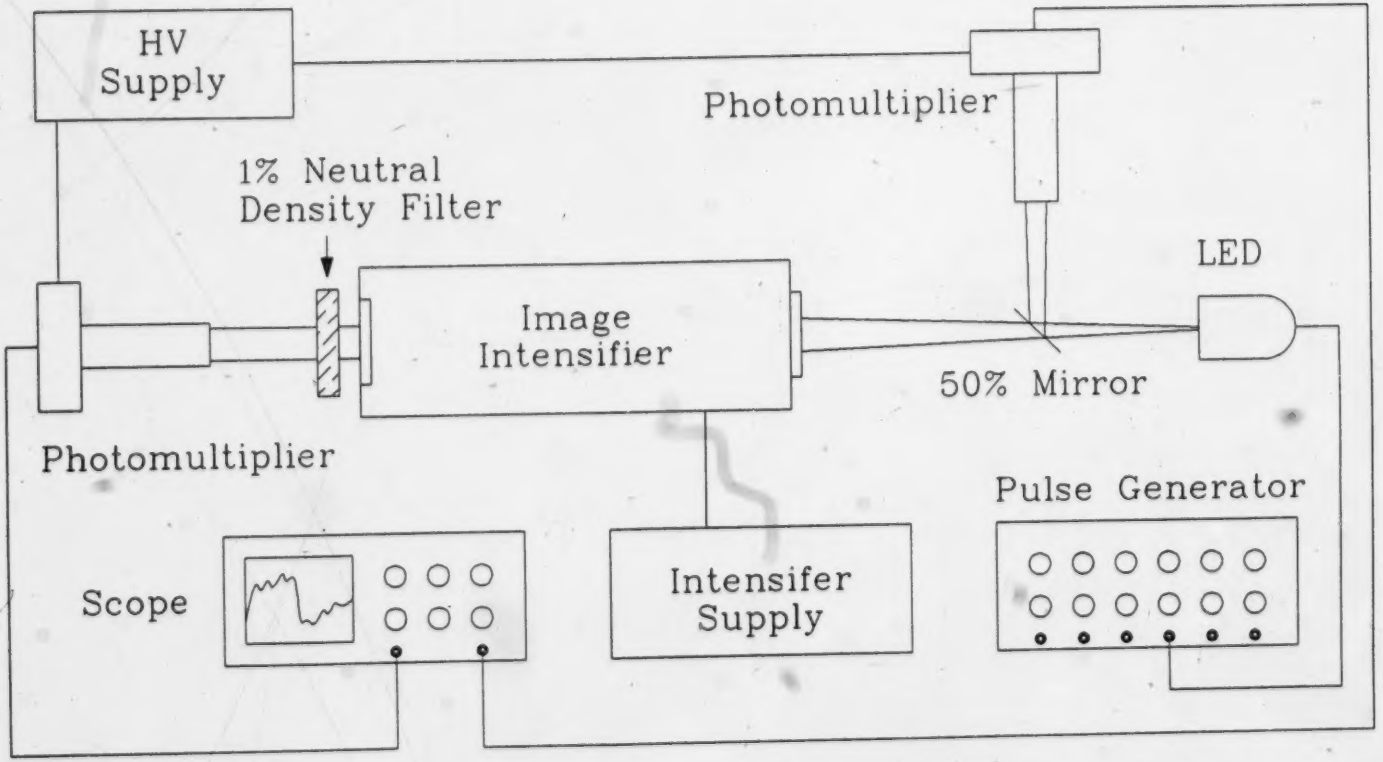

Figure I.1 Image Intensifier Experiment

silvered mirror, a pulse generator, a light emitting diode and a Tektronix model 7854 storage oscilloscope.

A type MV5054A-1 red light-emitting-diode (LED), was used to illuminate both the fibre-optic input of the image intensifier and the photomultiplier cathode. This LED was chosen because its output luminosity is linearly dependent upon diode current (Motorola, 1981). A WaveTek model #187 frequency/pulse generator was used as a signal source for the LED. This made it possible to perform controlled repeatable system analysis experiments.

The photomultipliers used to measure input and output luminosity give brightness ratings in units of voltage. Conventionally, luminosity is measured in units of lux or units of lumens per square meter; however, the available equipment to make luminosity measurements in these luminosity units was not sensitive at the low light intensity levels encountered. Thus, quantitative measurements from the photomultipliers did not present a problem in determining the mathematical theory presented in this investigation, since only the relative magnitude of luminosity gain, in the form of oscilloscope waveforms, was important. This made experimental evidence from these instruments acceptable determining the system transfer function. The specific values of the transfer function constants are not required, since only algebraic expressions are needed to understand how the intensifier

will operate under different luminosity conditions.

Experiments consisted of illuminating the image intensifier's plane fibre optic input with varying light intensities for a given excitation pulse. Also, the pulse width was stepped through varying durations for each input pulse. Input and output brightness were monitored on the oscilloscope, which utilized the output signals from the photomultipliers. These signals vary in current level depending upon light intensity.

3. EXPERIMENT CONSIDERATIONS

The sensitivity of both the image intensifier and the photomultiplier devices vary with wavelength; however, this does not present a problem in the formulation of a system transfer function for the intensifier. In the case of the photomultipliers used to monitor the input and output luminosity of the image intensifier, the "input" photomultiplier gives a signal which is referenced to the red (650nm) LED, while the "output" photomultiplier gives a signal which is referenced to the intensifier's output green (550nm) wavelength. As a result of the different wavelengths irradiating the "input" and "output" photomultipliers, observations taken from the resultant oscillogram waveforms of Plates I.1, I.2, and I.3, introduce a "wavelength" error in terms of the output-to-input luminosity gain. This error does not present a

problem in the derivation of an image intensifier transfer function since (for the purposes of this investigation) the expression is purely algebraic. The algebraic expression thus consists of "gain" proportionality constants which have no dependence on wavelength.

In the case of the image intensifier, the wavelength of light irradiating the input affects the amount of light gain. It is known from the manufacturer (EEV) that light radiation at 800nm will cause a higher degree of light amplification, in terms of peak photo-current, than light radiation at 850nm. Of course, when utilizing the intensifier to study combustion reactions, the burning mixtures will emit multiple wavelengths of light, depending upon the type of fuel involved and the air-fuel ratio. Therefore, this aspect has a direct effect in the magnitude of the intensifier's gain, since different wavelengths of light will be amplified to different extents, making the image intensifier amplification proportional with respect to wavelength. This characteristic introduces a wavelength dependency on "gain" terms in the intensifier's transfer function with respect to the light irradiating the intensifier. The effects of this amplification dependence on wavelength may be ignored when the intensifier is used in situations were the wavelength of light to be amplified remains constant.

4. TIME DOMAIN MODEL

In an attempt to model the intensifier's transfer function, experiments have produced enough information to formulate a mathematical model describing output brightness when excited by various light intensities. These input intensities were varied in unit steps. Observed waveforms displayed exponential curve characteristics demonstrated in three cases: Case 1 (normal), Case 2 (high), and Case 3 (excessively high) input intensities.

4.1 CASE 1: Normal Input Intensity

For a normal input intensity, the intensifier output's optical gain is steady and unsaturated but at a maximum. Plate I.1 displays the classical exponential growth waveform. In Figure I.2 the output luminosity rises exponentially towards a constant maximum in magnitude (G_{Fpk}) with time. This exponential, whose time constant is τ_{pk}, can be attributed to the phosphor plane fibre optic, since phosphor exhibits exponential decay/growth. The expression:

$$V_{out}(t) = V_{final} + (V_{initial} - V_{final})\, e^{-t/\tau_{pk}} \qquad (I.1)$$

where

$V_{out}(t)$	is the signal of optical intensity seen at the output-photomultiplier;
V_{final}	is final optical output level;
$V_{initial}$	is the initial optical output level;
τ_{pk}	is the time constant of the first exponential component which is dependent upon phosphor decay,

exhibits this characteristic in terms of the output-photomultiplier's signal, $V_{out}(t)$. Dividing I.1 by the input signal expression:

$$V_{in}(t) = V_{excit} \qquad (I.2)$$

where

$V_{in}(t)$ is the signal of optical intensity seen at the input-photomultiplier;
V_{excit} is the level of excitation irradiating the image intensifier's input.

results in an expression in terms of gain:

$$G(t) = \frac{V_{out}(t)}{V_{in}(t)} = G_{Fpk} + (G_{Ipk} - G_{Fpk})\, e^{-t/\tau_{pk}}. \qquad (I.3)$$

where

$G(t)$ is the optical gain in terms of output-to-input intensity;
G_{Ipk} is the initial "peak" gain for the first exponential component;
G_{Fpk} is the final "peak" gain for the first exponential component.

The constants G_{Ipk} and G_{Fpk} are defined as:

$$G_{Ipk} = \frac{V_{initial}}{V_{excit}}, \quad \text{and} \quad G_{Fpk} = \frac{V_{final}}{V_{excit}},$$

and when the initial condition is taken into account where the output is non-existent prior to the input step excitation (i.e. $G(t<0) = 0$), G_{Ipk} equates to zero. (This exponential expression is most commonly associated with the charging characteristics phenomena of capacitors).

When the gain equation of I.3 is taken to the limit as t approaches infinity:

$$\lim_{t \to \infty} G(t) = G_{pk} \tag{I.4}$$

it evaluates to a steady state output gain of G_{pk} as expected (Figure I.2).

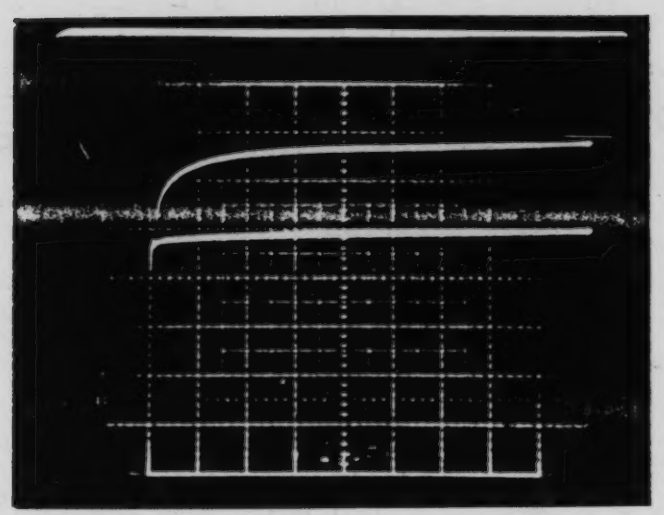

Plate I.1 Oscillogram of Image Intensifier's Output excited by Normal Input Intensity

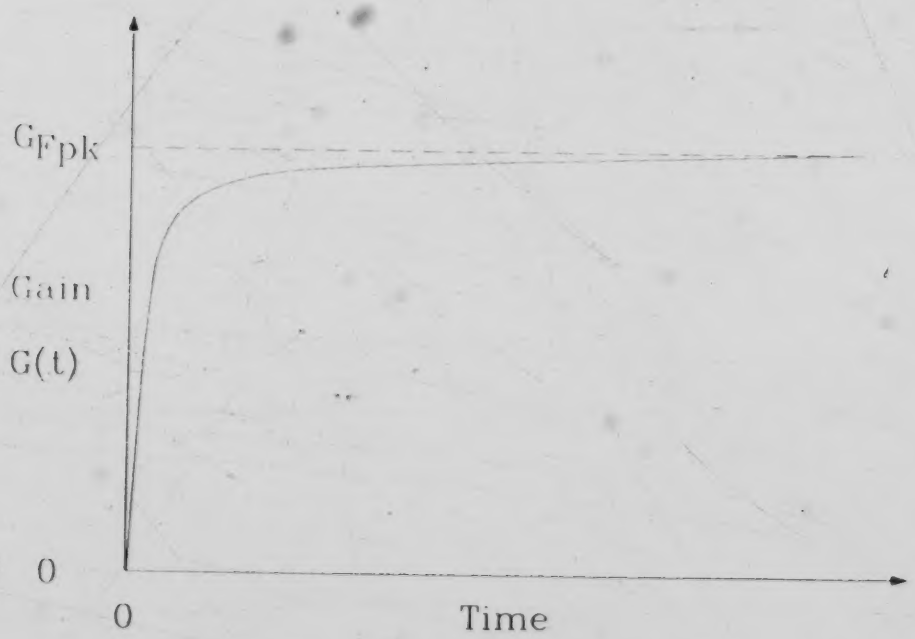

Figure I.2 Normal Input Intensity

4.2 CASE 2: High Input Intensity

With a high input intensity, Case 2 is demonstrated in Plate I.2 where automatic gain control tendencies are displayed. As in Figure I.3, the waveform overshoots the image intensifier's steady state optical level when the maximum possible gain causes the output brightness to be beyond the sustaining capability of the phosphor.

The gain initially rises toward a maximum point (G_{Fpk}, approximately 70,000). When it has become apparent that the brightness of the output is beyond a comfortable level - say approaching saturation - the automatic control of gain takes over to bring the output to a more reasonable level (G_{Fmid}), somewhat less than the maximum allowed. Notice that the time constant τ_{pk} of the first exponential has decreased because of the high input brightness, thus increasing the rate at which the first exponential is rising with respect to time. Also, it is obvious that time constant τ_{pk} is significantly less than that of the second exponential, τ_{mid}. An expression which exhibits these characteristics can be derived by a combination of the classical final/initial value exponential functions of I.3 and I.5, where I.3 is taken as $G_{Imid}(t)$:

$$G(t) = G_{Fmid} + (G_{Imid}(t) - G_{Fmid})\, e^{-t/\tau_{mid}}. \qquad (I.5)$$

where additional term definitions are:

$G_{Imid}(t)$ is the initial time dependent "middle" gain for the second exponential component;

G_{Fmid} is the final "middle" gain for the second exponential component;

τ_{mid} is the time constant of the second exponential component.

Substituting I.3 into I.5 for $G_{Imid}(t)$ and rearranging, will obtain a combined expression for gain:

$$G(t) = G_{Fmid} + (G_{Fpk} - G_{Fmid})\, e^{-t/\tau_{mid}} + (G_{Ipk} - G_{Fpk})\, e^{-t(1/\tau_{pk} + 1/\tau_{mid})}. \qquad (I.6)$$

When the gain equation of I.6 is taken to the limit as t approaches infinity:

$$\lim_{t \to \infty} G(t) = G_{Fmid} \qquad (I.7)$$

it evaluates to a steady state output gain of G_{Fmid} as expected (Figure I.3).

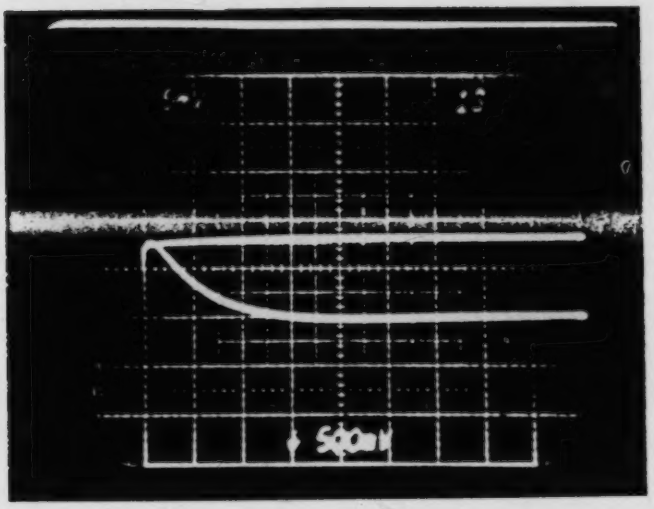

Plate I.2 Oscillogram of Image Intensifier's Output excited by High Input Intensity

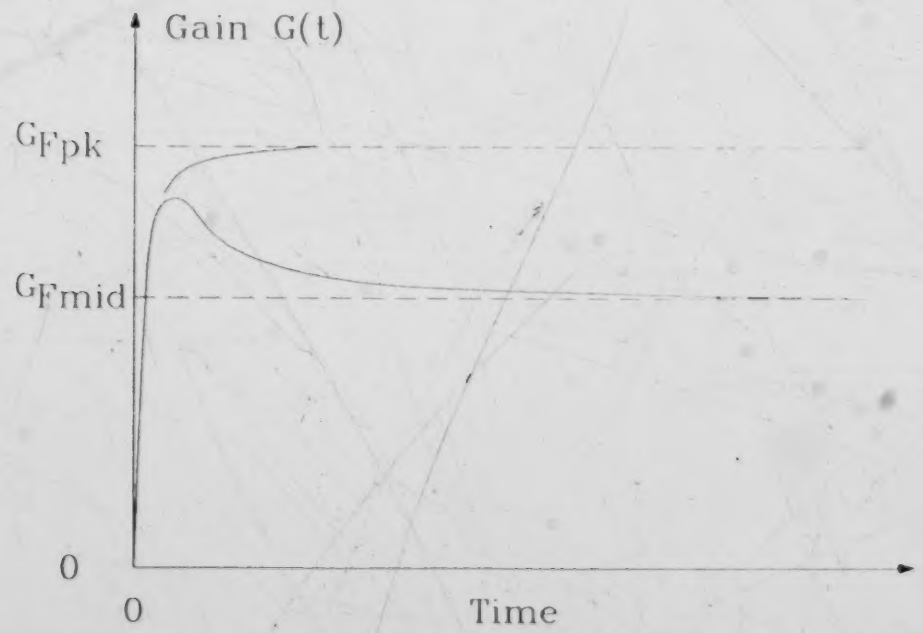

Figure I.3 High Input Intensity

4.3 CASE 3: Excessively High Input Intensity

When an excessively bright light is imposed upon the image intensifier's fibre optic input, a third exponential component as seen in Plate I.3, also seen in Figure I.4, is exercised. This results in an output waveform consisting of three exponentials exhibiting a somewhat oscillatory overshoot and undershoot characteristic.

As in Case 2, the output initially rises toward a level of maximum optical gain (G_{Fpk}), spurred on by the very intense input excitation V_{in}. But now, time constant τ_{pk} has greatly decreased due to the extreme input intensity causing a rapid and extreme peak of overshoot to occur. This peak, in turn, forces the unobtainable high magnitude of gain to be cut back toward a more reasonable level (G_{Fmid}); however, the second decaying exponential, whose lesser time constant τ_{mid} has also been affected by the intense input, now undershoots the favored moderate level of gain. Again, in an attempt to establish itself at this optimal gain (G_{Fss}), a third exponential (τ_{ss}) takes over to return the undershot level back up to the respectable steady state level of output. A gain expression which exhibits these characteristics admirably can be derived by a triple combination of the classical capacitor-like exponential functions of I.3, I.5, and I.8, where $G_{Iss}(t)$ is taken as I.5:

$$G(t) = G_{Fss} + (G_{Iss}(t) - G_{Fss})\ e^{-t/\tau ss}. \qquad (I.9)$$

where additional term definitions are:

$G_{Iss}(t)$ is the time dependent initial "steady state" gain of the third exponential component;

G_{Fss} is the final "steady state" gain of the third exponential component;

τ_{ss} is the time constant of the third exponential component.

Substituting I.3 into I.5, I.5 into I.9, and redistributing results in the following expression for gain:

$$\begin{aligned} G(t) = {} & G_{Fss} + (G_{Fmid} - G_{Fss})\ e^{-t/\tau ss} \\ & + (G_{Fpk} - G_{Fmid})\ e^{-t(1/\tau mid\ +\ 1/\tau ss)} \\ & + (G_{Ipk} - G_{Fpk})\ e^{-t(1/\tau pk\ +\ 1/\tau mid\ +\ 1/\tau ss)} \end{aligned} \qquad (I.10)$$

which ultimately describes how the system will respond in all three (Normal, High, Excessively High) cases. When the gain equation of I.10 is taken to the limit as t approaches infinity:

$$\lim_{t \to \infty} G(t) = G_{Fss} \qquad (I.11)$$

it evaluates to a steady state output gain of G_{Fss} as expected (Figure I.4).

At normal and moderately high input intensities, as described in Cases 1 and 2, the large exponential time constants τ_{mid} and τ_{ss} suppress the effects of the second and third exponentials, resulting in transient responses which are similar to equations I.3 and I.6, respectively.

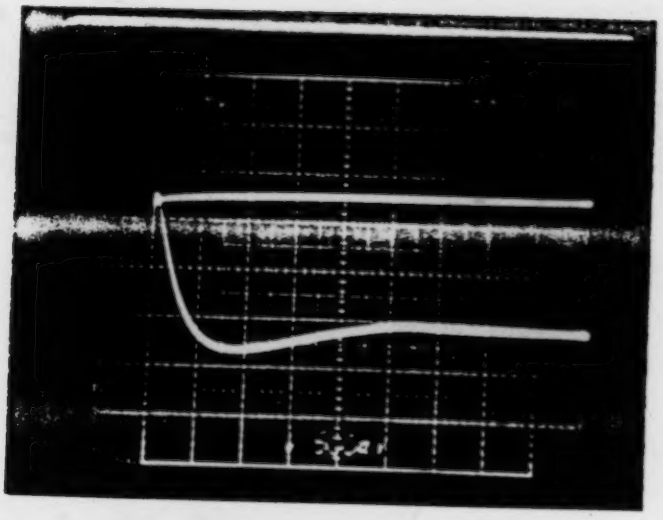

Plate I.3 Oscillogram of Image Intensifier's Output excited by Excessively High Input Intensity

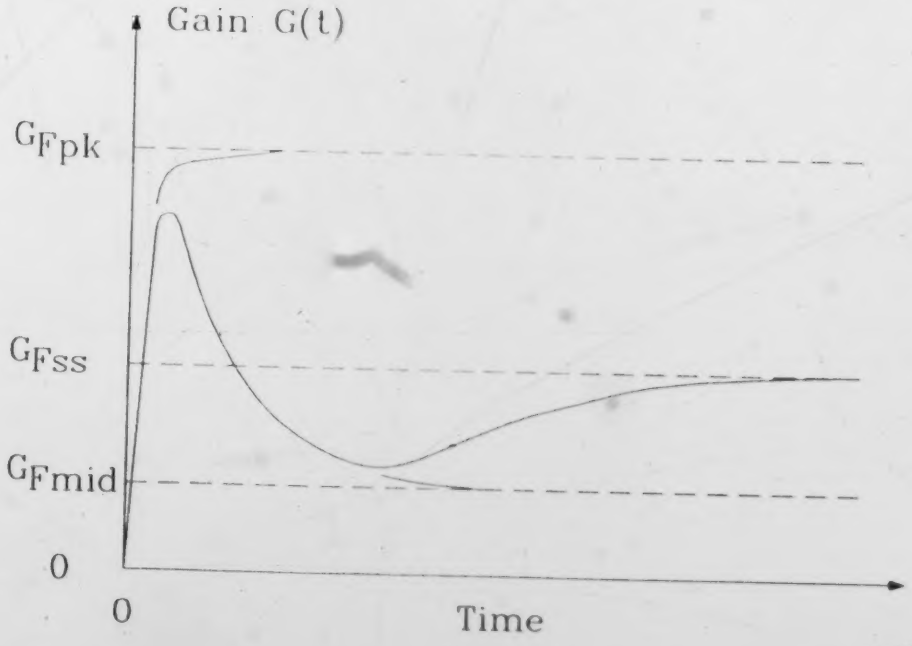

Figure I.4 Excessively High Input Intensity

5. PHOSPHOR DECAY CASE

When a step pulse excitation is exhausted at the end of pulse width time T, the light illuminated from the intensifier's output decreases exponentially because of phosphor decay. At time T, the magnitude of the output, $V_{out2}(t)$ of equation I.13, will have reached some non-zero value to become the initial condition for an exponential decrease in luminosity caused by phosphor decay. It will have an inherent phosphor decay time constant τ_{ph}. Mathematically, this can be modelled by the equation:

$$V_{out2}(0 < t < \infty) = V_{out1}(T)\ e^{-(t-T)/\tau_{ph}} \qquad (I.12)$$

where

V_{out1} is the optical intensity output signal before the excitation input is discontinued;
V_{out2} is the optical intensity output signal after the excitation input is discontinued;
T is the input excitation termination time.

which substitutes into latter part of the intensifier output expression modified from I.1 ($V_{out1}(t)$ of I.13 now becomes $V_{out}(t)$ from I.1) with respect to common time and time T:

$$V_{out}(t) = V_{out1}(t)\ u(T-t) + V_{out2}(t)\ u(t-T) \qquad (I.13)$$

where

$V_{out}(t)$ is the optical intensity output with respect to common time and time T;
$u(t-T)$ is a unit function in terms of common time and time T.

The unit function is defined as:

$$u(t-T) = \begin{cases} 0, & t < T \\ 1, & t \geq T. \end{cases}$$

In I.13 the unit function u(t-T) is used to switch in this phosphor decay activity, while u(T-t) terminates the case studied gain portion of the transfer function. The point at which this transfer occurs is mathematically continuous because the final value of $V_{out1}(t).u(T-t)$ becomes the initial value determined by $V_{out1}(t)$ evaluated at time T (i.e. $V_{out1}(T)$).

6. TIME EXPOSURE MODEL

Now that mathematical model I.13 has been established to describe the image intensifier's automatic gain control, the crucial role of this device as an integral part of the streak camera when photographing time versus distance images of combustion reactions will be qualified.

The correct time exposure of photographs is of concern in the streak camera, where circumstances sometimes require high speed photographs for studying events in detail. However, the sweep-time and streak-width characteristics of the streak camera often cause a reduction in the light intensity from the subject. An additional problem is that the self-illumination of the combustible reaction is sometimes not bright enough to correctly expose the Polaroid film used in the camera. Overcoming both problems

requires the use of some type of light amplifier to obtain a good exposure. Therefore, utilizing the image intensifier's light gain to enhance images from the reaction can provide useful experimental photographs.

The image intensifier's light amplification is only reliable if the intensifier can provide an output time exposure which is directly proportional to the input time exposure. Mathematically, this can be proven by considering the area of time transfer function I.16. Expression I.16 can be derived from I.15 divided by I.14, where the two parts of gain time transfer function I.15 are integrated over periods of zero to pulse duration time T, and T to infinity, respectively:

$$A_{in}(T) = \int_0^{\infty} V_{in}(t)\ u(T-t)\ dt \qquad (I.14)$$

$$A_{out}(T) = \int_0^{T} V_{out1}(t)\ u(T-t)\ dt + \int_T^{\infty} V_{out2}(t)\ u(t-T)\ dt \qquad (I.15)$$

where

$A_{in}(T)$ is the time-exposure area with respect to the input at time T;
$A_{out}(T)$ is the time-exposure are with respect to the output at time T.

Therefore,

$$G(T) = \frac{A_{out}(T)}{A_{in}(T)} = G_{ss}\ (T + \tau_{ph})$$

$$+ (G_{mid} - G_{ss})\ \frac{1}{T}\ [\tau_{ss} + (\tau_{ph} - \tau_{ss})\ e^{-T/\tau_{ss}}]$$

$$+ (G_{pk} - G_{mid})\ \frac{1}{T}\left[\ \frac{1}{\left[\frac{1}{\tau_{mid}} + \frac{1}{\tau_{ss}}\right]}\right.$$

$$\left. + \left[\tau_{ph} - \frac{1}{\left[\frac{1}{\tau_{mid}} + \frac{1}{\tau_{ss}}\right]}\right]\ e^{-T(1/\tau_{mid}\ +\ 1/\tau_{ss})}\ \right]$$

$$+ (G_I - G_{pk})\ \frac{1}{T}\left[\ \frac{1}{\left[\frac{1}{\tau_{pk}} + \frac{1}{\tau_{mid}} + \frac{1}{\tau_{ss}}\right]}\right.$$

$$\left. + \left[\tau_{ph} - \frac{1}{\left[\frac{1}{\tau_{pk}} + \frac{1}{\tau_{mid}} + \frac{1}{\tau_{ss}}\right]}\right]\ e^{-T(1/\tau_{pk}\ +\ 1/\tau_{mid}\ +\ 1/\tau_{ss})}\ \right] \qquad \text{(I.16)}$$

where

$G(T)$ is the optical gain in terms of output-to-input intensity with respect to time T.

Differentiating I.16 with respect to T then gives rise to an expression for the rate-of-change of the ratio of total output area to step pulse input area (time exposure):

$$\frac{d\,G(T)}{dT} = - G_{ss}\,\tau_{ph}$$

$$- (G_{mid} - G_{ss})\,\frac{1}{T}\left[\,\tau_{ss} + (\tau_{ph} - \tau_{ss})\left[\frac{1}{T} + \frac{1}{t_{ss}}\right] e^{-T/\tau_{ss}}\,\right]$$

$$-(G_{pk} - G_{mid})\,\frac{1}{T}\left[\,\frac{1}{\left[\frac{1}{\tau_{mid}} + \frac{1}{\tau_{ss}}\right] T}\right. \qquad \text{(I.17)}$$

$$\left. + \left[\tau_{ph} - \frac{1}{\left[\frac{1}{\tau_{mid}} + \frac{1}{\tau_{ss}}\right]}\right]\left[\frac{1}{T} + \frac{1}{\tau_{mid}} + \frac{1}{\tau_{ss}}\right] e^{-T(1/\tau_{mid} + 1/\tau_{ss})}\,\right]$$

$$- (G_I - G_{pk})\,\frac{1}{T}\left[\,\frac{1}{\left[\frac{1}{\tau_{pk}} + \frac{1}{\tau_{mid}} + \frac{1}{\tau_{ss}}\right] T}\right.$$

$$\left. + \left[\tau_{ph} - \frac{1}{\left[\frac{1}{\tau_{pk}} + \frac{1}{\tau_{mid}} + \frac{1}{\tau_{ss}}\right]}\right]\left[\frac{1}{T} + \frac{1}{\tau_{pk}} + \frac{1}{\tau_{mid}} + \frac{1}{\tau_{ss}}\right] e^{-T/\tau_{eq}}\,\right]$$

where the equivalent time constant τ_{eq} is defined as:

$$\tau_{eq} = 1 \Big/ \left[\,\frac{1}{\tau_{pk}} + \frac{1}{\tau_{mid}} + \frac{1}{\tau_{ss}}\,\right]$$

If the rate of change of equation I.17 can be found to be zero, then the image intensifier is qualified in its use as a linear light amplifier. Taking the limit of differential I.17 as T approaches infinity:

$$\lim_{T\to\infty} \frac{d\,G(T)}{d\,T} = 0 \qquad \text{(I.18)}$$

does indeed yield a zero equality. As a consequence, this also points to the conclusion that when I.16 is put to the limit as T approaches infinity:

$$\lim_{T\to\infty} G(T) = G_{ss} \qquad (I.19)$$

it equates to a constant, namely G_{ss}. However, for the case of a step input pulse of pulse width T, I.17 will equate to a non-zero value, which would not support the theory. But, if T is large in magnitude compared to each of the exponential time constants, then equation I.17 can be simplified by dropping terms which have little or no contribution. Consequently, when I.17 is evaluated at time T:

$$\frac{d\,G(T)}{dT} \simeq 0 \qquad (I.20)$$

it yields a small value which can be approximated to zero as desired. Also, experimental evidence shown in Figure I.5 supports this approximation. This exhibits evidence to validate the theory of a constant proportionality of output area to input area (i.e. time exposure).

7. CONCLUSION

Using the EEV P8079DC first generation 25mm cascade image intensifier as an integral part of the streak camera has been justified. A laboratory experimental study has has also established a model for the intensifier's gain

transfer function. This expression, coupled with experimental results, has provided the evidence of a sound basis for utilizing the automatic-gain-controlled image intensifier as a linear light amplifier to study flame structure in combustion.

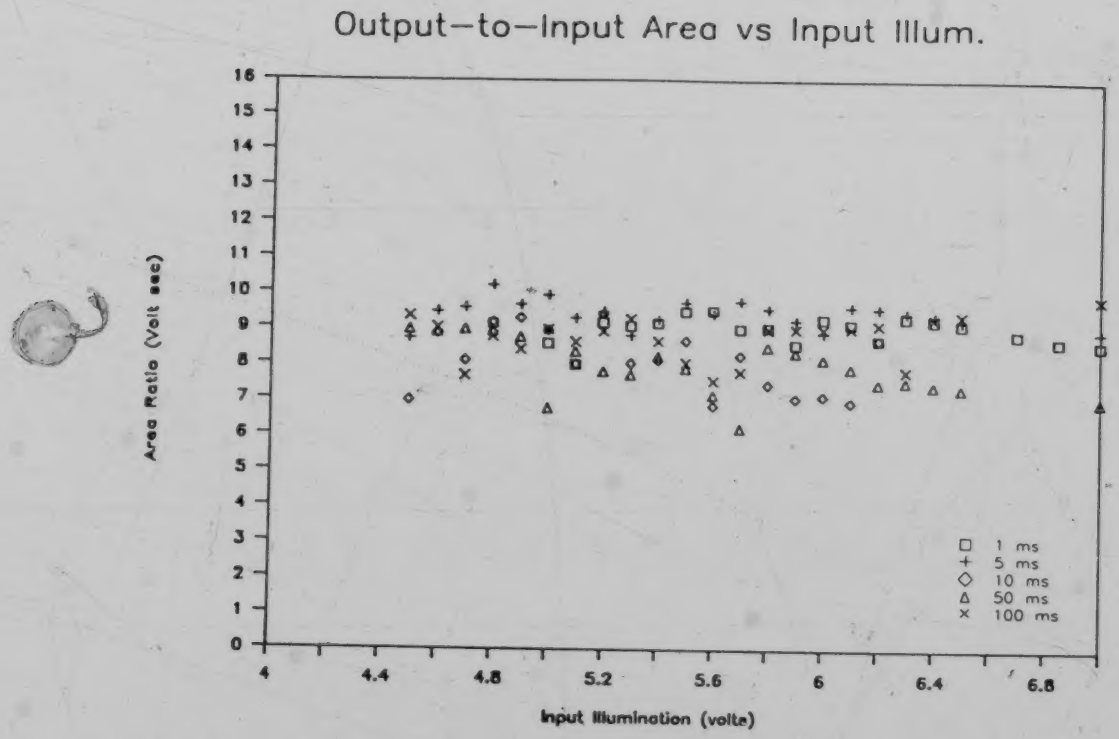

Figure I.5 Output-to-Input Luminosity Area vs Input Voltage